DEPARTMENT OF COMMERCE
LUTHER H. HODGES, Secretary

WEATHER BUREAU
F. W. REICHELDERFER, Chief

MONTHLY WEATHER REVIEW

JAMES E. CASKEY, JR., Editor

Volume 89, Number 9 Washington, D.C. September 1961

SOME ASPECTS OF A CYCLE OF AVAILABLE POTENTIAL ENERGY[1]

JAY S. WINSTON AND ARTHUR F. KRUEGER

Meteorological Satellite Laboratory, U.S. Weather Bureau, Washington, D.C.

[Manuscript received April 27, 1961]

ABSTRACT

A large-scale cycle of available potential energy in the Northern Hemisphere over a period of about two weeks during late December 1958 and early January 1959 has been investigated in some detail. During this cycle the zonal available potential energy first built up strongly to a maximum, and then when it began to decline, increases in eddy available and eddy kinetic energy took place. These changes in the energy parameters were well related to variations in the poleward heat transport, large values of which signify substantial conversions from zonal to eddy available potential energy, and to variations in the conversion between potential and kinetic energy. Furthermore some estimates of the generation of available potential energy show good consistency with the available potential energy variations. Examination of this cycle of available potential energy on a regional basis indicates that it was almost completely dominated by developments over North America and vicinity. The synoptic events associated with this energy cycle are also illustrated.

1. INTRODUCTION

Satellite observations of solar and terrestrial radiation will soon be available in sufficient quantity to provide the first direct measurements of the global heat budget. As radiation is measured on a continuing day-by-day basis it will be of great interest to study not only the large-scale spatial and temporal variations in this basic planetary heating, but also the manner in which the atmosphere reacts to it. Since this heating is indeed basic in nature, any clear-cut reactions of the atmosphere to it would most likely be found in some of the more fundamental atmospheric parameters that directly measure the large-scale energetics of the circulation. In particular it seems appropriate to investigate the role of radiational heating with respect to the zonal and eddy components of kinetic and available potential energy as defined, for example, by Lorenz [4].

These various energy components and the typical flow of energy from and to the environment and between various forms are illustrated schematically in figure 1 in the manner presented by Lorenz [3]. Here it is seen that diabatic heating of the atmosphere (actually differential heating between high and low latitudes) builds up the zonal available potential energy, which is basically a function of the latitudinal variance in temperature, or essentially a measure of the strength of latitudinal thermal gradients. As the zonal available energy keeps increasing, the strengthening thermal gradients lead to baroclinic instability and the growth of eddies. Thus eddy available potential energy (increasing thermal differences within latitude circles) increases at the expense of the zonal available energy as northward heat transport increases to relieve the excessive thermal gradients. Some of this increased eddy potential energy is then converted to eddy kinetic energy by means of direct thermal circulations (upward motion in the warm air, downward motion in the cold air) occurring in the eddies, or major cyclone waves. Differential heating relative to these eddies along

[1]This research has been supported by the National Aeronautics and Space Administration.

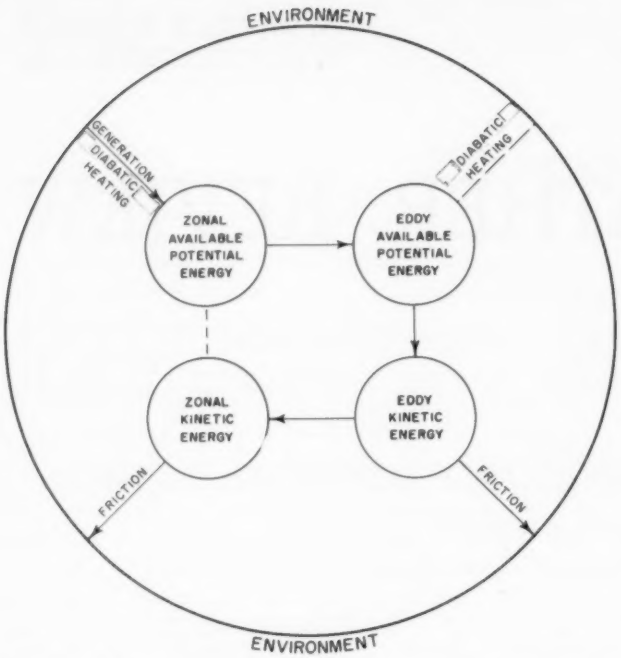

FIGURE 1.—Proposed energy cycle for the earth's atmosphere (after Lorenz [3]). Arrows indicate prevailing directions of energy transformations. Dashed lines indicate that there is apparently no prevailing direction.

latitude circles may either generate or dissipate the eddy available energy—a predominant trend in one direction or the other has not as yet been definitely established. Eddy kinetic energy is partially dissipated by friction and partially converted to zonal kinetic energy (much of the conversion being associated with the poleward transfer of momentum). The zonal kinetic energy is mainly subject to dissipation by friction, but a portion of it may be converted back into zonal available potential energy.

This typical energy flow picture has been generally substantiated by empirical evaluations of energy conversion terms (White and Saltzman [13]; Wiin-Nielsen [14]; Saltzman and Fleisher [10]; Jensen [1]). Although this mode of energy flux is representative of conditions that apparently must prevail on the average, it is realized that the generation and transformation of atmospheric energy may very well vary in both amount and direction at various times. This is the case both in the seasonal sense and also over time periods as short as a week or even a day, particularly when the energy in only one hemisphere or less is considered.

To investigate more closely the behavior of the energy cycle over various time and geographic scales a program for regular daily computation of several atmospheric energy parameters of the Northern Hemisphere has been initiated (Winston [16]). As a substantial sample of such calculations accumulate, it will be possible to document the energy cycle more precisely. Moreover, as radiation data observed by satellites also accumulate, there will be an opportunity to calculate the generation of available potential energy (primarily the zonal component) and to study the reactions of the energy cycle to variations in this radiant energy. These are areas of study for the future, however.

For the present it is of interest to illustrate an actual case of a pronounced cycle of available potential energy which occurred during a pilot period of 42 days of energy computations in the winter of 1958–1959 (Winston [16]). This case seemed to fit the idealized energy flow picture to such a marked degree that it was of interest to examine it in some detail. Presentation of this case is of special significance because it is, to our knowledge, the first time that a cycle of large-scale available potential energy has been investigated for the actual atmosphere. In general circulation model experiments, on the other hand (Phillips [8]; Smagorinsky [12]), there has been extensive "day-by-day" calculation of potential and kinetic energy and energy transformations. Yet it is surprising that there has not been a like body of data computed from the real atmosphere to check similarities of the models and the observed time variations of the atmospheric energetics. Occasionally the energy cycle in the models has been compared to the index cycle of the atmosphere, which was described in detail by Rossby and Willett [9], and indeed the energy cycle and index cycle in a gross sense are often similar phenomena. However, as some experience has been gained with energy parameters, it has been found that the index cycle and the energy cycle do not always occur at the same time and with the same degree of intensity. To a great extent this is due to physically real differences in the behavior of the zonal winds as contrasted with the energetics of the flow. But also it is in part due to the inadequacy of the zonal index as a general circulation parameter. In fact, if one stresses the broader connotation that the term "index cycle" has attained, particularly in terms of cold air penetrations to lower latitudes and expanded circumpolar westerlies (Namias [5]; Rossby and Willett [9]), then it is highly probable that the dynamic and thermodynamic consequences of the energy cycle are truly more descriptive of these typical "index-cycle" phenomena than any index variations themselves. Thus, the expedient of verifying energetics of general circulation models in the real atmosphere by means of the index cycle is a patently crude procedure. It must be pointed out, however, that there have been comparisons of the *average* energetics of models with *average* values of energy transformations computed for the atmosphere.

The first published calculations of available potential energy for the Northern Hemisphere in the actual atmosphere, which were made at about the same time as those calculated by us, are some average values for the month of February 1959 (Saltzman and Fleisher [10]). Their results consist not only of monthly average values of total, zonal, and eddy available potential energy, but also the components of the eddy available energy for individual

wave numbers around latitude circles. It is believed that the present study of one particular energy cycle provides some interesting material which is complementary to that of Saltzman and Fleisher and which also aids in the physical comprehension of the atmospheric energy cycle.

2. DEFINITIONS AND METHODS OF COMPUTATION

The average available potential energy per unit area over the entire earth's atmosphere may be expressed by the following approximate equation, as derived by Lorenz [4]:

$$\overline{A}=\frac{1}{2}\int_0^{\overline{p}_0}(\Gamma_d-\overline{\Gamma})^{-1}\overline{T}^{-1}\overline{(T')^2}dp, \tag{1}$$

where bars within the integral refer to averages over an entire isobaric surface, T is temperature, Γ_d is the dry adiabatic lapse rate, $\overline{\Gamma}$ is the lapse rate, T' is the deviation of the temperature at any given point on the isobaric surface from its average value in that surface, p is pressure, and $\overline{p_0}$ is the average pressure at the surface of the earth. It should be noted that over short time periods (i.e., of the order of days, weeks, or perhaps a month) variations of available potential energy are essentially dependent upon variations in the spatial variance of temperature on isobaric surfaces, $\overline{(T')^2}$, since the mean temperature and mean lapse rates within an isobaric surface are relatively constant with time. In a longer-period sense (e.g., over several months) the time variations in available potential energy are, however, also influenced to a moderate degree by changes in mean lapse rate and to a lesser extent by changes in mean temperature.

Available potential energy may also be expressed in terms of two components, a zonal and an eddy component (Lorenz [4]). The expression for zonal available potential energy is

$$\overline{A}_Z=\frac{1}{2}\int_0^{\overline{p}_0}(\Gamma_d-\overline{\Gamma})^{-1}\overline{T}^{-1}\overline{[T]'^2}dp, \tag{2}$$

where the bracket refers to a latitudinal average and $[T]'$ is the departure of the latitudinal average temperature from the overall mean temperature. The expression for eddy available potential energy is

$$\overline{A}_E=\frac{1}{2}\int_0^{\overline{p}_0}(\Gamma_d-\overline{\Gamma})^{-1}\overline{T}^{-1}\overline{(T^*)^2}dp, \tag{3}$$

where T^* is the departure of the temperature at any point from its latitudinal average value. Thus, zonal available potential energy is mainly dependent upon the variance of the average latitudinal temperatures, or essentially upon the strength of the north-south thermal gradients, while eddy available potential energy is mainly a function of the variance of temperature within latitude circles, having a minimum value when isotherms are parallel to the latitude circles and having maximum values when the isotherms display a wave pattern of large amplitude.

In attempting to calculate available potential energy in the actual atmosphere from synoptic data it is necessary to restrict the computations to a limited area where analyzed temperature data are available. In the calculations presented here, the area considered was the Northern Hemisphere from latitude 30° northward. Temperatures [2] at 700 mb. were used to represent the temperature field in the entire troposphere, and the calculations, which were made by means of a desk computer, were considered to apply to the layer between 1000 and 250 mb. No attempt has been made to weight these energy calculations for pressures less than 250 mb., since the available potential energy would tend to be much smaller in most of the more stable stratospheric layers than in tropospheric layers of comparable pressure intervals. A few tests comparing available potential energy computed from data throughout the troposphere and stratosphere, with values using 700-mb. temperatures only, show that the use of 700-mb. temperatures alone provides a good approximation to the available potential energy through the depth of the atmosphere. Another approximation in these calculations is the use of the standard atmosphere lapse rate for $\overline{\Gamma}$.

The average kinetic energy per unit area over the entire atmosphere may be expressed as follows (cf., Lorenz [4]):

$$\overline{K}=\frac{1}{2}g^{-1}\int_0^{\overline{p}_0}\overline{V^2}dp, \tag{4}$$

where g is the acceleration of gravity, V is the horizontal wind speed, and the bar within the integral again represents averaging over an entire isobaric surface. Kinetic energy may also be expressed in two components, zonal kinetic energy and eddy kinetic energy, the expressions for which are respectively as follows:

$$\overline{K}_Z=\frac{1}{2}g^{-1}\int_0^{\overline{p}_0}\overline{[V]^2}dp, \tag{5}$$

and

$$\overline{K}_E=\frac{1}{2}g^{-1}\int_0^{\overline{p}_0}\overline{(V^*)^2}dp, \tag{6}$$

where $[V]$ is the average wind for each latitude circle and V^* is the deviation of the wind from its latitudinal average value. Kinetic energy and its components were computed by means of a machine program which had previously been devised by C. L. Bristor. This program makes use of 500-mb. geostrophic winds obtained from 500-mb. height data of the Joint Numerical Weather Prediction (JNWP) Unit on their octagonal grid, which fully covers the area between about latitude 20° N. and the pole.

Expressions for time rates of changes of available potential and kinetic energy are also pertinent. Following Lorenz [4] we may write the following expressions for the local changes of energy:

[2] Temperature data recorded at 5° latitude and 10° longitude intervals (diamond grid) by the Extended Forecast Section of the Weather Bureau were used.

$$\frac{\partial \overline{A}}{\partial t}=-C+G \tag{7}$$

and

$$\frac{\partial \overline{K}}{\partial t}=C-D, \tag{8}$$

where

$$C=-Rg^{-1}\int_0^{\overline{p}_0} p^{-1}\overline{T\omega}\,dp, \tag{9}$$

$$G=g^{-1}\int_0^{\overline{p}_0}\Gamma_d(\Gamma_d-\overline{\Gamma})^{-1}\overline{T}^{-1}\overline{T'Q'}dp, \tag{10}$$

and

$$D=-g^{-1}\int_0^{\overline{p}_0}\overline{\mathbf{V}\cdot\mathbf{F}}dp. \tag{11}$$

In these expressions C represents the conversion between potential and kinetic energy, G is the generation of available potential energy, D is the frictional dissipation of kinetic energy, R is the gas constant for dry air, ω is equal to dp/dt (vertical motion in pressure coordinates), Q is the rate of addition of heat per unit mass, and $\mathbf{F}$ is the frictional force.

Generation of available potential energy is greatest when there is a high positive covariance between heating and temperature (equation (10)). In other words, when the atmosphere is heated where the temperature is high and cooled where the temperature is low there is considerable generation of available potential energy. The energy conversion term appears with opposite sign in equations (7) and (8). Energy is converted from available potential energy to kinetic energy when there is a correlation between vertical motion and temperature such that upward motion occurs in the warm air and downward motion occurs in the cold air (equation (9)). On the other hand, when the vertical motion field is reversed relative to the temperature field, i.e., downward motion in the warm air and upward motion in the cold air, the kinetic energy is converted to available potential energy.

It is obvious from these expressions that the place where radiational heating plays an important role is in the generation of available potential energy (equation (10)). This will be one of the most important terms to evaluate when satellite radiation data become available, and of course, it will be important to compare these evaluations of the generation term with the observed variations in available potential energy. At present, however, some calculations of the energy generation term can be made from indirect estimates of heating on a hemispheric scale (Wiin-Nielsen and Brown [15]).

The conversion term (equation(9)) is also of considerable interest in understanding the time variations of both kinetic and available potential energy. From data kindly provided by A. Wiin-Nielsen, some evaluations of this term have been made. These data are based on initial vertical motions and thicknesses available as a by-product of the operational baroclinic numerical prediction calculations of the JNWP Unit. These data were used by both Wiin-Nielsen [14] and Saltzman and Fleisher [10] to obtain calculations of this energy conversion term.

Expressions for conversion and generation of zonal and eddy components of available potential and kinetic energy are also given by Lorenz [4], but it is beyond the scope of this paper to present all of them here. It is pertinent, however, to write the expression for the conversion between zonal and eddy available potential energy, C_A, which is as follows:

$$C_A=-\frac{R}{g}\int_0^{\overline{p}_0}\frac{\overline{\theta}}{\overline{T}}\overline{\left([T^*v^*]\frac{\partial}{\partial y}+[T^*\omega^*]'\frac{\partial}{\partial p}\right)\left(\frac{\Gamma_d}{\Gamma_d-\overline{\Gamma}}\frac{[T]'}{\theta}\right)}\,dp, \tag{12}$$

where θ is potential temperature, * denotes a deviation from a latitudinal average value, and [ ]′ denotes a deviation of a latitudinal average value from the mean value over the entire isobaric surface. It will be noted that basically this conversion involves the products of the horizontal transport of sensible heat and the north-south temperature gradient and of the vertical transport of heat and the vertical temperature gradient.

In the discussion that follows only the northward heat transport itself is calculated. This transport, H, across a given latitude circle, ϕ_0, in a layer between two constant pressure surfaces, p_1 and p_2, is obtained through the following approximate expression:

$$H=\frac{c_p a\cos\phi_0(p_2-p_1)\Delta\lambda}{g}\sum v^*T^*, \tag{13}$$

where a is the radius of the earth, c_p is the specific heat at constant pressure, v is the meridional wind component, and λ is longitude. In the evaluation of (13), p_2 is taken as 850 mb. and p_1 as 500 mb., v^* and T^* are average values in the layer 850–500 mb., and the summation is over 72 intervals of $\Delta\lambda$, or 5° of longitude, around the latitude circle. Further treatment of the assumptions used in this calculation, including the use of geostrophic flow, has already been given elsewhere (Winston [16]).

3. DESCRIPTION OF THE ENERGY CYCLE AND VARIATIONS IN PARAMETERS ASSOCIATED WITH ENERGY CONVERSIONS

The day-to-day variations of the available potential energy, and its zonal and eddy components for the period of interest are shown in figure 2. It may be seen that the major cycle of buildup and breakdown in the total available potential energy between December 24 and January 7 mainly reflected the variation in the zonal component of the available potential energy. This is essentially indicative of the buildup of strong thermal gradients between latitude circles up to a peak on January 1, which was then followed by a very substantial breakdown in these thermal gradients between January 1 and 10. The eddy available potential energy remained at a nearly

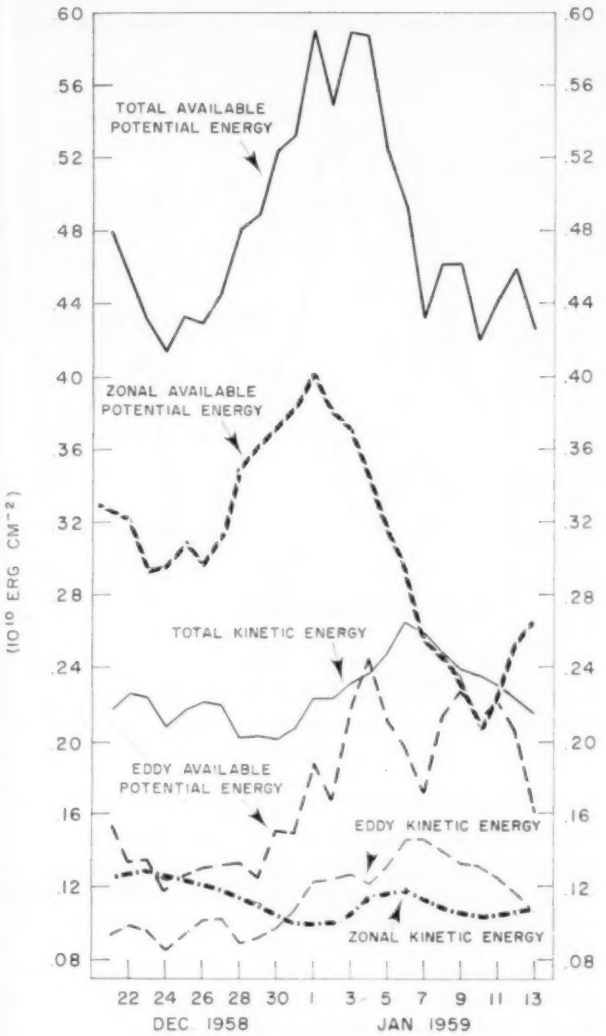
TOTAL AVAILABLE POTENTIAL ENERGY
ZONAL AVAILABLE POTENTIAL ENERGY
TOTAL KINETIC ENERGY
EDDY AVAILABLE POTENTIAL ENERGY
EDDY KINETIC ENERGY
ZONAL KINETIC ENERGY
(10^10 ERG CM^-2)
22 24 26 28 30 1 3 5 7 9 11 13
DEC. 1958
JAN. 1959

FIGURE 2.—Available potential energy, kinetic energy, and the zonal and eddy components of each for the period December 21, 1958–January 13, 1959. All quantities computed once daily at 0000 GMT.

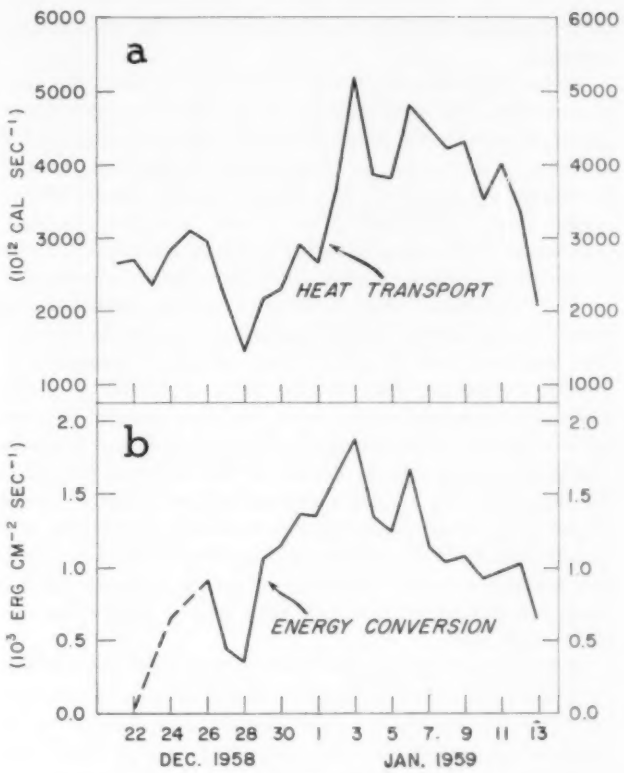

FIGURE 3.—(a) Total heat transport across all latitudes from 20° N. northward, and (b) the conversion between available potential and kinetic energy (positive for conversion to kinetic energy), for the period December 21, 1958–January 13, 1959. Both quantities computed once daily at 0000 GMT. Portion of energy conversion curve prior to December 26 is dashed since conversion data were unavailable for December 23 and 25.

constant, low level until December 29 and then began a general rise culminating in a peak value on January 4, when the zonal available potential energy was falling precipitously. Following this maximum the eddy available energy dropped at a rapid rate to reach a minimum on January 7, but a rapid rebound brought it to values only slightly less than peak values between January 8 and 12, when the zonal component reached its minimum value.

This overall behavior of the eddy relative to the zonal component of the available potential energy suggests very strongly that the increased level of eddy available energy was derived from the zonal available energy. In other words, strong thermal gradients developed *within* latitude circles at the expense of the thermal gradients *between* latitude circles. This is supported by the variation of the total northward heat transport (summed over all latitude circles) which is shown in figure 3. Note that heat transport was at a relatively low level during the buildup of zonal available potential energy, but spurted rapidly upward at the time when the zonal available energy began to decline after January 1. In view of the direct role that heat transport plays in the conversion from zonal to eddy available potential energy (equation (12)) there is little doubt that this increase in heat transport after January 1 signified a marked increase in this energy conversion.

Turning to the kinetic energy variations in figure 2, it is seen that the total kinetic energy also went through a cycle at this time, but it was almost completely dominated by the variations in the eddy kinetic energy. Note that the eddy (and total) kinetic energy generally increased for more than a week before reaching a maximum between about January 6 and 7, more than 2 days later than the peak in the eddy available potential energy. Thus the next step in the energy flow, the transformation from

eddy available to eddy kinetic energy (see fig. 1) evidently occurred.

As for the final step in the typical energy flow, the conversion from eddy kinetic to zonal kinetic energy, there appears to be very little evidence that any appreciable increase in conversion to zonal kinetic energy was realized in this period since the zonal kinetic energy showed rather small time variations. There was, however, a weak maximum in the zonal kinetic energy on January 6, about the same time as the maximum in the eddy kinetic energy.

The conversion between total available potential and total kinetic energy shown in figure 3 generally verifies the increased flow of energy from available potential to kinetic during the first several days of January. Comparison of this conversion with the time changes in total kinetic energy that can be deduced from figure 2 shows that they were generally related in the direction indicated by equation (8); i.e., the conversion term tended to be larger when kinetic energy was markedly increasing and smaller when kinetic energy was markedly decreasing (on the assumption that D always acts to decrease kinetic energy and that it does not vary nearly so much as the conversion term).

It is interesting that the time variation of the conversion term, which is a function of the spatial covariance between vertical motion and temperature, appears to be rather well correlated with the variations in total heat transport, which is a function of the spatial covariance between meridional motion and temperature. This tends to verify the deductions of Kuo [2] that northward heat transport (and hence conversion from zonal to eddy available potential energy) and conversions from potential to kinetic energy must be closely related. However, despite this good correspondence in these quantities, the actual curves of eddy available and eddy kinetic energy (fig. 2) are imperfectly correlated, particularly near the time of maximum values in the two eddy components (January 3–9). In fact, a secondary minimum in eddy available potential energy occurred on January 7, very close to the maximum in eddy kinetic energy. The explanation for this lack of agreement probably lies in the behavior of the generation of eddy available potential energy which apparently was responsible for the downturn in eddy available energy between January 3 and 7. Some evidence for this will be presented in the following sections.

4. THE GENERATION OF AVAILABLE POTENTIAL ENERGY

It was indicated earlier that for a closed region the available potential energy can change due to either a conversion term, depending on a correlation between vertical motion and temperature, or a generation term, depending on a correlation between diabatic heating and temperature (equations (7), (9), (10)). The variations of the conversion term have already been shown (fig. 3) and discussed above. Although readily computed through

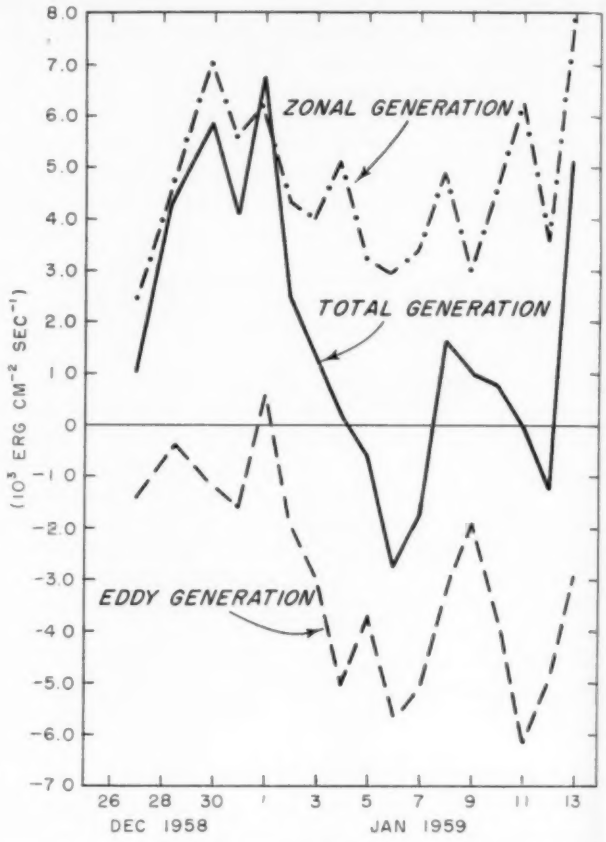

FIGURE 4.—Generation of available potential energy and its zonal and eddy components for the period December 27, 1958–January 13, 1959. Quantities computed once daily at 0000 GMT.

use of numerically calculated vertical motions its accuracy is not readily determinable. The problem of obtaining the diabatic heating, and consequently reliable estimates of the generation term however, is an even more difficult problem. Recently however, Wiin-Nielsen and Brown [15] have devised a method for computing the diabatic heating hemispherically on a daily basis. Their method essentially utilizes an equation derived from the thermodynamic energy equation where the vertical motion is estimated from the vorticity equation.

By utilizing their method it is now possible to estimate the generation of available potential energy from synoptic data, and indeed this was also done by Wiin-Nielsen and Brown. Their computations of the average generation term for the month of January 1959 indicate a value of about 1.5×10^3 ergs cm.$^{-2}$ sec.$^{-1}$, a value comparable to the average conversion from potential to kinetic energy for the same month (Wiin-Nielsen [14]). This represents the sum of 5.0×10^3 ergs cm.$^{-2}$ sec.$^{-1}$ for the zonal component and -3.5×10^3 ergs cm.$^{-2}$ sec.$^{-1}$ for the eddy component. Thus according to these calculations, the only source of available potential energy, at least during

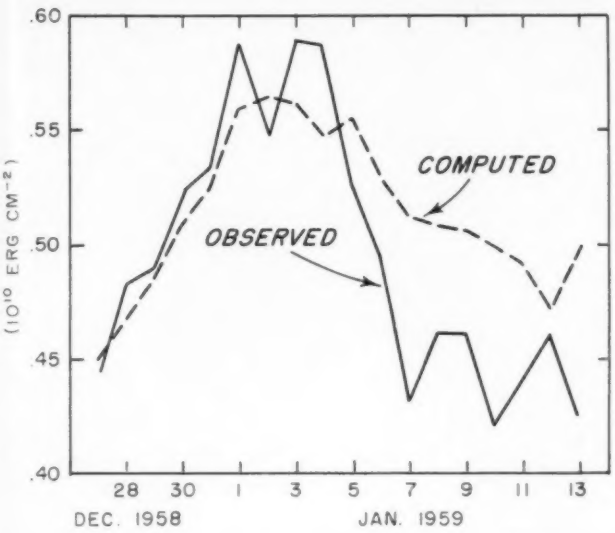

FIGURE 5.—Observed and computed available potential energy for the period December 27, 1958–January 13, 1959.

January 1959, was the latitudinal heating gradient. Apparently the heating within latitude circles, which represents the heating associated with the long planetary waves and transient disturbances, served only to reduce the available potential energy.

As part of the study of the cycle in available potential energy treated in this report, it was felt to be of interest to compare the interdiurnal variation of the generation term and its zonal and eddy components with that of the available potential energy. For this purpose Wiin-Nielsen has kindly made his computations for January 1959 available to us and these have been combined with similar computations made in the Meteorological Satellite Laboratory for the period December 27–31, 1958.

The time variations of these energy generation terms are shown in figure 4. As can be seen, the zonal generation was always positive, seldom dropping below 3 units, while the eddy generation was predominantly negative, averaging frequently below −2 units. The total generation, while usually positive, was occasionally negative, particularly between January 4 and 7, indicating that the heating field even in winter can at times act to destroy available potential energy. Of particular interest for this study was the similar behavior of the generation term and the total available potential energy (fig. 2) between December 27 and January 7. Both curves increased very markedly at the beginning of the period with the generation term reaching a maximum of 7×10^3 ergs cm.$^{-2}$ sec.$^{-1}$ about two days prior to the maximum in the available potential energy. At this time the eddy generation was small so that the total was nearly equal to the zonal component, reflecting a predominantly latitudinal heating distribution. Also significant is the fact that the generation term remained above 2 units for

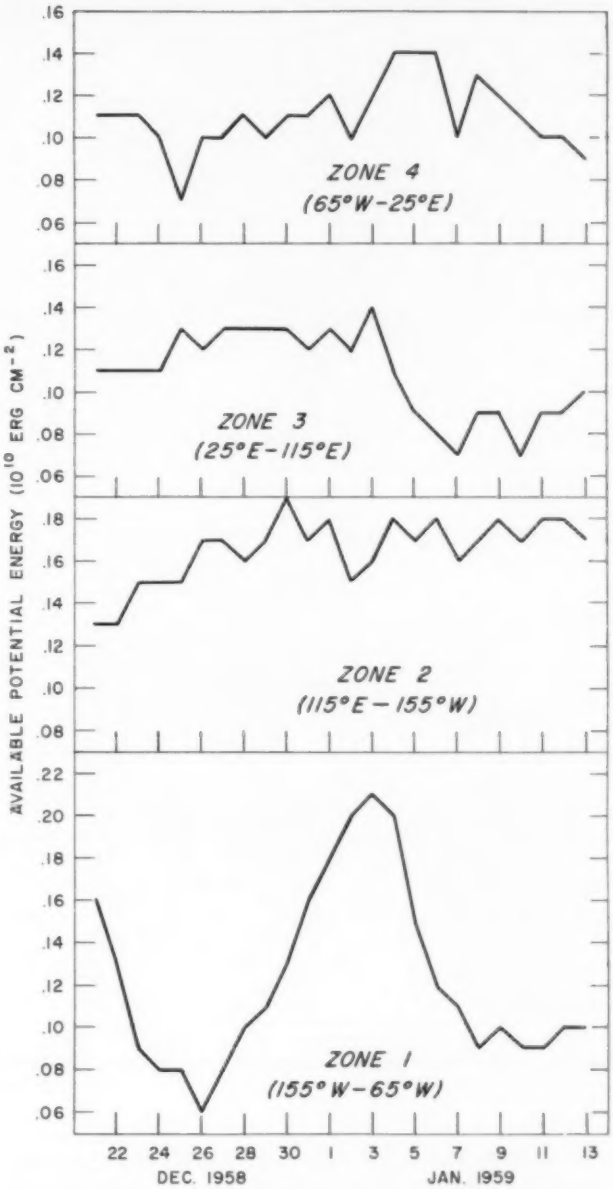

FIGURE 6.—Available potential energy in four zones extending northward from 30° N. within the indicated longitudinal boundaries for the period December 21, 1958–January 13, 1959. Quantities computed once daily at 0000 GMT.

about six consecutive days. Considering the magnitude of the energy conversion term (fig. 3) this was sufficient to cause an increase in available potential energy during this period.

After January 1 the intensity of the total generation of available potential energy was drastically reduced and within a few days it had even become negative. Much of this decline was due to the sudden drop in the eddy gen-

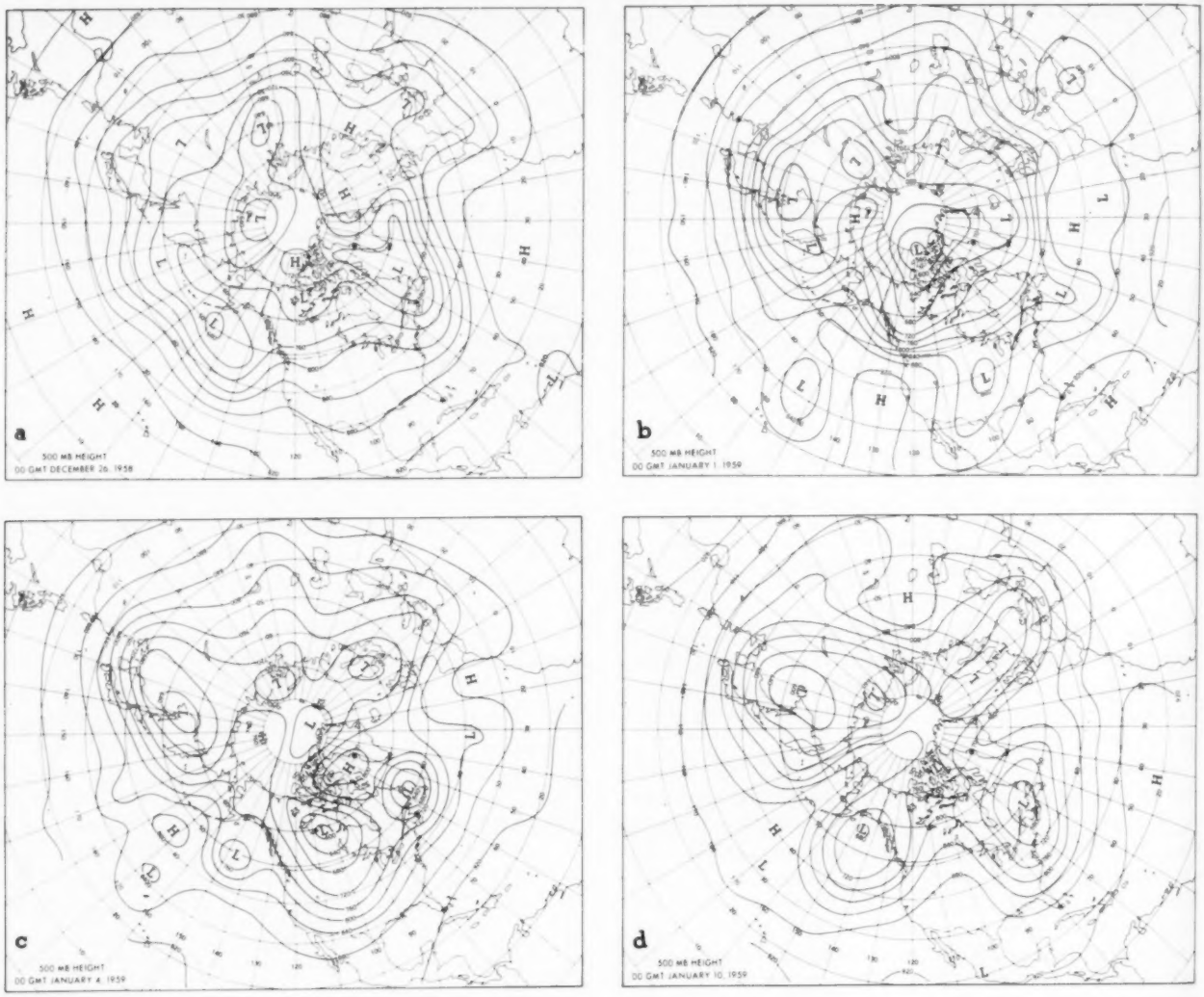

FIGURE 7.—500-mb. contour patterns for (a) December 26, 1958, (b) January 1, 1959, (c) January 4, 1959, and (d) January 10, 1959. Contour interval is 400 ft.

eration term which fell nearly 6 units during the same interval. This was the result of more intense cold air outbreaks and the consequent heating of polar air masses in middle and lower latitudes, as will be illustrated in the next section. The sudden dip in the eddy available potential energy between January 4 and 7 (fig. 2), which was discussed earlier, was probably a response to this strong heating and a direct consequence of the large negative value of the eddy generation. This was a period during which the computed values of both the (total) generation and (total) conversion terms contributed toward a decline in total available potential energy, agreeing with the observed decline. It is of interest in this regard to compare in more detail the computed behavior of the sum of C, the conversion term, and G the generation term, with the observed variation in available potential energy during this period. This will now be considered.

Equation (7) may be integrated to give

$$\overline{A}_n=\overline{A}_{n-1}+(G-C)\delta t, \tag{14}$$

where $\overline{A}_n$ is the value of available potential energy on a given day n, $\overline{A}_{n-1}$ is the value a day earlier, and δt is an interval of 1 day. Specifying the value of $\overline{A}_0$, which has been chosen here to be the observed value of the available potential energy on December 26, one can compute $\overline{A}_1$ and all succeeding values of $\overline{A}_n$ for as many days as one pleases, providing values of $G-C$ are available. These computed values of available potential energy are shown in comparison with the observed values for our period of

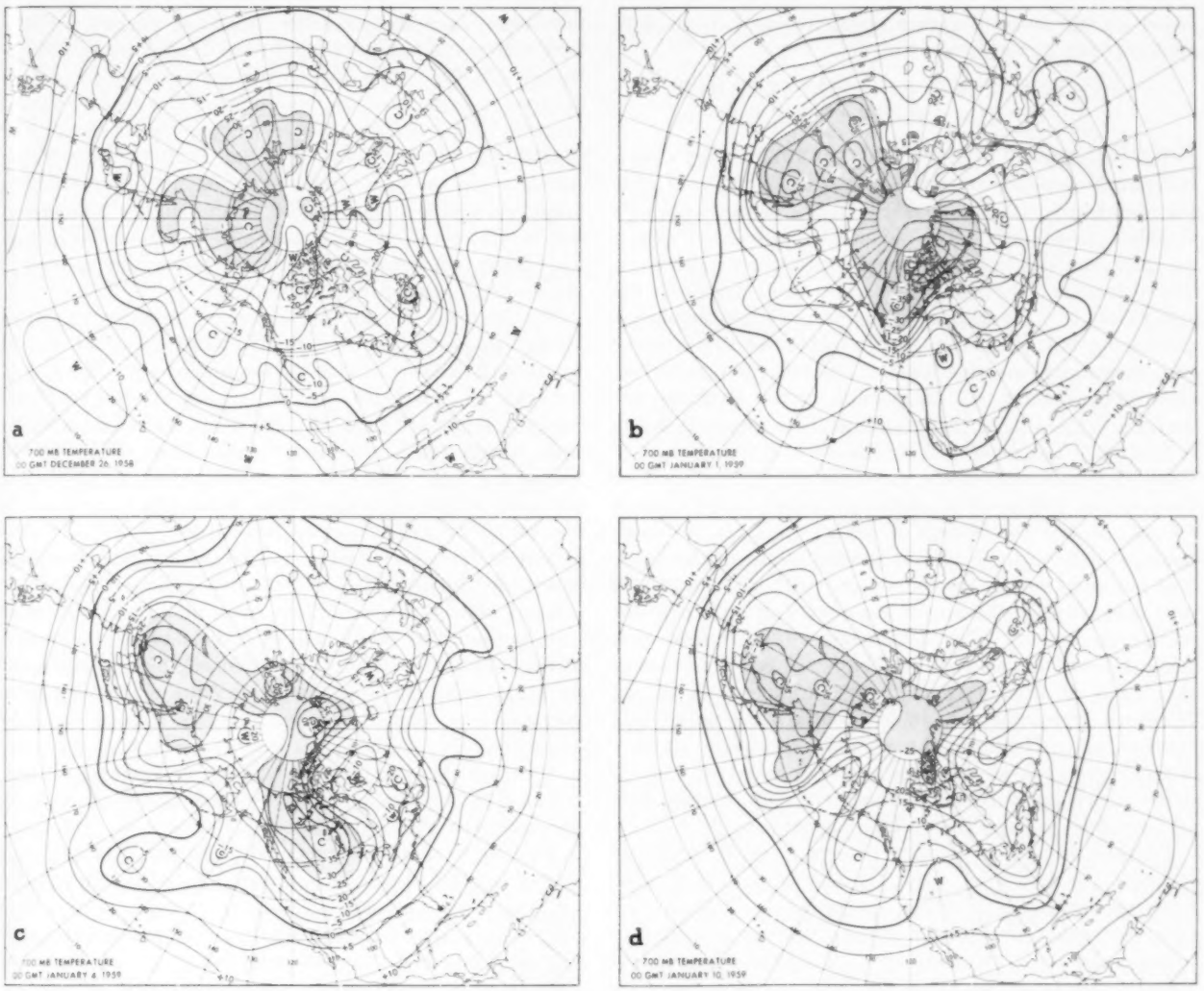

FIGURE 8.—700-mb. isotherms for (a) December 26, 1958, (b) January 1, 1959, (c) January 4, 1959, and (d) January 10, 1959. Interval is 5° C. with area below −25° C. stippled.

interest in figure 5. It is quite clear that the increase in available potential energy between December 27 and January 1 is explained very well by the sum of the generation and conversion terms, although the computed values do not rise to as high a maximum as the observed. The most serious discrepancy between computed and observed values occurred after January 3 during the period of strong decline in available potential energy. This period was represented by only a weak decline in the computed values, which suggests that the computed conversion term particularly after January 1, while indicating the correct trend, was too small. This is most likely attributable to the fact that the vertical velocities used in computing C are too small. Similar conclusions were were reached by Palmén [7], who suggested that the energy conversion computed by this method should be increased by about 40 percent or more. The weak values of the energy conversion probably also reflect the lack of inclusion of moist adiabatic processes in the vertical motion computations. Smagorinsky [11] has indicated that when these are included the upward motions are found to be much larger than those obtained by assuming dry adiabatic motions. Since moist adiabatic effects would be expected to be larger in warm air masses, the conversion from potential to kinetic energy would also be expected to be larger.

Despite these discrepancies, the encouraging fact is that such realistic estimates of the variations in available potential energy were obtained from the generation and conversion terms, particularly since these terms were com-

602484—61——2

puted on the basis of rather restrictive and incomplete models of the atmosphere.

5. REGIONAL AND SYNOPTIC FEATURES OF THE ENERGY CYCLE

The variations of total available potential energy shown in figure 2 were also examined from another point of view (as contrasted with the zonal and eddy components previously considered). The available potential energy was partitioned into four regional components representative of sectors 90° of longitude wide, stretching from the pole to 30° N. These four sectors were chosen somewhat arbitrarily, but roughly in such a fashion as to cover the two oceans and two continents. The longitudinal boundaries of each zone and the portion of the available potential energy contributed by each of these zones are shown in figure 6. The most striking feature of the variations of these regional components was that the major cycle of buildup and decline in available potential energy showed up only in the component of energy in Zone 1 (North America and vicinity). Thus the variations in the available potential energy for the whole Northern Hemisphere were basically dependent on the events in only this one particular region. The dominance of one area over another is not too unusual, of course, since differences in the types of flow patterns over various parts of the Northern Hemisphere have frequently been noted (cf., Namias [6]). However the virtually complete absence of an energy cycle at this time in three of the four zones is quite surprising, particularly since the total energy over all longitudes showed such a large variation.

Further insight into this energy cycle is attained through inspection of synoptic charts, which showed some interesting developments over North America and also over other portions of the hemisphere during this period. To illustrate these events, 500-mb. height and 700-mb. temperature fields for four selected days are presented in figures 7 and 8.

Confining our attention at first mainly to the North American area, we see that on December 26, when available potential energy was at a relatively low value, both over North America (Zone 1 in fig. 6) and over the hemisphere as a whole (fig. 2), there was a rather ill-defined circulation pattern (fig. 7a) with weak thermal gradients (fig. 8a). The high values of available potential energy which prevailed by January 1 were characterized by a deep cyclonic vortex over the Canadian Arctic (fig. 7b) with an associated extensive pool of cold air (fig. 8b). By January 4 a cyclonic vortex was located in western Canada, some 20° latitude south of the one in figure 7b, and the broad cyclonic flow to its south dominated most of the United States (fig. 7c). Accompanying these circulation developments, an extensive tongue of cold air covered western Canada and was also invading the United States (fig. 8c). This date marked the beginning of the overall drop in available potential energy over North America (fig. 6) and also the time of the maximum in eddy available potential energy for the hemisphere and of a very rapid drop in the zonal available energy (fig. 2). Thus the southward penetration of cold air over North America was one of the major instrumentalities in the breakdown of the strong supply of available potential energy that had built up over North America and the hemisphere as a whole. Undoubtedly a major part of its contribution to the energy breakdown was in its role in the conversion of zonal available into eddy potential energy and thence into eddy kinetic energy, all of which occurred at this time (fig. 3).

By the final day in this sequence, January 10, when available potential energy over North America (fig. 6) and the zonal available energy for the hemisphere (fig. 2) had dropped to relatively low values again, this cyclonic vortex was located near the Gulf of St. Lawrence with its main trough extending down the east coast of the United States (fig. 7d). The cold air associated with this system was now definitely weaker than before; in fact, most of the colder air (e.g., temperatures below −25° C.) over North America had disappeared (fig. 8d). This warming was undoubtedly reflective of two processes, one the descent of the cold air which contributed to conversion from potential to kinetic energy and the other the heating of the cold air mass as it proceeded off the east coast out over the Atlantic. Very large amounts of heating were computed by Wiin-Nielsen and Brown [15] on the days when the cold air moved off the coast (January 5–6) and it is evident that the strong heating of this cold air contributed to the strong negative values of computed eddy generation on these days (fig. 4).

Turning to other features of the flow and thermal fields it is of interest to note that a considerable amount of cold air was present over eastern Asia on each of the days shown in figure 8. This was very likely associated with the relatively high level of available potential energy in Zone 2 between December 26 and January 10 (fig. 6). Also, while a portion of this cold air was located farther west in Siberia (figs. 8a, 8b), the level of available energy in Zone 3 was fairly high, but as most of it moved east of Lake Baikal (figs. 8c, 8d) a noticeable drop in the energy in Zone 3 occurred. This more narrow longitudinal organization of the cold air near the Asian coast was accompanied by the sharpening of the Asian coastal trough subsequent to January 1 (fig. 7). Although the total energy for Zone 2 remained virtually the same, computations of longitudinal contributions to the northward heat transport (Winston [16]) showed that substantial heat transports were effected by the Asian coastal trough subsequent to January 1. This signified that increased transformations from zonal to eddy available energy occurred in this zone during the period of development of increased eddy energy in January (fig. 2). Thus, despite the lack of a cycle in the overall energy, it appears that eddy Zone 2 (eastern Asia to the east central Pacific) did contribute toward the increase or maintenance of eddy energy.

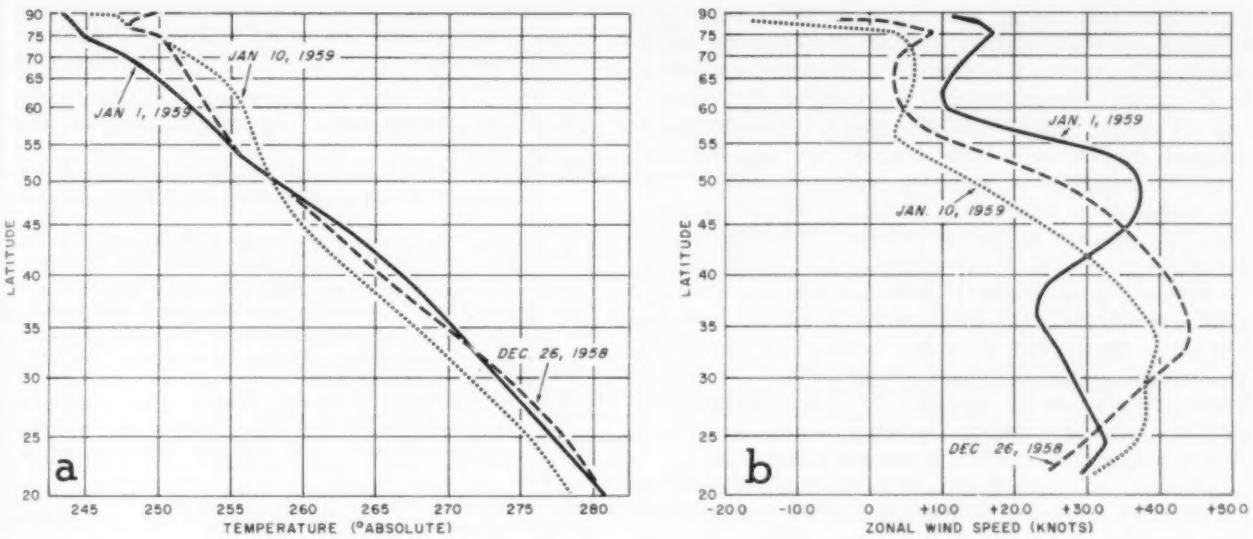

FIGURE 9.—Latitudinal profile of (a) temperature and (b) zonal wind speed for December 26, 1958 (dashed), January 1, 1959 (solid), and January 10, 1959 (dotted).

Finally it is worth noting that the overall hemispheric flow pattern at the end of the energy cycle (January 10, fig. 7d) consisted of four major, large-amplitude waves with large cyclone centers in middle latitudes. As indicated in figure 2, this was a day of minimum zonal available potential energy, but with fairly large eddy available potential energy. This pattern is to be contrasted with (1) the more heterogeneous (although mainly zonal) flow pattern of December 26 (fig. 7a), before zonal available energy started increasing; (2) the zonal flow at higher latitudes surmounting large-amplitude waves at lower latitudes of January 1 (fig. 7b), when zonal available energy was at its peak and eddy available energy was building up; and (3) the pattern of increasing wave amplitudes on January 4 (fig. 7c) when zonal available energy was dropping rapidly and eddy available energy was at a peak.

The latitudinal profiles of zonal wind and temperature for the whole hemisphere for three of these days summarize some of the differences at these different stages further (fig. 9). Note that at the beginning (December 26) and end (January 10) of the cycle there were rather broad zones of westerlies with maximum speeds located near latitude 35°. The flow at the end of the cycle was generally weaker than at the beginning except south of 30°. By way of contrast the westerlies on January 1 were concentrated in a narrow zone in middle latitudes (peak near 50°) with a definite minimum in the flow near 35° and a secondary maximum near 25°. These profiles are roughly characteristic of the zonal wind distributions at various phases of the index cycle (cf., Namias [5]), but it is worth pointing out that the profile for January 1 does not represent a case of extremely high zonal index (in latitudes 35°–55° N.).

The thermal profiles show rather definitely that the peak zonal available energy (January 1) was marked by rather low temperatures north of 55°, a cooling of up to 5° C. from December 26. This high-latitude cooling during a period when the westerlies were strengthening near latitudes 45°–55° was essentially the same type of development which Namias [5] described as containment of cold air in the polar cap during periods of strong westerly flow. By January 10, when the zonal available energy was at its lowest, temperatures were considerably higher north of 50°. The outflow of cold air into middle and lower latitudes in connection with the conversion of zonal available into eddy available energy is strikingly clear. Or putting it another way, the effects of the increased heat transports subsequent to January 1 were quite marked in the reduction of the northward thermal gradient.

6. SUMMARY

This observed cycle of available potential energy for the Northern Hemisphere possessed many characteristics which had been deduced from previous evaluations of some long-period averages of energy parameters and energy conversion terms. The buildup in zonal available energy to a high value and then its subsequent breakdown with the accompanying conversion into eddy available potential and eddy kinetic energy have all been clearly demonstrated. There was, however, little if any reaction to this potential energy cycle in the zonal component of the kinetic energy. The fact that estimates of energy

conversion and energy generation obtained from admittedly crude atmospheric models showed rather good correspondence with the observed short-period variations in the various energy parameters was especially interesting. The partition of available potential energy on a regional (longitudinal) basis showed that this clear-cut cycle in hemispheric available potential energy was dominated to a remarkable extent by events in only about one-quarter of the hemisphere. Investigations of the synoptic aspects of this energy cycle showed that this dominance by one region (North America and vicinity) was associated with the development of cold air over the Canadian Arctic and then the subsequent southward penetration of this large mass of cold air into the United States and out over the Atlantic. Obviously this signifies that studies of atmospheric energetics require close attention to geographical and synoptic-scale influences.

Although this cycle displayed many characteristics of the idealized energy cycle, it should not be concluded that this observed cycle is truly typical of most large-scale energy cycles. Cursory inspection of an accumulating record of available potential energy over more than a year indeed reveals that large-scale variations of the zonal and eddy components of the potential energy occur in a variety of ways. Study of the nature of other large-scale changes in the energy is contemplated, particularly with respect to probable differences in the manner in which the potential energy is generated.

ACKNOWLEDGMENTS

The authors are especially indebted to Dr. A. Wiin-Nielsen for several fruitful discussions concerning the energy problem and also for his generosity in making his data on the conversion and generation of energy readily available to us. Thanks are also due to several members of the Meteorological Satellite Laboratory for assisting in the various computational phases of the work.

REFERENCES

1. C. E. Jensen, "Energy Transformation and Vertical Flux Processes Over the Northern Hemisphere," *Journal of Geophysical Research*, vol. 66, No. 4, April 1961, pp. 1145–1156.
2. H. L. Kuo, "Application of Energy Integrals to Thermally Driven Motions," *Beiträge zur Physik der Atmosphäre*, vol. 31, No. 3/4, 1959, pp. 189–199.
3. E. N. Lorenz, "The Basis for a Theory of the General Circulation," Section IV of "Studies of the Atmospheric General Circulation," ed. by V. P. Starr, *Final Report* Part I, General Circulation Project, Contract AF 19(122)–153, Department of Meteorology, Massachusetts Institute of Technology, May 1954, pp. 522–534.
4. E. N. Lorenz, "Available Potential Energy and the Maintenance of the General Circulation," *Tellus*, vol. 7, No. 2, May 1955, pp. 157–167.
5. J. Namias, "The Index Cycle and Its Role in the General Circulation," *Journal of Meteorology*, vol. 7, No. 2, Apr. 1950, pp. 130–139.
6. J. Namias, "Thirty-Day Forecasting: A Review of a Ten Year Experiment," *Meteorological Monographs*, vol. 2, No. 6, American Meteorological Society, Boston, 1953, 83 pp.
7. E. Palmén, "On Generation and Frictional Dissipation of Kinetic Energy in the Atmosphere," *Societas Scientiarum Fennica, Commentationes Physico-Mathematicae* vol. XXIV, No. 11, 1960, 15 pp.
8. N. A. Phillips, "The General Circulation of the Atmosphere: A Numerical Experiment," *Quarterly Journal of the Royal Meteorological Society*, vol. 82, No. 352, Apr. 1956, pp. 123–164.
9. C. G. Rossby and H. C. Willett, "The Circulation of the Upper Troposphere and Lower Stratosphere, "*Science*, vol. 108, Dec. 10, 1948, pp. 643–652.
10. B. Saltzman and A. Fleisher, "The Modes of Release of Available Potential Energy in the Atmosphere," *Journal of Geophysical Research*, vol. 65, No. 4, Apr. 1960, pp. 1215–1222.
11. J. Smagorinsky, "On the Inclusion of Moist Adiabatic Processes in Numerical Prediction Models," In *Symposium über Numerische Wettervorhersage in Frankfort a.M. vom 23. bis 28. Mai 1956. Berichte des Deutschen Wetterdienstes*, Nr. 38, (Band 5), 1956.
12. J. Smagorinsky, "General Circulation Experiments with the Primitive Equations as a Function of the Parameters," (To be published) Abstract in *Programme of Meetings, International Association of Meteorology and Atmospheric Physics*, XII General Assembly, I.U.G.G., Helsinki, July 26–Aug. 6, 1960. pp. 22–23.
13. R. M. White and B. Saltzman, "On Conversions Between Potential and Kinetic Energy in the Atmosphere," *Tellus*, vol. 8, No. 3, Aug. 1956, pp. 357–363.
14. A. Wiin-Nielsen, "A Study of Energy Conversion and Meridional Circulation for the Large-Scale Motion in the Atmosphere," *Monthly Weather Review*, vol. 87, No. 9, Sept. 1959, pp. 319–332.
15. A. Wiin-Nielsen and J. A. Brown, Jr., "On the Distribution of Heat Sources and Sinks in the Lower Troposphere and the Corresponding Generation of Potential Energy," (To be published in the *Proceedings of the International Symposium on Numerical Weather Prediction, Tokyo, Japan, Nov. 7–13, 1960.*)
16. J. S. Winston, "Preliminary Studies of Atmospheric Energy Parameters," *Meteorological Satellite Laboratory Report to the National Aeronautics and Space Administration, No. 3*, U.S. Weather Bureau, January 1961, 30 pp.

LOW-LEVEL INVERSION FREQUENCY IN THE CONTIGUOUS UNITED STATES*

CHARLES R. HOSLER

U.S. Weather Bureau, Washington, D.C.

[Manuscript received May 3, 1961; revised June 19, 1961]

ABSTRACT

A tabulation of percent frequencies of inversion and/or isothermal conditions, based below 500 feet above station elevation, for Weather Bureau radiosonde stations in the contiguous United States for four observation times, provides a sampling of daytime and nighttime stability conditions for all time zones. These data are analyzed with respect to nighttime surface wind speed and cloud cover. Radiosonde data are compared to vertical temperature gradient data obtained from meteorologically instrumented towers and valley-ridge stations. Finally, an attempt is made to delineate, geographically and climatologically, the percent frequency of low-level stability for the entire country.

1. INTRODUCTION

Air pollution surveys of entire industrial regions and metropolitan areas are in demand by public and private agencies for purposes of evaluating levels of air contamination, air zoning regulations, and identification of obnoxious sources. In recent years meteorology has assumed an important role in the atomic energy industry for engineering and operational applications common to the industry generally, but in particular because of its application to the study of dispersion of airborne radioactivity by the atmosphere. Weather may play an important role in either conventional or nuclear industries and the proper appreciation of certain meteorological factors is paramount for an intelligent analysis and evaluation of air pollution phenomena.

In essence the dilution efficiency of the atmosphere depends on the wind and temperature gradients, both of which vary vertically, horizontally, and with time. Since the general spatial problems of slow atmospheric dispersion which affect large areas unquestionably arise at times when a stable stratified layer of air exists near the surface, a knowledge of the frequency of low-level stability for geographical and/or climatological areas will be helpful for assessing the potential for air pollution inherent to a given region. This study involves the compilation of inversion frequencies and the analysis of related meteorological parameters in an attempt to delineate, geographically and climatologically, the percent frequency of low-level stability for the contiguous United States.

2. INVERSION DATA

The initial step for obtaining statistics of inversion occurrence was to select upper air data that most nearly corresponds to daytime and nighttime periods. Table 1 gives the observation times for radiosonde soundings from which vertical temperature gradient data could be obtained. It was decided that a 2-year sampling of both 0300–1500 GMT and 0000–1200 GMT observation periods would be sufficient to give representative frequencies of daytime and nighttime inversion occurrence for each time zone. Accordingly, the National Weather Records Center at Asheville, N.C., tabulated for selected stations a percent frequency of inversions and/or isothermal layers based at or below 500 feet above the station elevation. This level was arbitrarily selected to define a minimum vertical depth of air, and it also permitted convenient tabulation of data from radiosonde sounding plots. These frequencies, given to the nearest whole percent, are based on all observations actually taken for a given time and season (Winter; December, January, February; Spring: March, April, May; etc.). These data are listed in the Appendix.

3. PROCEDURE

Rather than knowing only a percent frequency of inversions for any given observation time, it is desirable to have an estimate of inversion occurrence as a percent of total time sampled (seasonal or annual). Continuous

TABLE 1.—*Radiosonde observation times*

Date	Green-wich	Local standard time			
		Eastern	Central	Mountain	Pacific
Prior to Apr. 1, 1948	2300	1800	1700	1600	1500
	1100	0600	0500	0400	0300
April 1948–June 1957	0300	2200	2100	2000	1900
	1500	1000	0900	0800	0700
June 1957–present	0000	1900	1800	1700	1600
	1200	0700	0600	0500	0400

*Support for this study was jointly provided by the U.S. Atomic Energy Commission and the U.S. Public Health Service.

TABLE 2.—*Approximate number of nighttime hours (in 24-hour day)*

	Winter	Spring	Summer	Fall
North	15	11	9	13
Central	14	11	10	13
South	13	12	11	12

recording of vertical temperature gradient such as that obtained from towers gives such statistics, but the radiosonde data available do not permit such a tabulation directly. Therefore, to prepare frequencies of low-level stability as a percent of total seasonal hours from radiosonde data, the following hypothesis was used for analyzing data from *inland* stations: The entire nocturnal period was considered stable if an inversion was observed at any time during the night, and the maximum percent frequency of inversions for any one observation time within a nocturnal period was assumed applicable to the entire nighttime period; and, conversely, the entire daytime period was assumed to be unstable, and low values of inversion frequencies occurring at observation times during the daytime heating period were not considered in computation of inversion frequency as a percent of total hours.

A review of table 1 suggests that for the most part daytime observations are made either shortly after sunrise (transition period of stability to instability) or shortly before sunset (instability to stability); consequently, the "daytime" observations are not truly representative of the unstable solar heating period. In general, it is felt that ignoring the low frequency values for daytime observations compensated for the apparent overestimation arrived at from attributing the maximum frequency value to an entire nocturnal period.

A rough determination of length of nighttime periods was made from the Smithsonian Meteorological Tables [9] and resulted in three station categories: (a) the northern tier of States; (b) an area roughly between 30° and 40° N. latitude, comprising the largest number of stations; and (c) the southern regions along the Gulf of Mexico. The number of nighttime hours in each category by seasons is shown in table 2.

TABLE 3.—*Example of inversion percent frequency determination for inland stations*

Bismarck, N. Dak.					
	Maximum percent value (nighttime)	Observation time (LST)	Nighttime period (hours)	Fraction of 24-hour day	Inversion frequency (percent of total hours)
	A			*B*	*A*×*B*
Winter	67	0600	15	$\frac{15}{24}$=.625	67×.625=42
Spring	61	0600	11	$\frac{11}{24}$=.458	61×.458=28
Summer	77	2100 and 0600	9	$\frac{9}{24}$=.375	77×.375=29
Fall	69	2100	13	$\frac{13}{24}$=.542	69×.542=37

The method for computing a percent frequency of low-level stability for inland stations, defined as a percent of total seasonal (annual) hours, is exemplified in table 3, using radiosonde data from Bismarck, N. Dak. The results from this technique were compared to continuously recorded vertical temperature gradient data from towers (discussed later), and appear to be quite adequate for an overall climatological analysis.

In analyzing and computing the inversion frequency data, it became apparent that there was a notable exception to this technique. Inversion frequencies obtained from coastal stations reflect marine influences; that is, in coastal areas low-level stability may be either inhibited or enhanced by advection, in contrast to inland areas that, for the most part, exhibit radiation-type inversions. The coastal regions could be divided into (a) the Atlantic coastal sections of the Southeastern States and the entire coastal region of the Gulf of Mexico, where relatively warm water exists offshore, and (b) coastal sections of New England and the Pacific States where ocean waters are relatively cold. The effects of air-water-land temperature differential and associated land-sea breeze regimes on low-level stability are apparently reflected in the inversion frequency values of many coastal stations that are affected by a frequent flow of air from over the ocean. In general, for coastal areas along the South-

TABLE 4.—*Comparison of coastal and inland inversion frequencies (percent)*

Station	Winter				Spring				Summer				Fall			
Pacific Coast	*LST*	*16*	*19*	*04*	*07*	*16*	*19*	*04*	*07*	*16*	*19*	*04*	*07*	*16*	*19*	*04*	*07*
Oakland, Calif. (coastal)		10	66	77	88	14	23	45	35	34	29	21	13	15	58	62	62
Medford, Oreg. (inland)		16	75	65	70	2	35	74	40	0	13	80	32	6	63	76	73
Tatoosh Island, Wash. (coastal)		17	22	14	15	11	21	18	15	19	31	37	20	29	35	33	38
Seattle, Wash. (inland)		24	13	63	31	0	6	54	30	1	3	57	19	9	19	69	32
Gulf of Mexico	*LST*	*18*	*21*	*06*	*09*	*18*	*21*	*06*	*09*	*18*	*21*	*06*	*09*	*18*	*21*	*06*	*09*
Burrwood, La. (coastal)		46	63	69	36	18	57	51	11	4	26	11	1	13	38	33	3
Lake Charles, La. (inland)		12	61	58	30	3	53	58	5	5	62	71	3	9	75	61	12
Southeastern Atlantic	*LST*	*19*	*22*	*07*	*10*	*19*	*22*	*07*	*10*	*19*	*22*	*07*	*10*	*19*	*22*	*07*	*10*
Key West, Fla. (marine)		1	2	6	26	1	0	1	4	0	0	1	0	1	0	0	1
Miami, Fla. (coastal)		29	39	60	6	10	27	47	2	21	27	65	2	19	41	75	3
Jacksonville, Fla. (inland)		44	69	59	27	10	53	61	4	11	38	56	1	37	51	76	12
Northeastern and Middle Atlantic	*LST*	*19*	*22*	*07*	*10*	*19*	*22*	*07*	*10*	*19*	*22*	*07*	*10*	*19*	*22*	*07*	*10*
Hempstead, L.I., N.Y. (coastal)		18	21	24	7	36	36	32	3	22	45	21	1	24	48	30	1
Lakehurst, N.J. (inland)			41		17		47		2		51		2		59		12
Washington, D.C. (inland)		30	44	48	22	12	42	51	5	5	47	57	2	34	56	59	8

TABLE 5.—*Example of inversion percent frequency determination for coastal stations*

	Representative nighttime value (percent)	LST observation	Night fraction of 24-hour day	Representative daytime value (percent)	LST observation	Day fraction of 24-hour day	Inversion percent frequency for total hours
Miami, Fla.	A		A_1	B		B_1	AA_1+BB_1
Winter	39	2200	0.542	6	1000	0.458	21+3=24
Spring	27	2200	.500	2	1000	.500	14+1=15
Summer	27	2200	.458	2	1000	.542	12+1=13
Fall	41	2200	.500	3	1000	.500	20.5+1.5=22
Oakland, Calif.							
Winter	77	0400	.582	10	1600	.417	45+4=49
Spring	45	0400	.458	14	1600	.542	21+8=29
Summer	21	0400	.417	34	1600	.583	9+20=29
Fall	62	0400	.542	15	1600	.458	34+7=41

eastern States and Gulf of Mexico, a flow from over warm waters tends to inhibit inversion formation at night, while daytime sea breezes exhibit neutral stability. The net result is lower inversion frequency for coastal areas than for inland areas in these regions. The cold waters off the Pacific coast and northeastern Atlantic coast produce cool sea breezes which enhance low-level stability, resulting in higher frequencies of inversions, particularly during daytime hours, for these areas. Examples of these coastal regimes are given in table 4, where a list of inversion frequencies for coastal and nearby inland stations can be compared.

A review of these comparisons suggests that locations only a few miles inland from the coast exhibit a continental-type frequency of low-level stability (e.g., Lake Charles and Jacksonville). Consequently, in analyzing the radiosonde data for stations in coastal areas, it was necessary subjectively to classify by season each station as "inland" or "coastal" according to the marine effects reflected by the frequency data, as well as to consider station proximity to the water and prevailing wind directions. For stations designated coastal, both daytime and nighttime inversion frequency values were considered for computing an inversion frequency as a percent of total hours, instead of neglecting daytime values, as was done for inland stations. An example of attributing both a representative daytime and nighttime percent frequency value to the respective diurnal periods for computing inversion frequencies is shown in table 5 for the coastal cities of Oakland and Miami.

Isopleths of inversion frequency, expressed as a percent of total hours, for the contiguous United States are shown in figure 1 A–E.

Isopleths of the maximum inversion frequency value reported at any of the four observation times are shown in figure 2 A–E. Conservatively, these values show the percent frequency of nights (or days) that had *at least one hour* of inversion. However, it is reasonable to interpret these statistics to show a percent frequency of nights (or days, for some coastal areas) having several hours of inversions, since an inversion reported at any one hourly observation during the night (or day) implies that such stability will continue (or has continued) for more than one hour if it already exists. This has been shown by analysis of cumulative frequencies of inversions obtained from meteorological tower data [1, 4, 8, 10] at inland sites. Such data for four sites are shown in figure 3. These data are plotted on log-probability scales to enhance the "breaks" in the curves (abrupt changes in probability) which reflect the length of stable nocturnal periods. These analyses of tower data also support the concept used to determine inversion frequency for inland stations as a percent of total time. That is, a percent frequency of inversions at night for any one hour gives a value that is approximately representative for any hour during the nocturnal stable period.

The inherent shortcomings involved in this type of analysis are obvious. The subjectivity in the analytical methods, differences of topography, geography, observation time (relative to the diurnal cycle), and sampling periods are sources of possible error. However, a more exact quantitative assessment of low-level inversion frequency is not easily obtained from existing radiosonde data. It is hoped that this study may provide a means for comparing one section of the country to another, relative to inversion frequency, as well as furnishing information helpful for developing a diffusion climatology of the United States.

4. CLOUD COVER AND LOW WIND SPEED

Meteorologists, from experience, would expect clear skies and light surfaces winds at night to favor the formation of nocturnal radiation-type inversions over land. Cloud cover and wind speed data for available stations, tabulated for a 5-year period in *Summary of Hourly Observations* by the U.S. Weather Bureau were analyzed with respect to the inversion frequency data. These statistics are tabulated in the Appendix.

The inherent subjectivity involved in nighttime observations of cloud cover (e.g., thin cirrus), together with different exposures and elevations of anemometry, restricts any quantitative analysis. However, a statistical study was made of the relationship of nighttime cloud cover and wind speed to inversion frequency, resulting in poor correlation for all seasons. For example, figure 4 indicates a poor relationship, although a trend is evident, of observed maximum inversion frequency to occurrence of nighttime winds (≤ 7 m.p.h.) and nighttime cloud cover

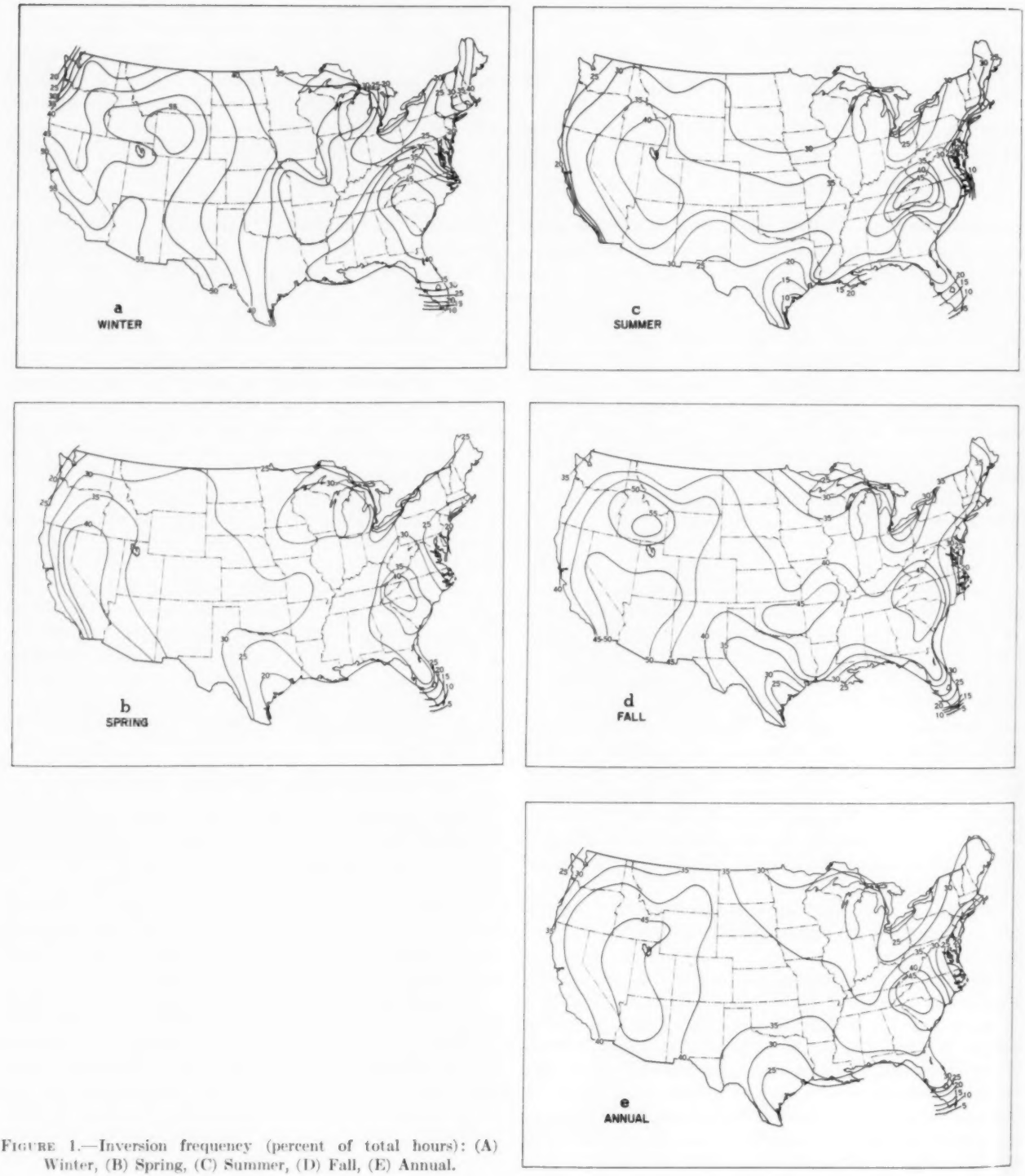

FIGURE 1.—Inversion frequency (percent of total hours): (A) Winter, (B) Spring, (C) Summer, (D) Fall, (E) Annual.

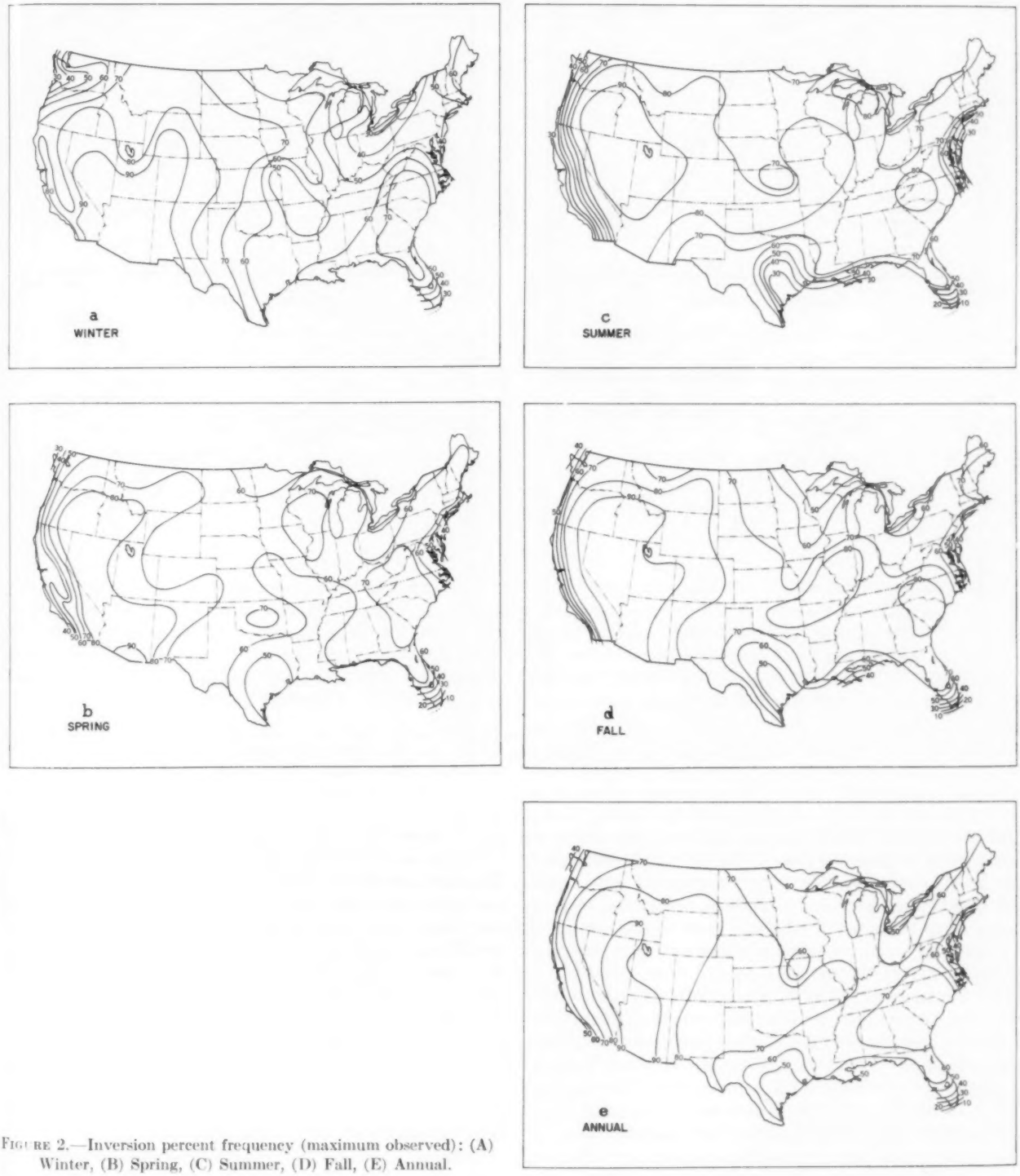

FIGURE 2.—Inversion percent frequency (maximum observed): (A) Winter, (B) Spring, (C) Summer, (D) Fall, (E) Annual.

602484—61——3

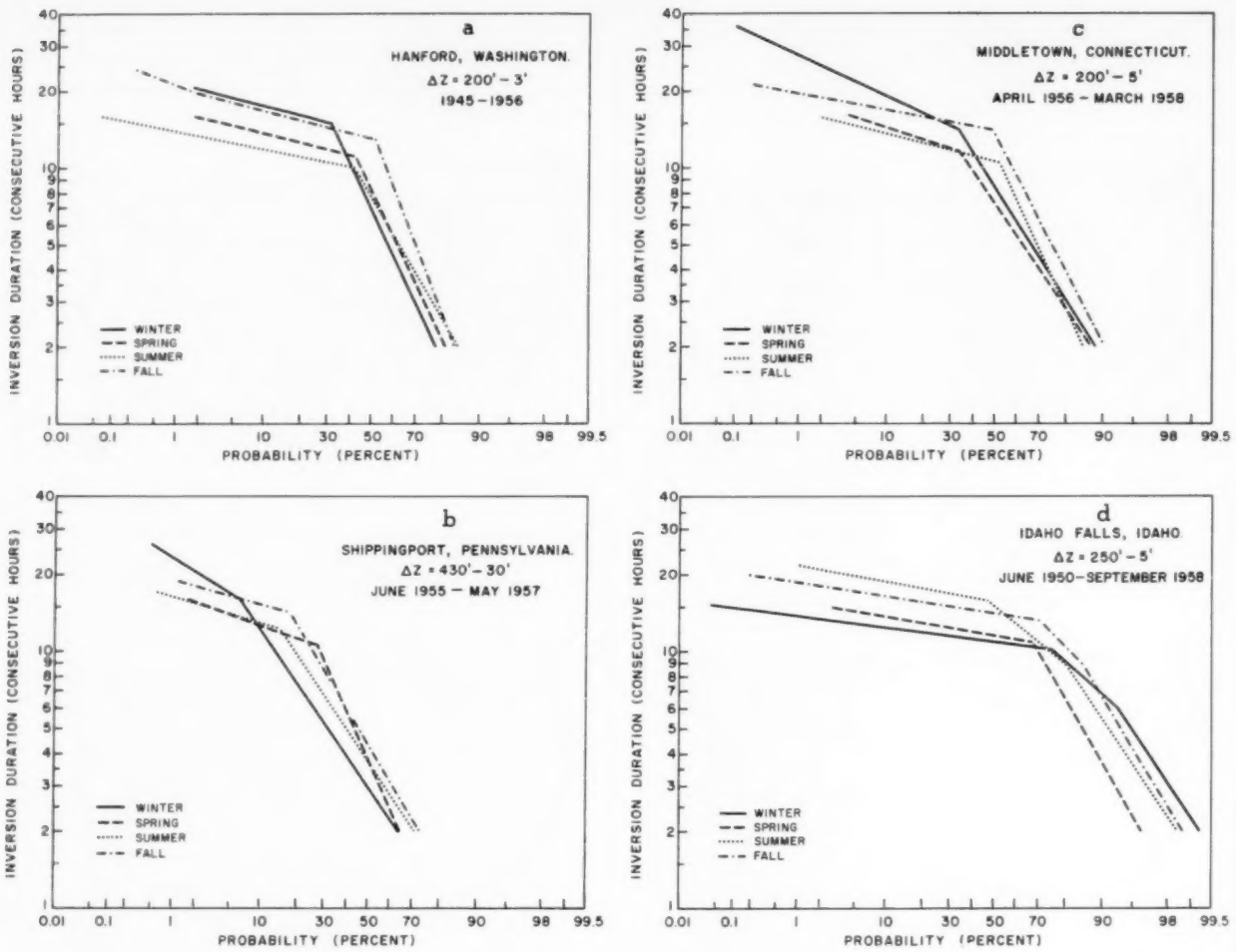

FIGURE 3.—Cumulative percent frequency of inversions from meteorological towers and valley-ridge stations: (A) Hanford, Wash., (B) Shippingport, Pa., (C) Middletown, Conn., and (D) Idaho Falls, Idaho.

($\leq 3/10$) respectively, for winter. Although this indicates that precise frequency values of low-level inversions may not be obtained for a specific location from wind speed and cloud cover data alone, isopleths of percent frequencies of cloud cover and wind speed, shown in figures 5 and 6 respectively, indicate that the general areas having a higher frequency of inversions are also characterized by a higher frequency of relatively clear nights with light winds, and vice versa. This relationship can be further illustrated by graphic addition of the cloud cover and light wind frequency values. The sums of these percent frequencies were divided by 2 to give conventional values within the range of 0–100. These isopleths of nighttime (cloud cover+wind speed)/2 are shown in figure 7.

5. CURRENT OBSERVATION DATA

Since two of the observation times (0300 and 1500 GMT) used in computing inversion frequency are no longer in use, it is desirable to compare the computed frequency values to those obtained from a current observation time. The 1200 GMT observation value was chosen for comparison, since this is the current local observation time in all four time zones that most nearly represents nighttime conditions. Such a comparison serves two purposes: (1) if percent frequencies from four different local observation times compare favorably to the computed frequency, this supports the hypothesis used for computing the percent values; and (2) additional 1200 GMT inversion frequencies, obtained either from towers or other upper air facilities, may be analyzed for relatively short sampling periods (months) to provide estimates of low-level inversion frequency for a given inland site.

However, since the 1200 GMT observation value was used more often than any other value to compute an inversion frequency, expressed as a percent of total time (i.e., of the available radiosonde data the maximum

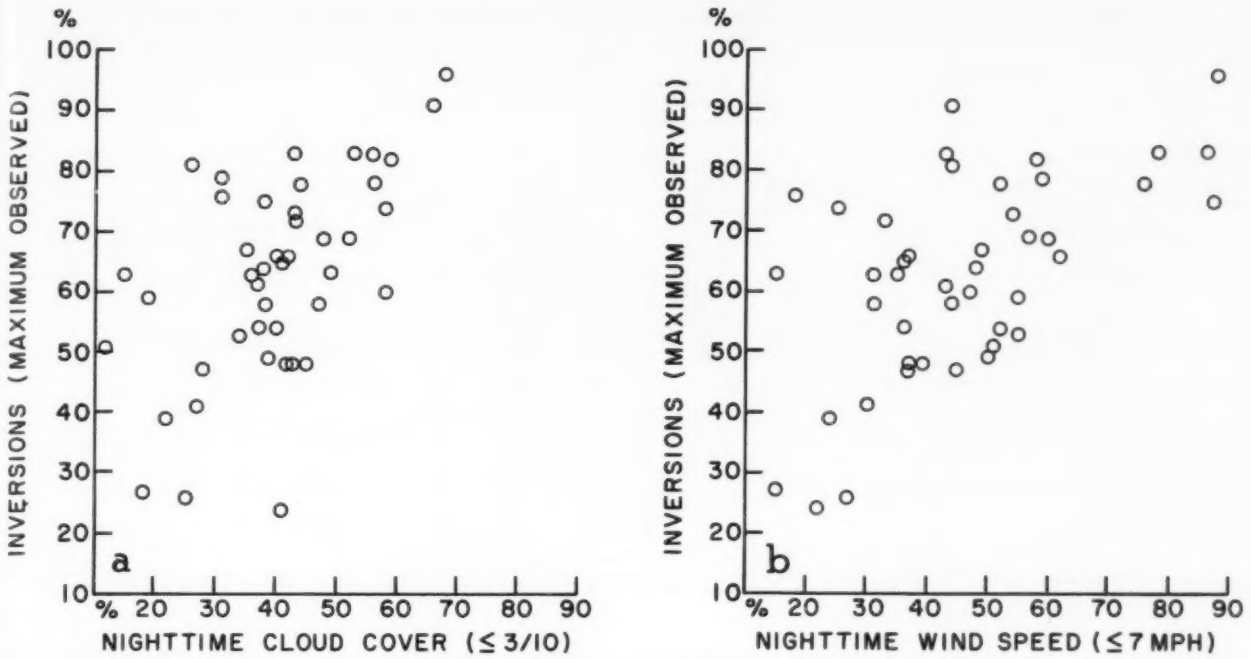

FIGURE 4.—Relationship of maximum observed nighttime inversion percent frequency to (A) nighttime cloud cover ≤3/10 and (B) wind speed ≤7 m.p.h. Occurrence for winter.

percent value was observed most often at 1200 GMT, in any season, for at least 60 percent of the stations), it was necessary to analyze the unrelated data to justify the selection of the 1200 GMT observation value as being representative of the nocturnal period, for all time zones. This was done for all inland stations by determining the variation of computed frequency, based on the 1200 GMT value, from the computed frequency based on the maximum observed value, for all cases when the maximum value was at an observation time other than 1200 GMT. This comparison showed that for any season the computed frequency determined from the 1200 GMT value, when averaged for all inland stations, differed by less than 3.4 percent from the computed frequency value determined from maximum frequencies at 0000, 0300, or 1500 GMT. On the other hand, since the fraction (nighttime hours)/24, attributed to the length of the nocturnal period is factored into the computed frequency value, it can be estimated that the 1200 GMT frequency value averages about 7 percent less than the maximum value, when the maximum frequency occurs at 0000, 0300, or 1500 GMT. This indicates that of the available radiosonde data analyzed, the 1200 GMT percent value is the most representative of the nocturnal period for all four time zones. Also, it was of interest to note that the 0300 GMT value yields a fairly close approximation of nighttime inversion frequency for fall and winter seasons; however, the 1500 GMT value appears to be unrepresentative of the nighttime period, except for western sections of the country in winter.

The next step was to relate empirically the computed inversion frequency to the currently observed 1200 GMT percent value. This is done in figure 8, which compares the computed percent value on the ordinate (Y) to the 1200 GMT percent value on the abscissa (X). Each point represents a station, and a least square fit provides the regression line. Coastal stations are not included in the regression analysis, but they are designated in the graphs. Their position relative to the regression line may provide an index to continentality. Since the ordinate is determined from the abscissa value for about 60 percent of the cases, no correlations were attempted. However, despite the related data inherent in the statistics, good relevance is indicated. In general, the relationships are sufficiently good to permit use of the 1200 GMT radiosonde data, for inland stations in all time zones, for determining inversion frequencies as a percent of total time.

6. TOWER DATA

Temperatures obtained from meteorological towers and valley-ridge field stations and an instrumented TV tower [1, 2, 4, 6, 7, 8, 10, 12] provide inversion frequency statistics that can be compared to inversion frequencies computed from nearby radiosonde stations. For all nine such stations temperature gradient data are continuously recorded and thereby readily provide frequencies in the form of percent of total hours. These statistics, which can be directly compared to the computed frequencies, are shown in table 6.

TABLE 6.—*Comparison of computed inversion frequency to tower and valley-ridge vertical temperature gradient data*

Station groups	Percent of total hours					Period of record	Vertical height (ft.)
	Winter	Spring	Summer	Fall	Annual		
Las Vegas, Nev. (radiosonde)	54	39	37	50	45	June 55–May 59	
Yucca Flat, Nev. (valley-ridge)	53	32	38	50	43	January 59–March 60	$\Delta Z = 500$
Toledo, Ohio (radiosonde)	23	22	30	36	28	1946–1950	
Enrico Fermi, Mich. (tower)	23	23	34	30	28	December 56–November 59	$\Delta Z = 100$–25
Mount Clemens, Mich. (radiosonde)	15	21	26	30	23	February 48–December 50	
Detroit, Mich. (TV tower)	23	23	36	34	30	December 56–November 59	$\Delta Z = 300$–20
Albany, N.Y. (radiosonde)	27	29	31	36	31	September 53–August 55	
Middletown, Conn. (tower)	33	23	27	32	29	June 57–May 59	
						April 56–March 59	$\Delta Z = 200$–5
Nashville, Tenn. (radiosonde)	31	27	32	40	33	June 55–May 59	
Greensboro, N.C. (radiosonde)	49	36	36	42	41	June 55–May 59	
Oak Ridge, Tenn. (towers)[1] (valley-ridge)	41	42	46	49	45	1955–1958	
Boise, Idaho (radiosonde)	51	38	36	50	44	June 55–May 59	
Idaho Falls, Idaho (tower)	52	37	45	57	48	January 56–June 58	$\Delta Z = 250$–5
Salem-Portland, Oreg. (radiosonde)	32	29	28	38	32	June 56–May 59	
Spokane, Wash. (radiosonde)	37	29	31	40	34	June 56–May 59	
Hanford, Wash. (tower)	45	32	27	42	37	1955–1958	$\Delta Z = 400$–50
Omaha, Nebr. (radiosonde)	42	27	33	38	35	June 56–May 59	
Sioux Falls, S. Dak. (valley-ridge) (Pathfinder Site)	37	50	47	37	43	May 58–April 60	$\Delta Z = 154$
Pittsburgh, Pa. (radiosonde)	24	31	27	34	29	June 56–May 59	
Shippingport, Pa. (valley-ridge)	14	19	23	28	21	April 55–May 57	$\Delta Z = 400$

[1] Average of Tower Shielding Facility (TSF), Melton Valley (MV), and Oak Ridge National Laboratory site (X–10 Sta.): For TSF, $\Delta Z = 300$ ft.; above a wooded ridge top, 500 ft. from valley floor; for MV, $\Delta Z = 60$ ft.; 5 ft. from the floor of a wooded valley; for X–10, $\Delta Z = 135$ ft.; 5 ft. atop a small ridge overlooking an industrial type valley, 90 ft. below.

While most of the towers give vertical temperature gradients within a height interval of less than 500 feet, this is not a serious obstacle for comparing the two sets of data, because nearly all nocturnal inversions (based below 500 feet above the surface) reported by inland radiosonde stations are based below 100 feet above the ground. In fact, most are surface based. The inherent discrepancies involved in differences of (a) periods and lengths of record, (b) geography, and (c) instrumentation are obvious; consequently, it is surprising to find that the frequency values compare so closely. In general, the tower data suggest that the methods of computation for determining inversion frequency from radiosonde data are sufficiently reliable for general climatological analysis.

7. OTHER CONSIDERATIONS

Since most of the Weather Bureau radiosonde stations are located at airports which are at the outskirts of cities, the inversion frequencies for the most part are representative of semi-rural or suburban areas. Consequently, one would expect higher frequencies of nocturnal inversions in the open country; but, lower frequencies for central city areas would be expected because of the mechanical turbulence and heat effects imposed by large metropolitan areas [3]. In the Rocky Mountain and Appalachian regions most of the weather stations are located in valleys; consequently, for these areas the percent values reflect inversion occurrence for elevations lower than the average for the region. Less frequent inversion occurrence would be expected on mountain slopes and tops.

The climatic-synoptic aspects of the west coast, particularly the coastal areas of California and southern Oregon, deserve special attention. The maritime influences and a semipermanent high pressure pattern produce dominating effects. The large-scale subsidence of air at altitudes above the ocean-cooled surface layer results in a stable layer which is semipermanent over the California and Oregon coasts during spring, summer, and fall months. The subsidence inversion acts as a "lid", limiting the vertical motions originating in the marine air below; consequently, it is an important contributor to the gross accumulation of air pollution since the inversion base limits the vertical volume of air in which pollutants may accumulate.

Because the subsidence inversion is often based between 500 and 2000 feet above ground along the coast, it is apparent that the data used in this study (inversion based $\leq$ 500 feet above ground) yield very conservative frequency values for the west coast area, relative to any assessment of atmospheric pollution potential for that area. Unlike studies for other areas of the country, a study of the diffusion climatology of the coastal areas of Oregon and California must consider a frequent and persistent occurrence of subsidence inversions based below 2000 feet above the ground, as well as radiation-type inversions based below 500 feet. It is important to note that the present study reflects for the most part only surface-based radiation-type inversions or low-level stability resulting from cool sea breezes. For further details of west coast inversions, the reader is referred to studies by Stanford Research Institute [11] and J. G. Edinger [5].

8. CLIMATIC-GEOGRAPHIC DELINEATION

A review of the distribution of inversion frequency over the country suggests a general delineation into regions according to climatological and geographical factors, and this classification is shown in figure 9. The factors relat-

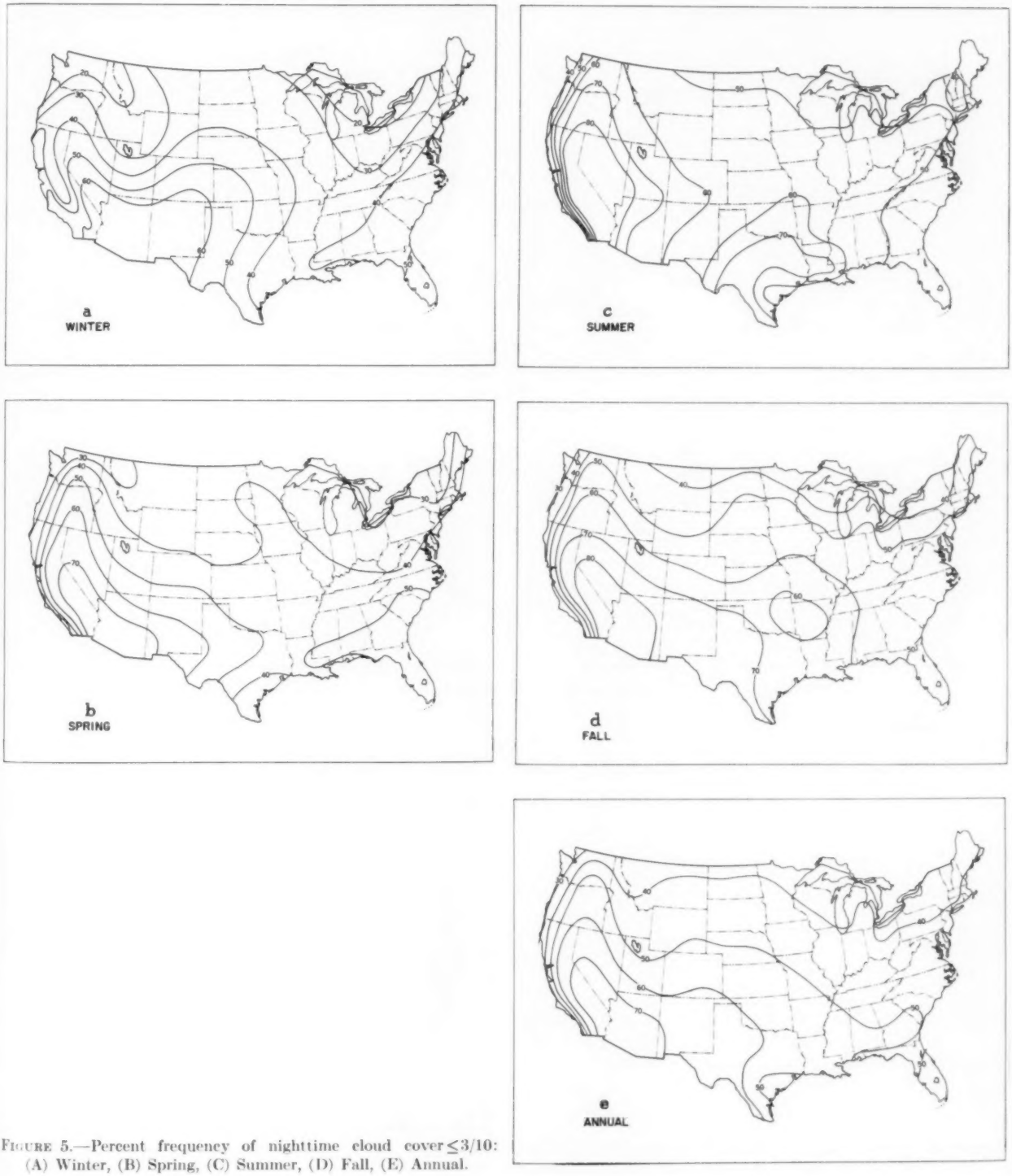

FIGURE 5.—Percent frequency of nighttime cloud cover ≤3/10: (A) Winter, (B) Spring, (C) Summer, (D) Fall, (E) Annual.

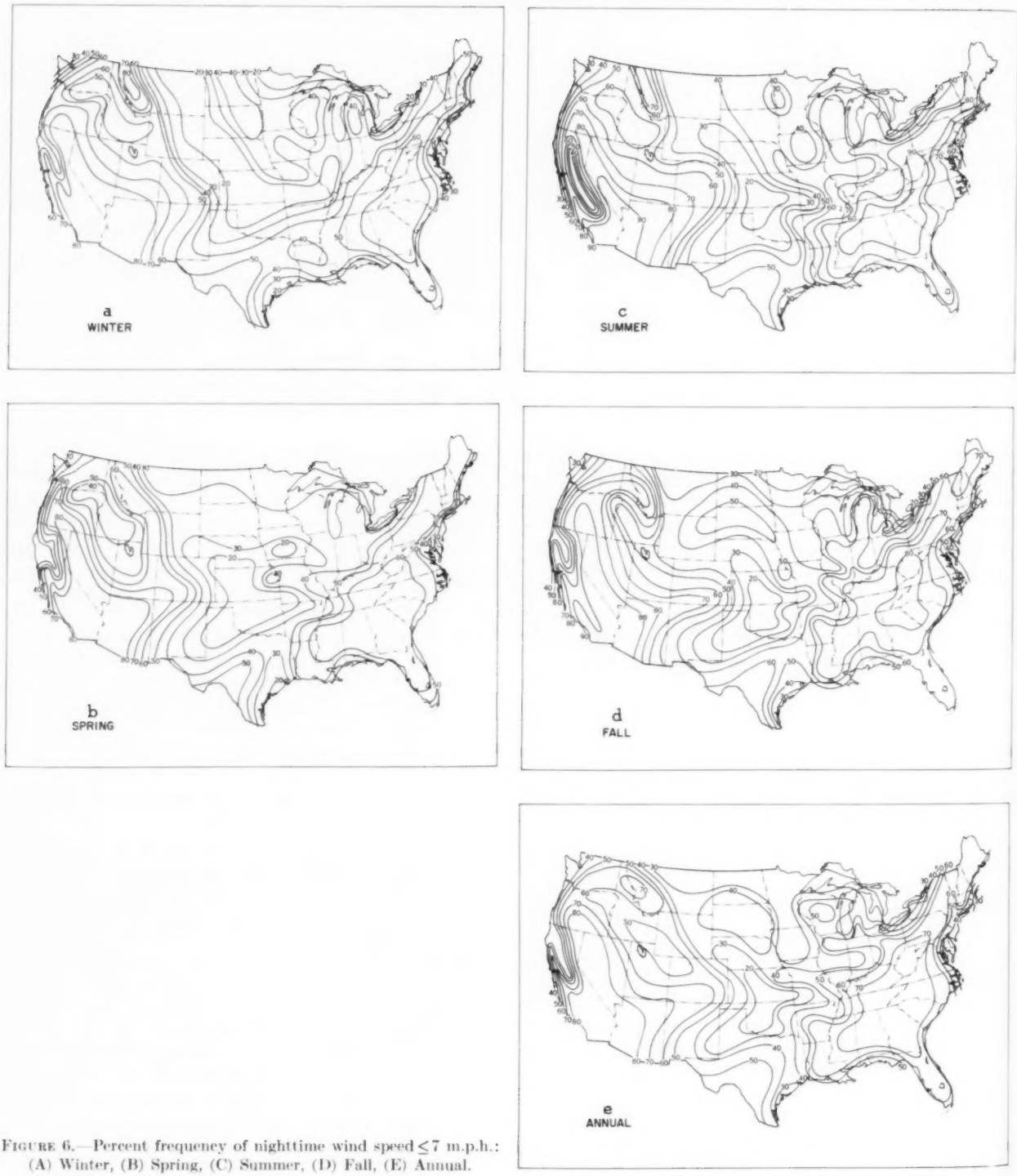

FIGURE 6.—Percent frequency of nighttime wind speed ≤ 7 m.p.h.: (A) Winter, (B) Spring, (C) Summer, (D) Fall, (E) Annual.

FIGURE 7.—Isopleths of nighttime [(percent cloud cover ≤ 3/10) + (percent wind speed ≤ 7 m.p.h.)]/2: (A) Winter, (B) Spring, (C) Summer, (D) Fall, (E) Annual.

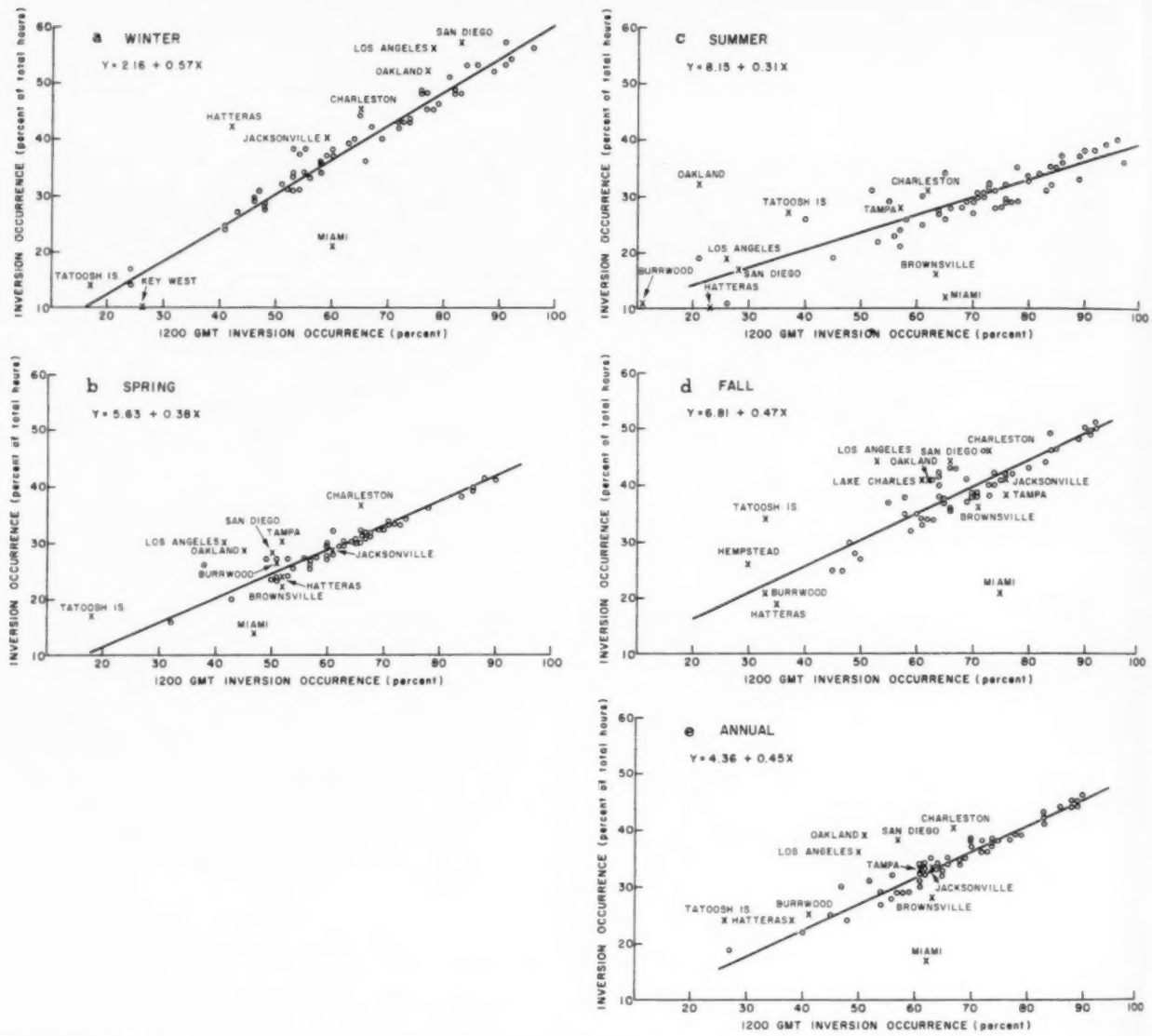

FIGURE 8.—Comparisons of computed inversion frequency (percent of total hours) on the ordinate (Y) to the 1200 GMT observed percent frequency of inversions on the abscissa (X): (A) Winter, (B) Spring, (C) Summer, (D) Fall, (E) Annual.

ing to inversion occurrence for each region are discussed below.

Great Lakes.—This area is characterized by frequent storm passages with their associated cloudiness and high winds, particularly from late fall to early spring, which result in relatively low frequencies of nocturnal radiation inversions. An analysis of climatological data for specific stations in this area shows a high occurrence of cloudiness during nighttime hours, which apparently reflects the effects of the Great Lakes imparting moisture to the air in its trajectory over the lake water. Summer and fall months show slightly higher frequencies of low-level stability than do the winter and spring months.

Generally, topography plays a small part in this area. However, the western slopes of the Appalachians probably enhance instability in western Pennsylvania and New York when the prevailing west and northwest winds blow. This is particularly true during the winter and spring, and is reflected by the frequent occurrence of snow shower activity in these areas. In summary, inversions based below 500 feet above the surface may be expected to occur about 20 to 30 percent of the time in any season in the Great Lakes area, although higher frequencies can be expected in remote sheltered valleys.

Appalachian Mountains.—Less storm frequency in the Southeastern States, compared to the area north of Vir-

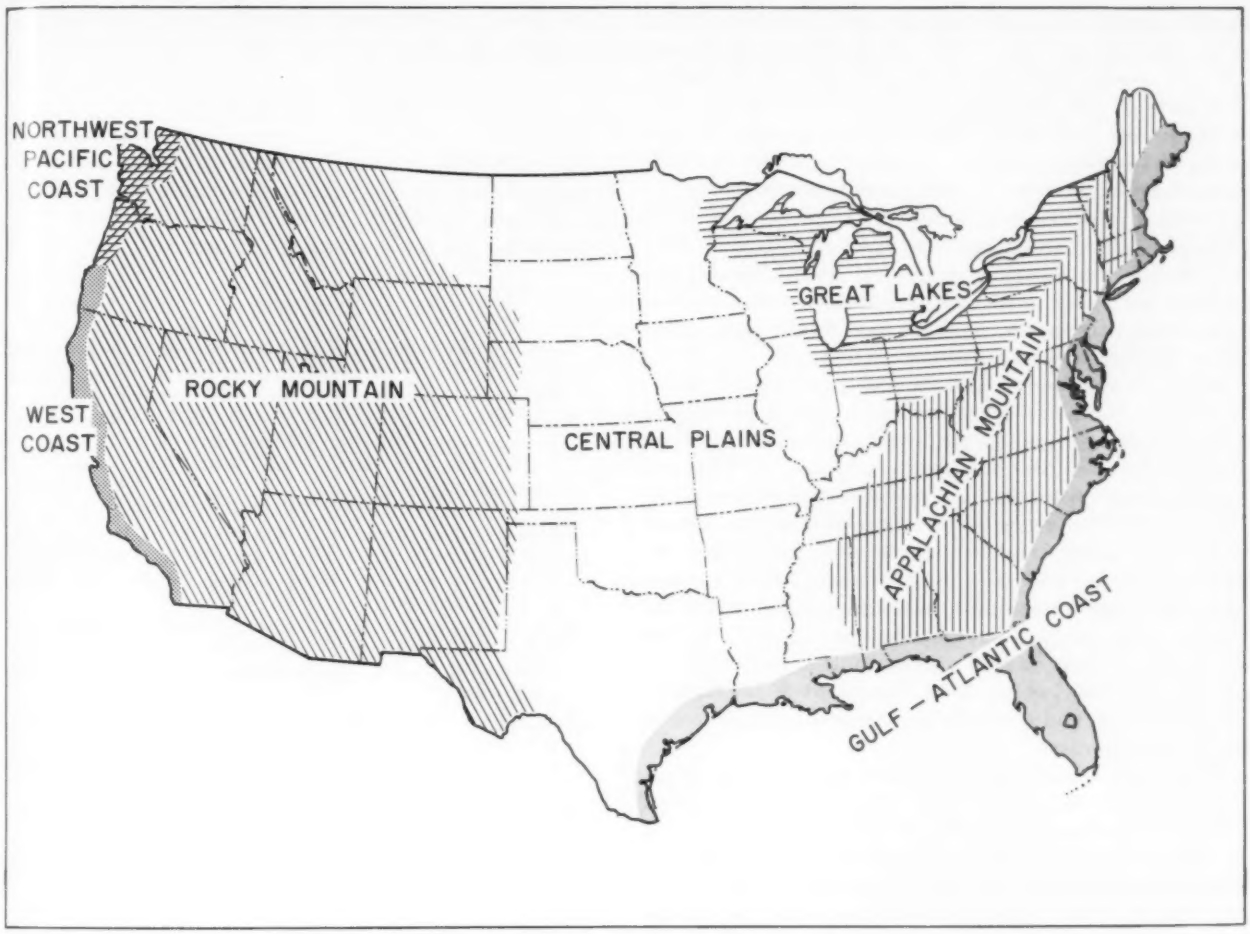

FIGURE 9.—Climatic-geographic delineation of low-level inversion frequency for contiguous United States.

ginia, undoubtedly contributes to the higher inversion frequency found over the southern Appalachian area. Mountain ridges afford protection to valley areas; consequently, light winds during nighttime hours are common in valleys. Frequent occurrence of anticyclonic flow over the Southeastern States, particularly during summer and fall months, also enhances nocturnal radiation inversion formation, since clear skies and light winds are associated with many of these high pressure systems. In general, low-level stabilization occurs 30 to 45 percent of the time in this area, while more topographically protected areas have more frequent occurrences of inversions.

Gulf–Atlantic Coast.—The warm waters of the Gulf of Mexico and Gulf Stream tend to inhibit inversion formation along the immediate coast in these regions. During the warmer months of the year the pressure gradient reinforces the sea breeze over most of the coastal areas of the Gulf of Mexico and Southeastern States. This reinforcement is sufficient to produce relatively strong winds during nights along immediate coastal areas, which helps to delay or inhibit nocturnal radiation inversion formation. Extreme southern Florida depicts minimum continentality, while stations farther inland (e.g., Jacksonville, Lake Charles, Charleston) show higher occurrences of nighttime stability. In general, from Long Island southward along the Atlantic coast to Hatteras, and along the Gulf coast and southern Florida, inversions may be expected 10 to 35 percent of the time. However, higher frequencies are indicated farther inland, as well as for the coastal area between Cape Hatteras and Jacksonville. The higher frequency of low-level stability along the New England coast, reflects the stabilizing effects of cold water off shore.

Central Plains.—The mid-section of the country has a pronounced continental type climate, and as such, has inversion frequencies closely related to the diurnal cycle; that is, there is a definite tendency for nocturnal stabilization and daytime instability in the lower levels. In general, inversions occur 20 to 30 percent of the time during the spring and summer, while during the fall and

602484—61——4

winter months inversions may be expected about 30 to 45 percent of the time. The higher frequency during fall and winter probably is a reflection of minimum storminess in fall and maximum length of a stable nocturnal period in winter. The opposite is true for the spring and summer months. During the colder months, particularly if snow cover exists, warm southerly advection over an existing cold surface may enhance low-level stability in these areas; however, such advection regimes are usually the incipient stages of warm fronts and cyclones with their associated precipitation and storminess, which ultimately produce less stable lapse rates below 500-foot elevations above ground.

Rocky Mountains.—This area also has marked continentality. With the exception of the northern regions during the winter and spring, storms occur infrequently, particularly over the southwestern areas. Unlike the Appalachian regions, dry air prevails most of the time, and inversion frequency is directly related to the diurnal cycle. Radiation inversions form near the surface on most nights, and they are dissipated shortly after sunrise. Since the longest nocturnal stable period and minimum daytime solar heating occur during the winter, it is this season that is potentially the most stable in this area. In general, inversions occur 40 to 55 percent of the time in fall and winter, and about 30 to 40 percent of the time in spring and summer.

West Coast.—Radiation inversions over interior areas, including areas only a few miles from the coast, are most prominent during the late fall and winter months. Along the immediate coast radiation inversions may merge with subsidence inversions, and low-level stability may persist until noon; or, on occasion, inversions persist for several days during which fog often occurs [11]. For the most part, the immediate coast has sufficient surface winds to provide good ventilation; however, the persistence of the subsidence inversion in addition to radiation inversions, the daily reversal of wind direction (land-sea breeze), and topographical sheltering of the valley and basin areas along coastal sections combine to create a potentially adverse climate as far as air pollution is concerned.

Pacific Northwest Coast.—Precipitation, cloudiness, and relatively high winds are dominant features of the climate of Washington and Oregon coastal areas. This region is situated far enough north of the high pressure cell which persists off the California coast to permit most storm systems from the Pacific to pass inland over the area. Consequently, storm activity is frequent, particularly during the winter and early spring. The instability associated with these frequent storm passages results in a relatively low frequency of radiation inversions. Radiation inversions are most frequent during the summer and early fall, when storm activity is at a minimum.

ACKNOWLEDGMENTS

The author is indebted to Messrs. Philip Jason and Benjamin Able for compilation of many of the climatological data. Also, the writer wishes to thank Mrs. Barbara Ritchie for drafting the diagrams.

REFERENCES

1. N. E. Bowne and R. R. Soller, A Meteorological Survey of the CANEL Site at Middletown, Connecticut, U.S. Weather Bureau, Middletown, Conn., July 1958 (unpublished).
2. W. M. Culkowski, Estimates of Accumulated Exposures and Environmental Build-up of Radioactivity, U.S. Weather Bureau Research Station, Oak Ridge, Tenn. (not dated) (unpublished).
3. G. A. De Marrais, "Vertical Temperature Difference Observed Over an Urban Area," U.S. Weather Bureau Research Station, Cincinnati, Ohio. (Paper presented at 190th National Meeting of American Meteorological Society, New York, N.Y., Jan. 26, 1961.)
4. G. A. De Marrais and N. F. Islitzer, "Diffusion Climatology of the National Reactor Testing Station," IDO–12015, U.S. Weather Bureau Research Station, Idaho Falls, Idaho, April 1960.
5. E. G. Edinger, "Variability of Low-Level Thermal Stratification Over Coastal Terrain in Southern California," University of California at Los Angeles, report on Contract Cwb–9666, May 1961.
6. E. M. Frisby, "Report on a Second Year of Hourly Climatological Observations Taken at the Pathfinder Atomic Power Plant Site Near Sioux Falls, South Dakota," South Dakota State College, Brookings, S. Dak., Sept. 15, 1960.
7. E. W. Hewson et al., "Meteorological Analysis" (Fifth Progress Report) 2515–5–P, College of Engineering, University of Michigan, Ann Arbor, June 1960.
8. D. E. Jenne, A Summary of the Persistence of Stable and Unstable Temperature Stratifications at Hanford for the Period 1946 through 1956, HW–53217, Hanford Laboratories Operation, General Electric Co., Richland, Wash., Oct. 1957 (unpublished).
9. R. J. List, Editor, *Smithsonian Meteorological Tables*, 6th Revised Edition, Smithsonian Institution, Washington, D.C., 1951.
10. D. H. Pack, C. R. Hosler, and T. B. Harris, A Meteorological Survey of the PWR Site at Shippingport, Pennsylvania, Special Projects Section, U.S. Weather Bureau, Washington, D.C., Dec. 1957 (unpublished).
11. Stanford Research Institute, "The Use of Meteorological Data in Large Scale Air Pollution Surveys," California Dept. of Public Health, Bureau of Air Sanitation, June 1958, 110 pp.
12. I. Van der Hoven, Personal Correspondence: Comparison of hygrothermograph traces at Yucca Weather Station and the 500-foot ridge station at the southwestern end of Yucca Dry Lake for January 1959–March 1960, U.S. Weather Bureau Research Station, Las Vegas, Nev., Aug. 29, 1960.

APPENDIX: CLIMATOLOGICAL DATA

Station	Season	Percent frequency of—						Station and period of record used	
		Inversion				Nighttime		Observations at 0300 and 1500 GMT	Observations at 0000 and 1200 GMT
		GMT 03	GMT 15	GMT 00	GMT 12	Total time	Surface Wind ≤7 mph	Cloud Cover ≤3/10	
Akron, Ohio	Winter						32	22	
	Spring						45	29	
	Summer						80	52	
	Fall						59	45	
Albany, N.Y.	Winter	47	11	31	43	27	45	28	Rome, N. Y., September 1953–August 1955.
	Spring	63	4	15	45	29	52	29	
	Summer	75	1	27	52	31	65	40	
	Fall	60	7	47	66	36	63	40	
Albuquerque, N. Mex.	Winter	67	72	8	82	48	58	59	Albuquerque, N. Mex., June 1955–May 1957.
	Spring	38	24	2	70	32	40	60	
	Summer	29	8	4	71	30	46	54	
	Fall	72	41	2	76	41	48	76	
Allentown, Pa.	Winter						49	36	
	Spring						53	35	
	Summer						79	53	
	Fall						64	48	
Amarillo, Tex.	Winter	71	68	16	74	43	25	58	Amarillo Air Force Base, Tex., June 1955–September 1956; Amarillo Air Terminal, October 1956–May 1957.
	Spring	45	18	4	65	30	15	54	
	Summer	48	10	3	82	34	23	55	
	Fall	71	43	6	70	38	26	71	
Asheville, N.C.	Winter						65	42	
	Spring						66	49	
	Summer						96	49	
	Fall						83	58	
Atlanta, Ga.	Winter	65	31	47	78	38	36	41	Atlanta, Ga., June 1953–May 1955
	Spring	67	5	17	71	31	41	49	
	Summer	70	2	13	70	29	65	47	
	Fall	70	10	51	75	38	55	55	
Augusta, Ga.	Winter						66	45	
	Spring						68	51	
	Summer						82	48	
	Fall						80	55	
Austin, Tex.	Winter						45	40	
	Spring						43	42	
	Summer						50	65	
	Fall						60	63	
Baltimore, Md.	Winter						36	37	
	Spring						34	40	
	Summer						47	55	
	Fall						42	53	
Baton Rouge, La.	Winter						41	43	
	Spring						54	53	
	Summer						81	71	
	Fall						71	70	
Billings, Mont.	Winter						27	29	
	Spring						35	35	
	Summer						38	55	
	Fall						35	49	
Birmingham, Ala.	Winter						51	38	
	Spring						59	49	
	Summer						86	54	
	Fall						68	57	
Bismarck, N. Dak.	Winter	65	57	37	67	42	49	35	Bismarck, N. Dak., June 1955–May 1957.
	Spring	59	19	2	61	28	38	39	
	Summer	77	9	2	77	29	52	51	
	Fall	69	41	15	65	37	49	50	
Boise, Idaho	Winter	79	75	19	81	51	44	26	Boise, Idaho, June 1955–May 1957
	Spring	61	59	2	84	38	38	45	
	Summer	68	33	1	97	36	54	68	
	Fall	90	81	8	92	50	46	60	
Boston, Mass.	Winter						17	39	
	Spring						18	35	
	Summer						29	48	
	Fall						23	48	
Brownsville, Tex.	Winter	53	51	7	66	36	37	42	Brownsville, Tex., June 1955–May 1957.
	Spring	21	11	1	52	22	26	32	
	Summer	9	2	2	63	16	45	71	
	Fall	57	23	4	71	36	54	69	
Buffalo, N.Y.	Winter	27	18	17	24	17	15	18	Buffalo, N.Y., June 1955—May 1957
	Spring	58	4	11	49	27	18	32	
	Summer	70	1	5	58	26	24	44	
	Fall	56	9	20	48	30	19	39	
Burbank, Calif.	Winter						81	59	
	Spring						83	52	
	Summer						85	65	
	Fall						91	68	
Burlington, Iowa	Winter						25	37	
	Spring						30	41	
	Summer						56	57	
	Fall						38	58	
Burrwood, La.	Winter	63	36	46	69	40			Burrwood, La., June 1955–May 1957
	Spring	57	11	18	51	26			
	Summer	26	1	4	11	11			
	Fall	38	3	13	33	21			
Cape Hatteras, N.C.	Winter	40	3	42	42	42			Hatteras, N.C., June 1955–February 1957; Cape Hatteras, March 1957–May 1957.
	Spring	51	6	43	52	24			
	Summer	14	3	11	23	10			
	Fall	29	5	31	35	19			

Burrwood, La., June 1957–May 1959.

Cape Hatteras, N.C., June 1957–May 1959.

APPENDIX—Continued

Station	Season	Percent frequency of—							Station and period of record used	
		Inversion					Nighttime			
		GMT 03	GMT 15	GMT 00	GMT 12	Total time	Surface Wind ≤7 mph	Cloud Cover ≤3/10	Observations at 0300 and 1500 GMT	Observations at 0000 and 1200 GMT
Caribou, Maine	Winter	49	27	39	60	38			Caribou, Maine, June 1955–May 1957	Caribou, Maine, June 1957–May 1959.
	Spring	57	7	24	38	26				
	Summer	69	1	27	40	26				
	Fall	52	9	49	49	28				
Charleston, S.C.	Winter	78	23	59	65	45	52	44	Charleston, S.C., June 1955–May 1957	Charleston, S.C., June 1957–May 1959.
	Spring	79	4	23	66	36	57	51		
	Summer	74	2	11	62	31	76	43		
	Fall	85	9	63	73	46	73	51		
Charlotte, N.C.	Winter						69	41		
	Spring						66	46		
	Summer						79	43		
	Fall						74	53		
Chattanooga, Tenn.	Winter						62	35		
	Spring						66	46		
	Summer						91	54		
	Fall						83	53		
Cheyenne, Wyo.	Winter						21	48		
	Spring						27	41		
	Summer						43	58		
	Fall						35	56		
Chicago, Ill.	Winter						29	30		
	Spring						39	36		
	Summer						72	54		
	Fall						47	50		
Cincinnati, Ohio	Winter						31	26		
	Spring						38	36		
	Summer						69	55		
	Fall						50	54		
Cleveland, Ohio	Winter						22	22		
	Spring						38	30		
	Summer						63	54		
	Fall						38	42		
Columbia, Mo.	Winter	53	38	27	52	31			Columbia, Mo. June 1955–May 1957	Columbia, Mo., June 1957–May 1959.
	Spring	52	4	1	67	31				
	Summer	84	5	5	78	35				
	Fall	80	24	20	66	43				
Columbia, S.C.	Winter						68	44		
	Spring						66	51		
	Summer						84	46		
	Fall						83	54		
Columbus, Ohio	Winter						54	25		
	Spring						48	32		
	Summer						86	53		
	Fall						72	50		
Corpus Christi, Tex.	Winter						26	40		
	Spring						26	34		
	Summer						38	66		
	Fall						30	66		
Dallas, Tex.	Winter						44	47		
	Spring						33	50		
	Summer						30	71		
	Fall						51	68		
Dayton, Ohio	Winter	40	21	17	41	24	30	27	Dayton, Ohio, June 1955–May 1957	Dayton, Ohio, June 1957–May 1959.
	Spring	41	6	2	57	26	40	41		
	Summer	57	4	4	66	28	71	57		
	Fall	69	15	31	65	37	50	51		
Denver, Colo.	Winter	82	75	54	83	48	43	53	Denver, Colo., June 1954–May 1956	Denver, Colo., June 1957–May 1959.
	Spring	58	22	5	65	30	47	46		
	Summer	54	15	8	84	35	52	56		
	Fall	78	49	22	80	43	55	62		
Des Moines, Iowa	Winter						20	36		
	Spring						20	40		
	Summer						36	53		
	Fall						29	57		
Detroit, Mich.	Winter						27	25		
	Spring						40	34		
	Summer						63	55		
	Fall						47	49		
Dodge City, Kans.	Winter	78	69	47	77	45			Dodge City, Kans., June 1955–May 1957.	Dodge City, Kans., June 1957–May 1959.
	Spring	52	16	7	67	31				
	Summer	64	8	1	85	35				
	Fall	76	46	28	77	42				
Duluth, Minn.	Winter						25	34		
	Spring						28	37		
	Summer						43	46		
	Fall						26	38		
El Paso, Tex.	Winter	71	91	3	84	53	44	66	El Paso, Tex., June 1955–May 1957	El Paso, Tex., June 1957–May 1959.
	Spring	45	33	2	67	31	34	68		
	Summer	34	11	1	61	25	37	57		
	Fall	76	55	4	69	41	49	75		
Ely, Nev.	Winter	79	91	22	86	53			Ely, Nev., June 1955–May 1957	Ely, Nev., June 1957–May 1959.
	Spring	52	52	0	78	36				
	Summer	63	42	1	96	40				
	Fall	86	89	9	91	49				
Evansville, Ind.	Winter						36	32		
	Spring						44	41		
	Summer						63	57		
	Fall						62	57		
Fargo, N. Dak.	Winter						24	37		
	Spring						21	41		
	Summer						30	52		
	Fall						22	46		

APPENDIX—Continued

Station	Season	Percent frequency of—							Station and period of record used	
		Inversion					Nighttime			
		GMT				Total time	Surface Wind ≤7 mph	Cloud Cover ≤3/10	Observations at 0300 and 1500 GMT	Observations at 0000 and 1200 GMT
		03	15	00	12					
Flint, Mich.	Winter	25	15	28	46	29			Mount Clemens Air Force Base, Mich., June 1954–May 1956.	Flint, Mich., June 1957–May 1959.
	Spring	49	9	4	65	30				
	Summer	72	5	2	70	27				
	Fall	47	10	21	63	34				
Fort Worth, Tex.	Winter	58	38	13	55	34			Fort Worth, Tex., June 1955–May 1957.	Fort Worth, Tex., June 1957–May 1959.
	Spring	42	7	2	51	23				
	Summer	45	2	2	53	22				
	Fall	69	27	18	55	37				
Fort Wayne, Ind.	Winter						39	25		
	Spring						41	34		
	Summer						75	53		
	Fall						60	50		
Fresno, Calif.	Winter						84	39		
	Spring						64	63		
	Summer						48	91		
	Fall						81	73		
Galveston, Tex.	Winter						20	35		
	Spring						18	36		
	Summer						22	56		
	Fall						31	63		
Glasgow, Mont.	Winter	75	75	56	76	48			Glasgow, Mont., June 1955–May 1957.	Glasgow, Mont., June 1957–May 1959.
	Spring	68	38	7	72	33				
	Summer	50	14	4	84	32				
	Fall	79	53	17	83	44				
Grand Junction, Colo.	Winter	81	86	8	91	53			Grand Junction, Colo., June 1955–May 1957.	Grand Junction, Colo., June 1957–May 1959.
	Spring	60	32	0	67	31				
	Summer	67	17	4	90	38				
	Fall	90	75	6	84	49				
Grand Rapids, Mich.	Winter						43	20		
	Spring						44	33		
	Summer						76	51		
	Fall						57	45		
Great Falls, Mont.	Winter	73	74	41	76	48	18	31	Great Falls, Mont., June 1955–May 1957.	Great Falls, Mont., June 1957–May 1959.
	Spring	32	36	1	68	31	26	32		
	Summer	34	28	2	75	28	32	51		
	Fall	66	70	8	70	38	27	45		
Green Bay, Wis.	Winter	54	31	29	53	34			Green Bay, Wis., June 1955–May 1957.	Green Bay, Wis., June 1957–May 1959.
	Spring	58	8	9	71	33				
	Summer	76	9	4	76	29				
	Fall	59	16	22	61	33				
Greensboro, N.C.	Winter	73	15	58	72	43	54	43	Greensboro, N.C., June 1955–May 1957.	Greensboro, N.C., June 1957–May 1959.
	Spring	70	3	13	66	32	56	49		
	Summer	78	1	11	66	33	79	48		
	Fall	74	4	52	74	40	68	58		
Harrisburg, Pa.	Winter						60	32		
	Spring						54	32		
	Summer						85	52		
	Fall						77	47		
Hartford, Conn.	Winter						50	34		
	Spring						54	32		
	Summer						81	39		
	Fall						66	41		
Helena, Mont.	Winter						69	26		
	Spring						63	33		
	Summer						67	55		
	Fall						69	48		
Houston, Tex.	Winter						22	31		
	Spring						26	39		
	Summer						40	68		
	Fall						34	61		
Indianapolis, Ind.	Winter						24	30		
	Spring						29	38		
	Summer						57	57		
	Fall						40	55		
International Falls, Minn.	Winter	55	48	12	53	34			International Falls, Minn., June 1955–May 1957.	International Falls, Minn., June, 1957–May 1959.
	Spring	51	15	2	57	26				
	Summer	70	4	2	65	26				
	Fall	45	19	7	47	25				
Jackson, Miss.	Winter	54	32	31	58	34	47	38	Jackson, Miss., June 1944–January 1945, February 1956–May 1957.	Jackson, Miss., June 1957–May 1959.
	Spring	59	10	7	60	27	62	49		
	Summer	68	4	11	72	30	83	61		
	Fall	70	24	29	58	38	70	62		
Jacksonville, Fla.	Winter	69	27	44	59	40	60	48	USNAS, Jacksonville, Fla., June 1955–October 1955; WBAS, Jacksonville, November 1955–May 1957.	WBAS, Jacksonville, Fla., June 1957–May 1959.
	Spring	53	4	10	61	28	63	54		
	Summer	38	1	11	56	23	75	44		
	Fall	51	12	37	71	41	63	47		
Joliet, Ill.	Winter	46	25	29	56	33			Joliet, Ill., March 1951–February 1953.	Peoria, Ill. June 1957–May 1959.
	Spring	63	5	3	63	29				
	Summer	82	7	4	65	34				
	Fall	71	15	39	73	38				
Kansas City, Mo.	Winter						39	47		
	Spring						34	43		
	Summer						47	57		
	Fall						47	62		
Key West, Fla.	Winter	1	2	6	26	9			Key West (Navy), Fla., June 1955–May 1957.	Key West (Navy), Fla., June 1957–May 1959.
	Spring	1	0	1	4	1				
	Summer	0	0	1	0	<1				
	Fall	1	0	0	1	<1				
Knoxville, Tenn.	Winter						55	34	Data sparse throughout period.	
	Spring						57	44		
	Summer						78	50		
	Fall						73	53		

APPENDIX—Continued

Station	Season	Percent frequency of—							Station and period of record used	
		Inversion					Nighttime			
		GMT 03	GMT 15	GMT 00	GMT 12	Total time	Surface Wind ≤7 mph	Cloud Cover ≤3/10	Observations at 0300 and 1500 GMT	Observations at 0000 and 1200 GMT
LaCrosse, Wis.	Winter						44	32		
	Spring						39	35		
	Summer						66	49		
	Fall						46	48		
LaGuardia, N.Y.	Winter						22	41		
	Spring						28	36		
	Summer						47	48		
	Fall						36	50		
Lake Charles, La.	Winter	61	30	12	58	36	43	37	Lake Charles, La., June 1955–May 1957.	Lake Charles, La., June 1957–May 1959.
	Spring	53	5	3	58	27	56	44		
	Summer	62	3	5	71	30	76	65		
	Fall	75	12	9	61	41	72	63		
Lakehurst, N.J.	Winter	41	17	--	--	24			Lakehurst (Navy), N.J., June 1953–May 1955.	Station closed July 1955.
	Spring	47	2	--	--	22				
	Summer	51	2	--	--	21				
	Fall	59	12	--	--	32				
Lander, Wyo.	Winter	82	90	50	91	57			Lander, Wyo., June 1955–May 1957.	Lander, Wyo., June 1957–May 1959.
	Spring	50	37	3	67	31				
	Summer	63	18	4	89	33				
	Fall	81	59	18	85	46				
Lansing, Mich.	Winter						31	23		
	Spring						24	35		
	Summer						58	57		
	Fall						33	50		
Las Vegas, Nev.	Winter	88	92	2	92	54			Las Vegas, Nev., June 1955–May 1957.	Las Vegas, Nev., June 1957–May 1959.
	Spring	52	54	0	86	39				
	Summer	52	41	1	89	37				
	Fall	92	88	0	90	50				
Little Rock, Ark.	Winter	49	17	32	46	29	50	39	Little Rock, Ark., June 1955–May 1957.	Little Rock, Ark., June 1957–May 1959.
	Spring	60	11	5	51	27	55	48		
	Summer	73	1	7	61	30	83	59		
	Fall	76	9	24	64	42	77	59		
Los Angeles, Calif.	Winter	48	77	27	78	56	76	56	Long Beach, Calif., March 1954–February 1956.	Santa Monica, Calif., June 1957–May 1959.
	Spring	25	31	20	42	30	79	45		
	Summer	24	14	20	26	19	90	41		
	Fall	51	49	32	53	44	90	51		
Louisville, Ky.	Winter						48	36		
	Spring						54	41		
	Summer						83	62		
	Fall						67	59		
Madison, Wis.	Winter						35	33		
	Spring						37	38		
	Summer						65	50		
	Fall						44	50		
Medford, Oreg.	Winter	75	70	16	65	44	87	38	Medford, Oreg., June 1955–May 1957.	Medford, Oreg., June 1957–May 1959.
	Spring	35	40	2	74	34	77	40		
	Summer	13	32	0	80	33	86	64		
	Fall	63	73	6	76	41	87	38		
Memphis, Tenn.	Winter						31	38		
	Spring						39	49		
	Summer						66	59		
	Fall						55	61		
Miami, Fla.	Winter	39	6	29	60	24	47	58	Miami, Fla., June 1955–May 1957.	Miami, Fla., June 1957–May 1959.
	Spring	27	2	10	47	15	49	59		
	Summer	27	2	21	65	13	75	49		
	Fall	41	3	19	75	22	64	48		
Midland, Tex.	Winter	64	67	12	73	43			Midland, Tex., June 1955–May 1957.	Midland, Tex., June 1957–May 1959.
	Spring	40	18	1	65	30				
	Summer	45	2	3	64	27				
	Fall	63	29	8	61	34				
Milwaukee, Wis.	Winter						26	32		
	Spring						33	43		
	Summer						57	51		
	Fall						36	48		
Minneapolis, Minn.	Winter						35	39		
	Spring						30	41		
	Summer						46	54		
	Fall						36	50		
Missoula, Mont.	Winter						81	14		
	Spring						68	29		
	Summer						76	54		
	Fall						86	45		
Mobile, Ala.	Winter						28	37		
	Spring						40	44		
	Summer						67	54		
	Fall						45	58		
Moline, Ill.	Winter						39	37		
	Spring						41	40		
	Summer						68	57		
	Fall						56	54		
Montgomery, Ala.	Winter	66	29	24	55	38	62	40	Maxwell Field, Montgomery, Ala., December 1952–November 1954.	Donnelly Field, Montgomery, Ala. June 1957–May 1959.
	Spring	64	5	4	60	29	73	50		
	Summer	70	6	10	72	30	90	54		
	Fall	77	16	33	64	42	84	56		
Mount Clemens, Mich.	Winter	25	15	28	46	29			Selfridge Air Force Base, Mich., June 1954–May 1956.	Flint, Mich., June 1957–May 1959.
	Spring	49	9	4	65	30				
	Summer	72	5	2	70	27				
	Fall	47	10	21	63	34				
Nantucket, R.I.	Winter	55				32			U.S. Navy Marine Climatic Atlas of the World. (See References.)	
	Spring	65				30				
	Summer	82				34				
	Fall	70				38				

APPENDIX—Continued

Station	Season	Percent frequency of—							Station and period of record used	
		Inversion					Nighttime			
		GMT 03	GMT 15	GMT 00	GMT 12	Total time	Surface Wind ≤7 mph	Cloud Cover ≤3/10	Observations at 0300 and 1500 GMT	Observations at 0000 and 1200 GMT
Nashville, Tenn.	Winter	51	24	35	53	31	55	34	Nashville, Tenn., June 1955–May 1957.	Nashville, Tenn., June 1957–May 1959
	Spring	60	4	8	56	27	68	47		
	Summer	76	1	6	73	32	93	56		
	Fall	74	16	38	64	40	77	59		
Newark, N.J.	Winter						38	41		
	Spring						39	39		
	Summer						61	52		
	Fall						55	52		
New Orleans, La.	Winter						42	37		
	Spring						57	45		
	Summer						81	61		
	Fall						61	63		
New York, N.Y.	Winter	21	7	18	24	14			Hempstead Air Force Base, N.Y., September 1954–August 1956.	International Airport, N.Y., June 1957–May 1959.
	Spring	36	3	36	32	16				
	Summer	45	1	22	21	19				
	Fall	48	1	24	30	26				
Norfolk, Va.	Winter	28	28	40	48	28	37	43	Norfolk, Va., Fleet Weather Central, September 1953–August 1955.	Norfolk, Va., Municipal Airport, June 1957–May 1959.
	Spring	31	8	15	50	23	42	45		
	Summer	21	3	9	45	19	61	50		
	Fall	29	21	30	50	27	52	53		
North Platte, Nebr.	Winter	68	63	36	74	43			North Platte, Nebr., June 1955–May 1957.	North Platte, Nebr., June 1957–May 1959.
	Spring	55	18	3	69	32				
	Summer	74	9	4	76	32				
	Fall	79	51	20	67	43				
Oakland, Calif.	Winter	66	83	10	77	49	78	43	Oakland, Calif., June 1955–May 1957.	Oakland, Calif., June 1957–May 1959.
	Spring	23	35	14	45	29	64	48		
	Summer	29	13	34	21	29	67	40		
	Fall	58	62	15	62	41	81	51		
Ogden, Utah	Winter	77	66	17	79	46			Ogden, Utah, June 1954–May 1956.	Salt Lake City, Utah, June 1957–May 1959.
	Spring	63	23	1	73	33				
	Summer	62	28	2	94	39				
	Fall	84	69	3	84	46				
Oklahoma City, Okla.	Winter	63	38	33	59	37	15	49	Oklahoma City, Okla., June 1955–May 1957.	Oklahoma City, Okla., June 1957–May 1959.
	Spring	70	15	6	61	32	14	47		
	Summer	88	5	3	86	37	21	60		
	Fall	85	27	16	72	46	19	67		
Omaha, Nebr.	Winter	61	57	43	72	42	33	43	Omaha, Nebr., June 1955–May 1957.	Omaha, Nebr., June 1957–May 1959.
	Spring	58	23	8	60	27	29	40		
	Summer	70	15	9	80	33	45	50		
	Fall	71	42	22	64	38	44	59		
Philadelphia, Pa.	Winter						38	38		
	Spring						39	36		
	Summer						62	49		
	Fall						54	43		
Phoenix, Ariz.	Winter	88	92	0	96	56	88	68	Phoenix, Ariz., June 1955–May 1957.	Yuma, Ariz., June 1957–May 1959.
	Spring	58	68	0	86	39	83	71		
	Summer	59	38	0	86	36	81	67		
	Fall	95	88	0	92	51	92	82		
Pittsburgh, Pa.	Winter	33	24	20	41	24			Pittsburgh, Pa., June 1955–May 1957.	Pittsburgh, Pa., June 1957–May 1959.
	Spring	34	6	5	68	31				
	Summer	55	1	4	64	27				
	Fall	56	15	25	62	34				
Pocatello, Idaho.	Winter						45	28		
	Spring						42	42		
	Summer						58	66		
	Fall						54	59		
Port Arthur, Tex.	Winter						23	38		
	Spring						32	45		
	Summer						72	72		
	Fall						49	67		
Portland, Maine	Winter	53	29	48	64	40	48	38	Portland, Maine, June 1955–May 1957.	Portland, Maine, June 1957–May 1959.
	Spring	60	6	48	53	27	56	35		
	Summer	78	4	41	55	29	79	42		
	Fall	70	16	65	71	38	66	46		
Portland, Oreg.	Winter	36	41	8	51	32	51	12	Portland, Oreg., June 1954–May 1956.	Salem, Oreg., June 1957–May 1959.
	Spring	19	20	1	63	29	71	30		
	Summer	14	3	0	74	28	75	51		
	Fall	49	43	2	71	38	76	35		
Providence, R.I.	Winter						40	41		
	Spring						37	37		
	Summer						63	45		
	Fall						54	51		
Pueblo, Colo.	Winter						62	60		
	Spring						60	50		
	Summer						68	61		
	Fall						76	68		
Raleigh, N.C.	Winter						60	42		
	Spring						60	49		
	Summer						76	45		
	Fall						75	55		
Rapid City, S. Dak.	Winter	73	71	49	77	48			Rapid City, S. Dak., June 1955–May 1957.	Rapid City, S. Dak., June 1957–May 1959.
	Spring	64	29	3	66	30				
	Summer	71	11	12	78	29				
	Fall	77	48	19	74	42				
Richmond, Va.	Winter						54	44		
	Spring						57	41		
	Summer						76	47		
	Fall						69	53		

APPENDIX—Continued

Station	Season	Percent frequency of—							Station and period of record used	
		Inversion					Nighttime		Observations at 0300 and 1500 GMT	Observations at 0000 and 1200 GMT
		GMT 03	GMT 15	GMT 00	GMT 12	Total time	Surface Wind ≤7 mph	Cloud Cover ≤3/10		
Rochester, N.Y.	Winter						29	17		
	Spring						35	34		
	Summer						61	49		
	Fall						50	39		
Sacramento, Calif.	Winter						51	37		
	Spring						34	65		
	Summer						20	88		
	Fall						52	71		
Salem, Oreg.	Winter	36	41	8	51	32			Portland, Oreg., June 1954–May 1956.	Salem, Oreg., June 1957–May 1959.
	Spring	19	20	1	63	29				
	Summer	14	3	0	74	28				
	Fall	49	43	2	71	38				
Salt Lake City, Utah	Winter	77	66	17	79	46	59	31	Ogden, Utah, June 1954–May 1956.	Salt Lake City, Utah, June 1957–May 1959.
	Spring	63	23	1	73	33	46	43		
	Summer	62	28	2	94	39	40	62		
	Fall	84	69	3	84	46	50	61		
San Antonio, Tex.	Winter	54	34	9	47	31	52	40	San Antonio, Tex., June 1955–May 1957.	San Antonio, Tex., June 1957–May 1959.
	Spring	27	6	2	43	20	43	37		
	Summer	8	0	2	26	11	50	56		
	Fall	46	15	6	45	25	66	58		
San Diego, Calif.	Winter	27	61	22	83	57	86	56	San Diego, Calif., June 1954–May 1956.	San Diego, Calif., June 1957–May 1959.
	Spring	14	22	9	51	28	82	31		
	Summer	8	4	8	28	17	94	27		
	Fall	31	37	17	66	44	94	46		
San Francisco, Calif.	Winter						55	43		
	Spring						32	53		
	Summer						20	54		
	Fall						42	56		
Santa Monica, Calif.	Winter	48	77	27	78	56			Long Beach, Calif., March 1954–February 1956.	Santa Monica, Calif., June 1957–May 1959.
	Spring	25	31	20	42	30				
	Summer	24	14	20	26	19				
	Fall	51	49	32	53	44				
Sault Ste. Marie, Mich.	Winter	48	53	35	58	36			Sault Ste. Marie, Mich., June 1955–May 1957.	Sault Ste. Marie, Mich., June 1957–May 1959.
	Spring	63	29	14	60	29				
	Summer	84	12	12	73	32				
	Fall	55	25	38	66	36				
Savannah, Ga.	Winter						46	47		
	Spring						56	54		
	Summer						69	47		
	Fall						57	54		
Seattle, Wash.	Winter	13	31	24	63	39	31	15	Seattle, Wash., June 1954–May 1956.	Seattle, Wash., June 1957–May 1959.
	Spring	6	30	0	54	25	31	28		
	Summer	3	19	1	57	21	35	44		
	Fall	19	32	9	69	37	38	32		
Shreveport, La.	Winter	52	31	6	54	31	36	37	Barksdale Air Force Base, La., June 1955–December 1955; Municipal Airport, Shreveport, La., January 1956–May 1957.	Municipal Airport, Shreveport, La., June 1957–May 1959.
	Spring	54	10	3	57	26	42	46		
	Summer	66	3	5	68	28	61	64		
	Fall	75	31	10	63	41	59	63		
Sioux City, Iowa.	Winter						38	40		
	Spring						38	39		
	Summer						57	56		
	Fall						50	58		
Sioux Falls, S. Dak.	Winter						37	36		
	Spring						34	38		
	Summer						52	50		
	Fall						45	53		
Spokane, Wash.	Winter	53	59	16	54	37	55	19	Spokane, Wash., June 1955–May 1957.	Spokane, Wash., June 1957–May 1959.
	Spring	23	41	0	63	29	57	39		
	Summer	16	26	1	83	31	66	62		
	Fall	57	57	4	73	40	68	47		
Springfield, Ill.	Winter						18	36		
	Spring						27	41		
	Summer						55	60		
	Fall						33	57		
Springfield, Mo.	Winter						17	44		
	Spring						18	45		
	Summer						26	60		
	Fall						23	61		
St. Cloud, Minn.	Winter	57	60	14	53	38			St. Cloud, Minn., June 1955–May 1957.	St. Cloud, Minn., June 1957–May 1959.
	Spring	60	13	1	63	29				
	Summer	76	6	3	76	29				
	Fall	65	25	14	58	35				
St. Louis, Mo.	Winter	63	24	.....		37			1947–51.	
	Spring	60	11	.....		27				
	Summer	82	7	.....		34				
	Fall	81	13	.....		44				
Syracuse, N.Y.	Winter						40	19		
	Spring						47	30		
	Summer						67	46		
	Fall						53	39		
Tampa, Fla.	Winter	69	17	28	60	37	57	52	Tampa, Fla., June 1956–May 1957.	Tampa, Fla., June 1957–May 1959.
	Spring	59	1	7	52	30	61	57		
	Summer	62	8	14	57	28	81	41		
	Fall	63	2	25	76	38	67	46		

APPENDIX—Continued

Station	Season	Percent frequency of—							Station and period of record used	
		Inversion					Nighttime			
		GMT				Total time	Surface Wind ≤7 mph	Cloud Cover ≤3/10	Observations at 0300 and 1500 GMT	Observations at 0000 and 1200 GMT
		03	15	00	12					
Tatoosh Island, Wash.	Winter	22	15	17	14	17	.....	.....	Tatoosh Island, Wash., June 1955–May 1957.	Tatoosh Island, Wash., June 1957–May 1959.
	Spring	21	15	11	18	17	.....	.....		
	Summer	31	20	19	37	27	.....	.....		
	Fall	35	38	29	33	34	.....	.....		
Toledo, Ohio	Winter	39	14	.....	.....	23	24	22	Toledo, Ohio, June 1946–December 1950.	
	Spring	49	4	.....	.....	22	31	32		
	Summer	73	1	.....	.....	30	63	51		
	Fall	67	5	.....	.....	36	45	49		
Topeka, Kans.	Winter	44	30	16	48	28	39	45	Topeka, Kans., June 1955–May 1957.	Topeka, Kans., June 1957–May 1959.
	Spring	41	13	2	53	24	40	42		
	Summer	53	7	2	69	29	50	56		
	Fall	64	24	11	60	35	50	60		
Tulsa, Okla.	Winter	.....	.....	.....	.....	.....	27	47		
	Spring	.....	.....	.....	.....	.....	28	48		
	Summer	.....	.....	.....	.....	.....	41	60		
	Fall	.....	.....	.....	.....	.....	35	59		
Tucson, Ariz.	Winter	65	83	2	89	52	.....	.....	Davis Monthan Air Force Base, Tucson, Ariz., June 1955–February 1956; Municipal Airport, Tucson, March 1956–May 1957.	Municipal Airport, Tucson, Ariz., June 1957–May 1960 (September 1958–June 1959 06Z & 18Z only).
	Spring	29	61	1	90	41	.....	.....		
	Summer	19	15	4	74	31	.....	.....		
	Fall	77	70	1	89	48	.....	.....		
Washington, D.C.	Winter	44	22	30	48	28	37	43	Washington, D.C., June 1955–May 1957.	Washington, D.C., June 1957–May 1959.
	Spring	42	5	12	51	23	38	38		
	Summer	47	2	5	57	24	58	49		
	Fall	56	8	34	59	32	54	53		
Wichita, Kans.	Winter	.....	.....	.....	.....	.....	19	49		
	Spring	.....	.....	.....	.....	.....	17	45		
	Summer	.....	.....	.....	.....	.....	13	56		
	Fall	.....	.....	.....	.....	.....	13	63		
Winnemucca, Nev.	Winter	.....	.....	6	82	48	.....	.....	Station opened May 1, 1956.	Winnemucca, Nev., June 1957–May 1959.
	Spring	.....	.....	0	88	41	.....	.....		
	Summer	.....	.....	0	92	38	.....	.....		
	Fall	.....	.....	1	91	49	.....	.....		
Yakima, Wash.	Winter	.....	.....	.....	.....	.....	76	26		
	Spring	.....	.....	.....	.....	.....	55	50		
	Summer	.....	.....	.....	.....	.....	49	70		
	Fall	.....	.....	.....	.....	.....	61	55		
Youngstown, Ohio	Winter	.....	.....	.....	.....	.....	28	23		
	Spring	.....	.....	.....	.....	.....	40	33		
	Summer	.....	.....	.....	.....	.....	72	57		
	Fall	.....	.....	.....	.....	.....	49	48		

Weather Note

THE EFFECT OF DIFFERENTIAL FRICTION BETWEEN LAND AND WATER ON THE MOVEMENT OF DONNA IN THE VICINITY OF EASTERN NORTH CAROLINA

EUGENE W. HOOVER

U.S. Weather Bureau, Washington National Airport, Washington, D.C.

Manuscript received March 27, 1961; revised May 1, 1961]

The small-scale irregularities in the movement of hurricane Donna over eastern North Carolina in September 1960 support the conclusion of Dunn et al. [1] on the effects of differential wind friction between land and water surfaces. They suggested that the increase in surface friction and the greater cross-isobaric flow over land contributed to an increase in pressure in the forward right quadrant. This increase in surface pressure caused a temporary deviation to the left and brief slowing in the forward speed of the hurricane. The duration of these small-scale irregularities was contingent upon the time required for the core of strongest wind to move inland. These vacillations were noted by Dunn et al. [1] in the tracks of hurricanes Connie, Diane, and Ione and by Dunn [2] in the track of Donna.

The unusually large dimensions of the eye in the vicinity of North Carolina make Donna a remarkable hurricane to illustrate the concept of differential friction. The magnitude of time and distance elements of deviations in the storm track are large enough to evaluate quantitatively.

The track of the radar fixes of the center of Donna over eastern North Carolina (fig. 1) deviated inland to the left about one degree of latitude, which is approximately the same as the reported diameter of the eye. The forward speed (see data table in fig. 1) slowed from 27 kt. over water (segment E to F) to 13 kt. over land (segment B to C).

The differential friction effect reversed as the hurricane moved off shore. The decreasing friction over water permitted the winds to increase and become more nearly parallel to the isobars off shore. According to the suggested hypothesis, this flow results in a depletion of air near the coast. This depletion of air causes the hurricane to be temporarily displaced to the right, and simultaneously to accelerate forward briefly. The radar fixes of Donna in figure 1 illustrate the turn to the right and the forward acceleration to an average speed of 38 kt. between points C and D (see data table in fig. 1). Both the magnitude and geographical position of the observed vacillations over eastern North Carolina are in agreement with those suggested by the differential friction hypothesis.

REFERENCES

1. Gordon E. Dunn, Walter R. Davis, and Paul L. Moore, "Hurricanes of 1955," *Monthly Weather Review*, vol. 83, No. 12, Dec. 1955, pp. 315–326.
2. Gordon E. Dunn, "The Hurricane Season of 1960," *Monthly Weather Review*, vol. 89, No. 3, Mar. 1961, pp. 99–108.

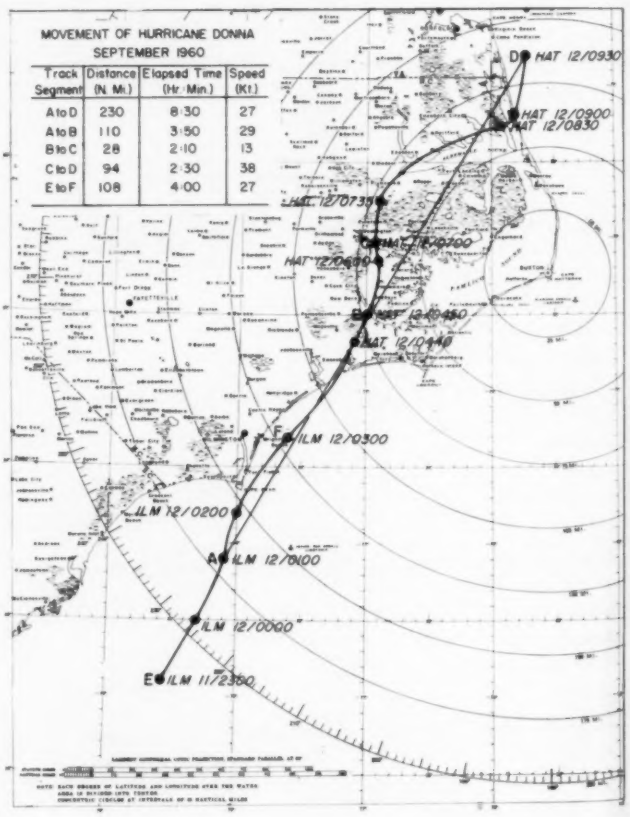
MOVEMENT OF HURRICANE DONNA
SEPTEMBER 1960
Track Segment | Distance (N. Mi.) | Elapsed Time (Hr. Min.) | Speed (Kt.)
A to D | 230 | 8:30 | 27
A to B | 110 | 3:50 | 29
B to C | 28 | 2:10 | 13
C to D | 94 | 2:30 | 38
E to F | 108 | 4:00 | 27
D HAT 12/0930
HAT 12/0900
HAT 12/0830
HAT 12/0730
HAT 12/0700
HAT 12/0630
HAT 12/0450
HAT 12/0440
F ILM 12/0300
ILM 12/0200
A ILM 12/0100
ILM 12/0000
E ILM 11/2300

FIGURE 1.—Track of radar fixes on center of hurricane Donna, 2300 GMT September 11 to 1930 GMT September 12, 1960.

MOISTURE AND COTTON AT HARVEST TIME IN THE MISSISSIPPI DELTA

J. A. RILEY

Delta Agricultural Weather Project, U.S. Weather Bureau, Stoneville, Miss.
[Manuscript received February 28, 1961; revised May 18, 1961]

ABSTRACT

The moisture content of cotton at time of harvest has a direct effect on cotton quality. Weather, in particular relative humidity, strongly influences variation in cotton moisture content. This paper summarizes three years of observations of weather in and around cotton fields at harvest time in the Mississippi Delta.

Detailed studies of the variation of relative humidity, temperature, wind, sunlight, dew, and evaporation have been made in leafed fields and in fields where leaves were removed artificially. Single weather variables and combinations of variables have been related to dew intensity and to the rate of evaporation. Surface weather maps are presented to show the average pressure patterns associated with extremes in dew and evaporation. A preliminary cotton picking guide, developed jointly by the Weather Bureau and the Cotton Harvesting Section of the U.S. Department of Agriculture, which gives the farmer an objective estimate of when to start picking cotton on the basis of weather variation, illustrates how weather information can improve farm efficiency.

1. INTRODUCTION

Dry weather is good cotton picking weather. In the humid Cotton Belt, over 8 million bales with a cash value of over a billion dollars were harvested in 1959. Some of this cotton was harvested too wet and the consequent reduction in quality resulted in a price drop of $10 to $15 per bale; thus damp cotton in the humid belt is a problem of considerable economic importance.

Wet weather in the form of excessive rain gives poor harvest conditions; mechanical equipment is inoperative when soils are water-logged; if the rain persists, maturity may be delayed until the plants are caught by frost; and frequent soaking of lint by rain stains the cotton. This type of wet weather damage has no control. Wet weather in the form of high humidity is damaging to quality if the cotton is picked while wet. If the cotton is not harvested until the lint has dried, higher quality results. This type of wet weather damage does have a control; a harvest program that restricts operations to periods of optimum moisture conditions of cotton on the stalk.

When cotton is picked too wet or with a seed cotton moisture content above about 10 percent, staining is more frequent and more trash adheres to the lint [1,2]. By the middle of the harvest season, most gins are overloaded and many trailer loads of cotton are kept waiting at the gin yard. The delay accelerates bacterial activity which causes increased discoloration and general deterioration of fiber and seed. After wet cotton reaches the gin, fairly high temperatues are necessary for drying the lint to an acceptable moisture level. This makes the fiber brittle and staple length is often reduced.

Research has shown that relative humidity exerts the greatest control over seed cotton moisture variation with the exception of actual rainfall. Wooten and Montgomery found that after a morning dew a relative humidity of approximately 50 percent is the dividing line between cotton dry enough to pick and cotton that is too wet. Under the usual harvest weather conditions, relative humidity can be used to give a realistic estimate of the seed cotton moisture content on the stalk [3,4].

Defoliation, or the removal of leaves by chemical application, is now practiced on over half of the cotton acreage in the humid belt. Its original purpose was to reduce leaf trash gathered by the ever increasing number of mechanical pickers [5]. In the last few years, it has been recognized as an aid in reducing the moisture content of seed cotton [6]. This study illustrates the change in microclimate that results in cotton fields from defoliation.

The objective of this study is the development of an understanding of moisture variation within cotton fields which will form the basis of a technique for forecasting "safe" picking conditions.

The history of weather observation programs designed to increase the efficiency of the cotton industry dates back many years. The Organic Act of the Weather Bureau enacted in 1890 states its mission in part as ". . . the reporting of temperature and rainfall conditions for the cotton interests . . ." This Act is still in effect and its most

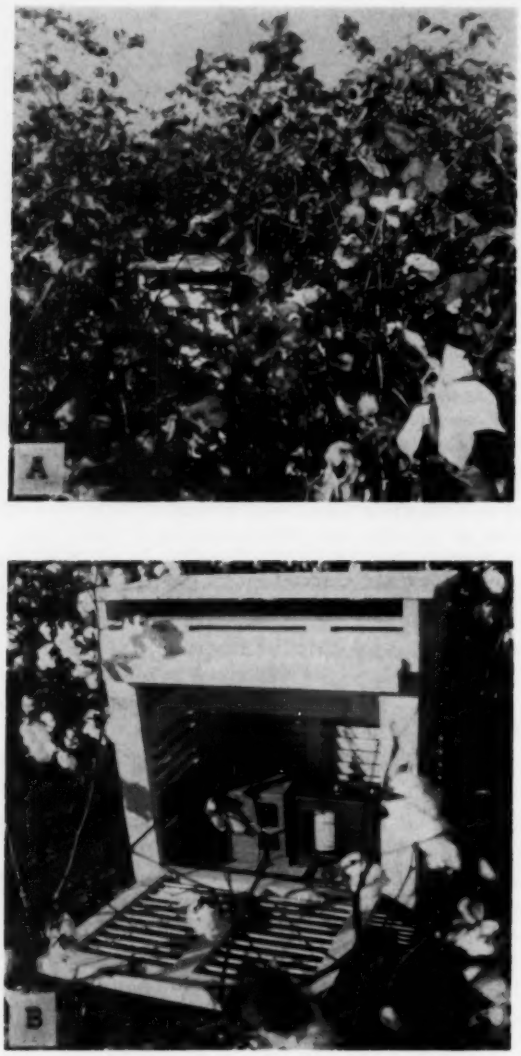

FIGURE 1.—Hygrothermographs in (A) leafed and (B) defoliated cotton fields.

recent implementation is the Delta Agricultural Weather Project, under which the work reported here was done. This study summarizes observations and tests made in cotton fields during the fall seasons of 1958 through 1960. All tests were made in cooperation with the Cotton Harvesting Section of the U.S. Department of Agriculture and the Delta Branch of the Mississippi Agricultural Experiment Station.

Observations were made in Delta Experiment Station cotton fields about one mile south of the Administration Building. The area is free from obstructions and typical of most Delta cotton fields. Deer Creek makes a wide loop around the area at a distance of about 0.4 mile north of the observation site, 0.8 mile to the east, and 0.3 mile to the south. Trees about 50 feet high are scattered along the creek. Measurements were made in both defoliated and undefoliated cotton fields with similar crop cover extending several hundred yards in all directions from the instrument site.

TABLE 1.—*Cross section of leaf, stalk and lint in square feet per cubic foot of space occupied by defoliated and undefoliated cotton plants.*

Leaf cover	Leaf area	Stalk and lint area	Total area
Defoliated	2.5	16.5	19.0
Undefoliated	110.5	16.5	127.0

Because of the remarkably uniform growth characteristics of cotton grown in this experimental field and the scientific farming practices, cotton stands of great similarity were available for microweather observations during the three fall seasons. The average height of the cotton plants did vary slightly: in 1958–59 cotton averaged 5 feet high and in 1960, 4 feet. Leaf density was very similar; table 1 shows the 3-year average values of leaf, and stalk and lint cross-section area in square feet for each cubic foot of space occupied by plants. The leaf area, or the area available for transpiration, in the defoliated field was only 2 percent of the leaf area in the undefoliated field. The total area of leaf, stalk and lint, or the area available for obstruction to wind and sunlight, in the defoliated field was 15 percent of the area in the undefoliated.

2. RELATIVE HUMIDITY AND TEMPERATURE

Relative humidity shows considerable variation in cotton fields and in turn is a key to the variation in seed cotton moisture. The air surrounding cotton plants receives vapor from the transpiring plants, evaporation from moist soil and rainfall, and from mixing with moist air moving northward from the Gulf of Mexico. At night, the air frequently loses water vapor by dew formation but this is usually returned the following day by evaporation. Vapor losses of more importance occur with rising air currents, especially when accompanied by strong dry winds. Most of the diurnal variation in relative humidity, which is an important variable in designing a picking program, is caused by variation in temperature rather than in absolute content of moisture.

Hygrothermographs were placed in instrument shelters at a height of 10 inches above the ground (see fig. 1) and at 54 inches above the ground (top of cotton averaged 60 inches) in both defoliated and undefoliated cotton fields. Table 2 shows the average daily minimum relative humidity and maximum and minimum temperature and temperature range for 35 days without rain from September 22–November 5, 1959.

The minimum daily humidity deep within the plant zone averaged 9 percent lower in the defoliated field than in the leafed field. At the top of the plant zone, relative humidity was slightly higher in the defoliated field. Highest maximum temperatures, which are approximately concurrent with minimum relative humidity, occurred in

TABLE 2.—*Average daily minimum relative humidity and maximum and minimum temperature and temperature range for 35 days without rain from Sept. 22–Nov. 5, 1959, Stoneville, Miss.*

Exposure	Minimum relative humidity	Maximum temperature	Minimum temperature	Temperature range
	Percent	*°F.*	*°F.*	*°F.*
54-inch undefoliated	48.0	75.0	57.8	17.2
10-inch undefoliated	56.8	74.3	57.9	16.2
54-inch defoliated	48.8	79.6	58.0	18.4
10-inch defoliated	47.7	80.9	57.4	23.5

the defoliated field. The largest temperature range was at the low level in the defoliated field and the smallest range was within the plant cover of the leafed field.

The vertical variation of relative humidity in the defoliated field was similar to the variation that occurs above bare ground. In this case, the relative humidity was slightly less near the ground than at the top of the plant. Geiger [7] calls this distribution the "dry type" and indicates that it is very rare, and indeed, he stated that it has been observed only in southern India, particularly over the black cotton soils. It is possible that the instruments used in this experiment are not precise enough to detect a 1 percent difference; however, it was unusual that the relative humidity was not higher near the ground.

The variation in relative humidity in a leafed field is mainly the result of exposure. The low level is sheltered from the sun and wind; thus moisture is not as free to disperse into the atmosphere as from the top of the plant zone. A smaller effect is the lower temperatures caused by shading. Using the 1959 data as an example (table 2), if the maximum temperature of 74.3° F. observed at the 10-inch level were raised to 75.0° F. (the maximum at 54 inches), the relative humidity of the air parcel would be reduced less than one percent. Since the difference in relative humidity between the two levels was actually 8.8 percent, the difference in temperature alone cannot account for the measured difference. The higher humidity at the low level must have been caused by the lack of mixing with drier air above the plant zone.

Observations made during the fall seasons of 1958 and 1960 conformed in pattern to the detail given above for 1959. For the 3-year period, the relative humidity averaged between 8 and 10 percent higher within the plant zone of the leafed field, and the humidity remained below 50 percent for one additional hour in the defoliated field.

3. WIND AND SUNLIGHT

Wind variation.—Air movement acts in both the vertical and the horizontal plane to change the moisture level on and near cotton plants. Wind can completely change temperature and moisture characteristics of air surrounding cotton plants at times of air mass change and cause minor modifications at other times. Vertical air movement mixes the air near the plant with air of differing characteristics at some height above the ground.

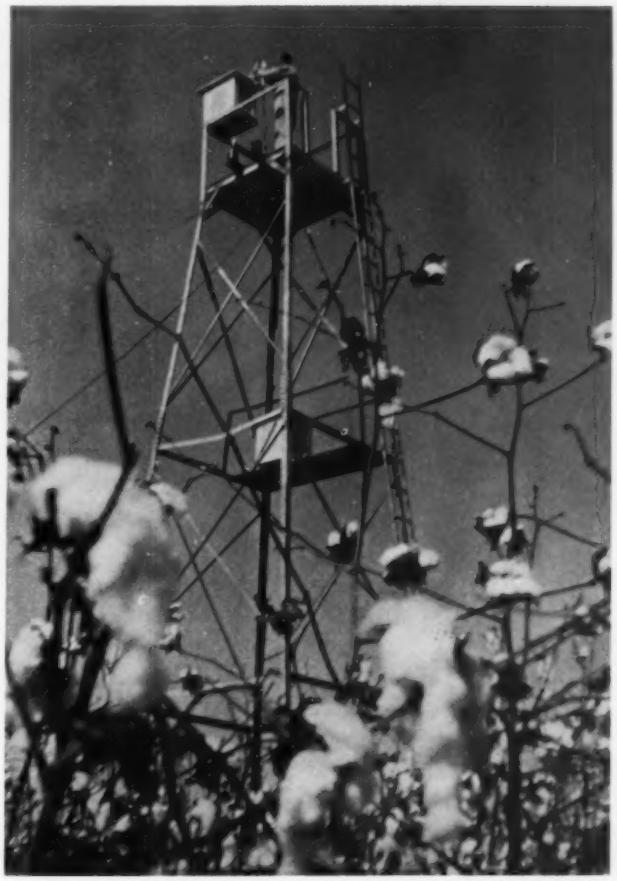

FIGURE 2.—Weather tower in cotton field. Anemometer, hygrothermograph, and Livingston atmometers located on top of tower.

Vertical air movement was not measured directly; however, the air stability which is related to vertical movement was measured. The temperature at 5 feet above the ground minus the temperature at 35 feet was the measurement of air stability used in this study. When the difference was positive, i.e., the temperature near the ground was higher than the temperature at the upper level, the air was more likely to undergo vertical motion by way of turbulent eddies. In this portion of the report, stability and wind are represented by daytime average (7 a.m. to 5 p.m. LST) and nighttime average (5 p.m. to 7 a.m. the next morning). From September 30–November 8, 1960, the daytime stability averaged +1.45° and the nighttime stability, −2.18°; consequently vertical motion was much more of a factor in the daytime than at night.

The wind was measured at 40 feet above the ground on top of the observation tower shown in figure 2 and at 7 feet above the ground which was 3 feet above the defoliated

FIGURE 3.—Anemometer, instrument shelter, and Livingston atmometer (observer refilling atmometer) in cotton fields.

cotton tops shown in figure 3. The wind on the tower averaged 5.27 m.p.h. and at the lower level averaged 2.45 m.p.h. During the daytime, the upper wind averaged 6.50 m.p.h and the lower 3.65 m.p.h.; thus, the lower level was 56 percent of the upper level. At night, the wind averaged 4.40 m.p.h. at the upper level and 1.55 m.p.h. at the lower level. At night the lower wind was only 35 percent of the upper level.

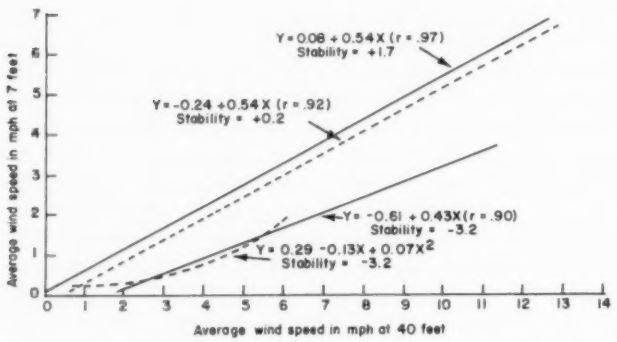
Y = 0.08 + 0.54X (r = .97)
Stability = +1.7
Y = -0.24 +0.54 X (r = .92)
Stability = +0.2
Y = -0.61 + 0.43X (r = .90)
Stability = -3.2
Y = 0.29 -0.13X + 0.07X²
Stability = -3.2
Average wind speed in mph at 7 feet
Average wind speed in mph at 40 feet
0 1 2 3 4 5 6 7
0 1 2 3 4 5 6 7 8 9 10 11 12 13 14

FIGURE 4.—Relationship between wind speed at 40 feet and 7 feet above the ground, above 4-feet high cotton, as a function of air stability at Stoneville, Miss., September 30–November 8, 1960.

The diurnal variation of wind with height above the cotton field is related to the diurnal variation of stability of the air column. Figure 4 shows the relation between winds at the upper and lower levels as a function of stability. The top solid line represents 34 cases of stability between $+1°$ and $+3°$ with an average stability of $+1.7°$. The wind at 7 feet was a little more than half as strong as the wind at 40 feet.

The dashed straight line represents 22 cases of air stability between $+1°$ and $-1°$, with an average stability $+0.2°$. This average stability figure means that the temperature at the 5-foot level averaged nearly the same as the temperature at the 35-foot level. In this case there was practically no wind at the 7-foot level when the wind at 40 feet was 0.7 m.p.h. or less. The wind at 7 feet was usually about half as strong as the wind at 40 feet with a wind of 5 m.p.h. or more at the 40-foot level.

The lower solid straight line represents 24 cases when the air stability was between $-1°$ and $-6°$, or an average of $-3.2°$. All of these cases occurred at night and represent very stable air; i.e., there was little or no vertical mixing of the air in the lower 40 feet above the ground. On this type of night, the wind was practically zero at the 7-foot level with a wind of 2 m.p.h. at 40 feet. With an average wind speed of 10 m.p.h. at 40 feet, the

TABLE 3.—*The average wind speed in defoliated and leafed fields at 2 feet above the ground (cotton plants 4 feet high) and at 7 feet and 40 feet above the ground, Nov. 1–8, 1960, Stoneville, Miss.*

Time (1st)	Undefoliated, 2 feet above ground	Defoliated, 2 feet above ground	7 feet above ground	40 feet above ground
7 a.m.–5 p.m.	0.33	1.29	5.22	9.02
5 p.m.–7 a.m.	0.01	0.04	1.96	5.66

wind at 7 feet was only about 3 m.p.h. under stable conditions.

The dashed curved line is a parabola representing the same conditions shown in the lower solid straight line (stable air). This curve is valid only for wind speeds of about 1 to 6 m.p.h. at 40 feet and is included to emphasize the stilling influence of very stable conditions; the air was practically calm at 7 feet with less than 4 or 5 m.p.h. at the 40-foot level.

During the period of November 1–8, 1960, wind readings were made at a height of 2 feet above the ground in fields of defoliated and undefoliated cotton about 4 feet high. During this period, the defoliated field offered only about 30 percent as much surface leaf, stalk, and boll obstruction to wind as did the leafed field. Table 3 shows the average daytime and nighttime wind speed in the defoliated and leafed fields at 2 feet above the ground and at the 7-foot and 40-foot levels.

Practically no wind occurred within the cotton foliage at night unless the prevailing wind was relatively strong, at least 10 m.p.h. Daytime wind speeds in the defoliated cotton averaged only 25 percent of the wind at 7 feet and the wind in the leafed cotton was only 6 percent of the wind at 7 feet. At night, the wind speed in the defoliated cotton was only 2 percent of the 7-foot wind while the wind in the leafed field was less than 1 percent of the 7-foot wind.

Sunlight variation.—The difference between the amount of water evaporated from a white and a black Livingston atmometer gives an indication of sunlight or solar radiation [8]. Table 4 shows the total evaporation from the white and black atmometers at 32 feet (unobstructed location) and at 26 inches (within a leafed field) and the percentage of increase in evaporation of the black over the white.

At the unobstructed location, evaporation from the black atmometer totaled 57 percent more than from the white atmometer. Within the leafed field, evaporation from the black atmometer totaled 16 percent more than from the white atmometer. The percentage increase in the leafed field amounted to only 28 percent of the percentage increase at the unobstructed location. This 28 percent can be assumed to approximate the amount of sunlight that reached the inner zone of a leafed cotton field. Less than a third of the sunlight that was available to the top of a 4- to 5-foot cotton plant was available to the middle of the plant.

TABLE 4.—*Evaporation from Livingston atmometers and percent increases of black over white at an unobstructed area and within cotton foliage, Sept. 30–Nov. 8, 1960, Stoneville, Miss.*

Exposure	Evaporation		Percent increase of black over white
	White	Black	
32 feet—unobstructed	1012	1591	57.2
26 inches—within leafed cotton	300	349	16.3

Both wind and vertical air currents are at a maximum in the daytime and are usually quite small at night. Wind increases with increasing height and with decreasing amounts of leaf obstruction. Sunlight is much reduced within the leaf canopy. Higher humidity and consequently higher seed cotton moisture content in well leafed fields, as compared with defoliated fields, is in part related to the absence of wind and sunlight in the leafed area.

4. DEW INTENSITY

Dew is a frequent and important cause of wet cotton and must be considered in designing a cotton harvest program. The daily probability of rain is under 20 percent while the probability of dew is over 80 percent in the Delta during the harvest season.

Dew was collected at the observation site on thin, painted, metal sheets. On nights with heavy dew, approximately 2 $cm.^3$ of water condensed on each 100 $cm.^2$ of surface. This is assumed to be fairly representative of dew that formed on cotton plants and is the moisture equivalent of about 0.01 inch of rain. For purposes of this report dew was classified as: none, light, moderate, heavy. Rain fell on 5 nights of the 40-day observation period, September 30–November 8, 1960 and these intervals were omitted from this portion of the report.

Huschke [9] lists the following conditions as favorable for dew formation: " (a) a radiating surface, well insulated from the heat supply of the soil, on which vapor may condense; (b) a clear, still atmosphere with low specific humidity in all but the surface layers, to permit sufficient effective terrestrial radiation to cool the surface; and (c) high relative humidity in the surface air layers, or an adjacent source of moisture such as a lake."

The availability of moisture is very rarely the limiting factor in dew formation in the Delta because of the many lakes and ponds in the area. During periods of extended drought, the availability of moisture is vastly reduced. Many of the lakes and ponds dry out and trees and crops under moisture stress do not supply much moisture by transpiration. During the drought years in the early 1950's the lack of local moisture was a limiting factor in dew formation; however, it has not been a factor in the 3 years of current Weather Bureau experiments in cotton fields.

Relative humidity in relation to dew intensity.—To determine the relationship between relative humidity and

TABLE 5.—*Relative humidity at 5 feet above the ground, 1 foot above defoliated cotton, as related to dew intensity Sept. 30–Nov. 8, 1960, Stoneville, Miss.*

Dew intensity	Average relative humidity 1 a.m.–6 a.m.	Percent of nights relative humidity did not reach 100 percent	Average relative humidity on preceding day		
			10 p.m.–12 midnight	7 p.m.–9 p.m.	1 p.m.–3 p.m.
Heavy	100	0	98	92	42
Moderate	100	0	96	89	43
Light	91	22	78	66	53
None	83	67	83	83	54

TABLE 7.—*Relation of dew intensity and average wind speed in m.p.h. from 5 p.m. to 7 a.m. at two levels above cotton fields at Stoneville, Miss., Sept. 30–Nov. 8, 1960.*

Dew intensity	Average speed 7 feet above the ground or 3 feet above defoliated cotton plants	Average speed 40 feet above the ground
	m.p.h.	*m.p.h.*
Heavy	0.42	2.46
Moderate	.89	2.99
Light	1.75	5.46
None	3.10	6.81

dew intensity on cotton fields, the humidity was measured at a height of 5 feet above the ground, which was 1 foot above the top of a defoliated cotton field. As shown in table 5, the relationship varied with the time of day. After midnight, there was a close direct relation between relative humidity and dew intensity. Between the preceding afternoon's relative humidity and dew occurrence next morning, the relation was inverse. There was very little relation between humidity during the early evening and dew intensity the following morning.

During nights with heavy dew the air remained saturated; relative humidity equaled 100 percent from 1 a.m. to 6 a.m. During 5 of the 7 nights with moderate dew, the humidity was 100 percent continuously during that period, but with light or no dew it was never continuously 100 percent for the 5-hour period.

On nights with heavy dew the average time of saturation was 12 p.m. (midnight) and the latest time of saturation was 1 a.m. With moderate dew, the air reached saturation about 1½ hours later. On nights of light or no dew, the air was saturated for only very brief periods if at all.

Table 5 shows that the highest humidities for nighttime periods before midnight occurred with moderate to heavy dew. In the case of light dew and no dew, higher humidities occurred with no dew. At such times, fairly high humidity in the evening was accompanied by cloudiness but the clouds persisted through the night and prevented the ground from cooling and thereby prevented saturation.

The last column of table 5 shows that low afternoon humidities often preceded high dew intensity. This merely indicates that clear days were usually followed by clear nights and the large diurnal temperature change gave low relative humidities in the day and high values at night.

Cloud cover in relation to dew intensity.—The variable used to represent cloud cover in this experiment was the percent of opaque sky cover, excluding obstruction by fog, from the hours of 7 p.m. through 6 a.m. as measured by the Greenwood FAA station 43 miles to the east. The distance between the two observation points introduces a small error; however, the difference is usually quite small. Table 6 shows that an average of 72 percent opaque sky cover occurred on nights with no dew formation. The effect of lesser cloud amounts was indeterminate.

Wind speed in relation to dew intensity.—Table 7 shows the average wind speed from 5 p.m. to 7 a.m. as recorded at 7 feet above the ground and at 40 feet above the ground. The speed at 7 feet is indicative of conditions 3 feet above defoliated cotton plants and the speed at 40 feet compares with wind observations at airport stations in the area. Moderate to heavy dew was associated with average winds at 40 feet of less than 3 m.p.h., light dew with average winds of 5–6 m.p.h., and no dew with an average of about 7 m.p.h.

Table 8 shows the relation of dew intensity to air stability. On nights with no dew, the average stability was not far from zero; this means that the air in the first 30 feet above the cotton plant was near neutral stability; i.e., vertical motion was possible most of the time. On nights with dew, the air was normally quite stratified and little vertical motion occurred. Occasionally heavy dew occurred on cotton plants while the top of the tower was dry, indicating a very shallow temperature inversion. Since the inversion height is normally above the tower top, the stability measurements of this experiment can differentiate between dew and no dew but cannot be used to forecast dew intensity.

TABLE 6.—*Relation of percent opaque sky cover, excluding fog, as measured by the Greenwood, Miss., FAA station during the hours of 7 p.m. through 6 a.m., to dew intensity at Stoneville, Miss. Sept. 30–Nov. 8, 1960.*

Dew intensity	Percent of opaque sky cover
Heavy	8
Moderate	5
Light	4
None	72

TABLE 8.—*Relation of dew intensity to air stability as measured by the temperature at 5 feet above the ground minus the temperature at 35 feet above the ground from 5 p.m. to 7 a.m. Sept. 30–Nov. 8, 1960, Stoneville, Miss.*

Dew intensity	Average stability
Heavy	−2.49
Moderate	−2.63
Light	−3.90
None	−.27

Combined effect of cloud cover and wind on dew intensity.—Cloud cover and wind speed normally do not undergo extreme changes during the night, but there are exceptions. For example, a thundershower or a front may move through the area during the evening giving gusty winds and cloudy skies up until midnight, while after midnight, clear calm conditions may prevail. Clear calm weather normally produces a moderate to heavy dew. Both cloud cover and wind speed are represented by a nightly average in this experiment; thus it is not possible to account for the rare occurrences of radically changing weather during the night.

Figure 5 shows the four classes of dew intensity as a function of cloud cover and wind speed at 40 feet. In table 6, the lower range of cloud cover shows little relation to dew intensity. Consequently, in figure 5, the classes of dew intensity for cloud cover of less than 20 percent are related almost exclusively to wind speed.

As both wind and cloud cover are regularly forecast, it might be possible to use the relation shown in this graph to make regular forecasts of dew intensity. This has not been tested on independent data.

5. EVAPORATION

Evaporation from a water surface in an enclosed container is a relatively simple process compared with evaporation from a field of cotton. Inside the container, an equilibrium is established between water molecules escaping from the water surface and those returning to the surface. In an open cotton field equilibrium is a rare condition; normally moisture is being taken away by evaporation or added by dew formation.

Evaporation was measured at 3 levels in both defoliated and undefoliated fields during the period 7:45 a.m. to 5:00 p.m. on 35 days without rain, September 22–November 5, 1959. Table 9 shows that evaporation at the 10- and 21-inch levels in the defoliated field was nearly twice that in the undefoliated field. Even at the 54-inch level, which was only 6 inches below the top of the plant, evaporation was greater in the defoliated field.

The evaporation observations during 1960 included the addition of two black Livingston atmometers. Because of the different radiation absorption characteristics of the white and black atmometers, the difference in evaporation between the two atmometers gives a measure of solar radiation. Observations in 1960 also included

TABLE 9.—*Average evaporation from Livingston atmometers in 5-foot-high defoliated and undefoliated cotton fields on 35 days without rain during the period 7:45 a.m. to 5:00 p.m., Sept. 22–Nov. 5, 1959, Stoneville, Miss.*

Height above ground (inches)	Evaporation (cm.³)	
	Undefoliated	Defoliated
10	9.8	18.1
21	10.7	19.2
54	23.1	24.9

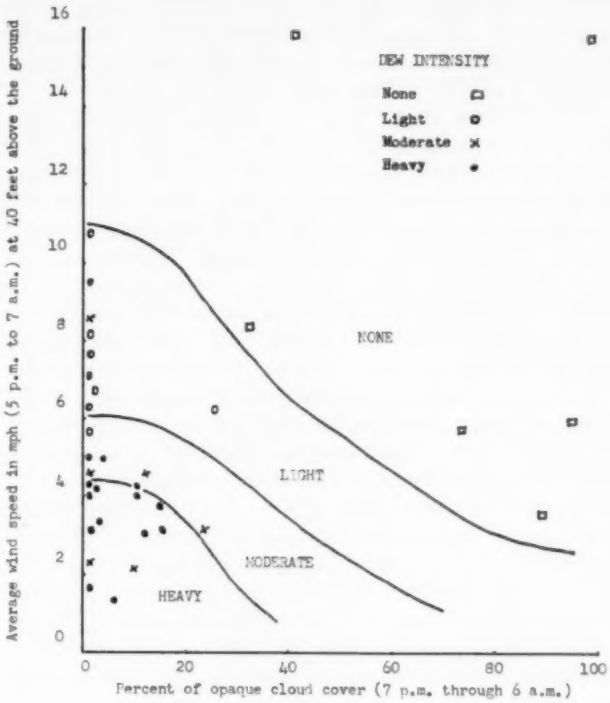

FIGURE 5.—Dew intensity in relation to percent of opaque cloud cover from 7 p.m. through 6 a.m. and to average wind speed in m.p.h. from 5 p.m. to 7 a.m. at 40 feet above the ground, Stoneville, Miss., September 30–November 8, 1960.

evaporation readings, both black and white, made on the weather tower shown in figure 2.

Table 10 summarizes evaporation readings made during the period 7 a.m.–5 p.m., September 30–November 8, 1960. Evaporation was directly proportional to the height above the ground and inversely proportional to the amount of obstruction. Within the two types of cotton fields, evaporation was almost twice as great in the defoliated field, in agreement with measurements made the year before.

The variation in evaporation between the 5-foot and

TABLE 10.—*Average evaporation from Livingston atmometers at different heights and different exposures during the period 7 a.m.–5 p.m., Sept. 30–Nov. 8, 1960, Stoneville, Miss. The latter two columns relate evaporation at individual locations to evaporation at 5-foot level*

Height	Type	Exposure	Average evaporation	Estimation of 5-foot evaporation	Correlation coefficient
32.2 feet	White	Unobstructed	25.3	$Y=1.31+1.21X$	0.972
32.2 feet	Black	Unobstructed	39.8	$Y=4.51+1.78X$	.982
5.0 feet	White	1 foot above defoliated.	19.8		
26 inches	White	Defoliated	15.9	$Y=0.44+0.78X$	.976
18 inches	White	Defoliated	14.0	$Y=0.28+0.69X$	.970
26 inches	White	Undefoliated	8.9	$Y=-1.74+0.53X$	.935
18 inches	White	Undefoliated	7.5	$Y=-1.77+0.47X$	.892
18 inches	Black	Undefoliated	8.7	$Y=-2.03+0.54X$	.908

32-foot levels was primarily due to stronger winds at the upper level. The variation between readings in fields of different leaf cover was caused by differing relative humidity, amounts of sunshine, and wind speeds.

The fifth column in table 10 contains regression equations which estimate the evaporation at the 5-foot level as a function of the individual location. The last column gives correlation coefficients which show the relation between the evaporation at the various observation points and the evaporation at the 5-foot level. The evaporation at each of the various observation points appears to be closely related to the evaporation at the 5-foot level.

Readings within the leafed field, although highly correlated showed the poorest relation. This lower correlation is believed to have been caused by a slight change in leaf cover that occurred during the experiment, and not by any fundamental difference in relation to measured variables. A light frost occurred October 21 and a few top leaves were killed. They dried up during the last of October and subsequent frosts killed more leaves early in November. Besides offering less resistance to wind and sunlight, the dried leaves late in the season did not transpire as much moisture; thus the sheltered, moist climate that extisted through the first two-thirds of October was modified considerably by the end of the period.

To obtain an estimate of how the evaporation within the leafed field increased during the experiment, the 10-day total evaporation at the 5-foot level was divided into the 10-day total evaporation from the various levels within the cotton fields. Table 11 shows these measures.

Evaporation in the undefoliated cotton field using the 5-foot reading as a standard shows some increase during the third period and a sharp increase during the last 10-day period. This undoubtedly was due to the reduction of leaf cover, and to a lesser extent to the aging of the existing leaf cover as cold weather advanced. One interesting point is that the black atmometer in the leafed field had less evaporation than the white atmometer 8 inches higher during the first 30 days of the period; but, during the last 10 days, the condition reversed. This was caused by the increase in sunlight within the leafed field as the leaf cover gradually became less. For comparison purposes, evaporation at the same heights in the defoliated field are included. Variations occurred there too, but were smaller and in the opposite direction to the changes in the leafed field; this tends to emphasize the drying effect that occurred in the leafed field with the advance of the season.

TABLE 11.—*10-day total evaporation (cm.³) from different instruments within cotton fields divided by the 10-day total at the 5-foot level*

Periods	Defoliated cotton		Undefoliated cotton		
	White		White	White	Black
	26 in.	18 in.	26 in.	18 in.	18 in.
Sept. 30–Oct. 9	0.810	0.719	0.354	0.268	0.341
Oct. 10–Oct. 19	.895	.783	.364	.296	.340
Oct. 20–Oct. 29	.816	.719	.487	.391	.459
Oct. 30–Nov. 8	.752	.668	.544	.508	.572

Evaporation is measured by a number of different methods and each tends to give a different estimate of the same elusive weather element. Pan evaporation was measured regularly at the Stoneville weather station from April 1 to October 31. For the month of October, the evaporation from the 5-foot Livingston atmometer was related significantly, at the 1 percent level, to pan evaporation. Total evaporation from the Livingston atmometer was 710 cm.³ and from the pan, 3.44 inches. It is much easier to read 2-cm.³ evaporation from the Livingston atmometer than it is to read the comparable evaporation of 0.01 inch from the pan. In addition the Livingston atmometer can be moved more easily. The aerodynamics of the two different evaporimeters are different and it is believed that Livingston atmometers are much better suited to this type of investigation.

To evaluate weather elements that influence evaporation, and thus drying power near cotton plants, various measurements of sunshine, relative humidity, wind, and temperature were related to the daily evaporation at the 5-foot level for the period September 30–November 8, 1960.

Sunshine intensity in total langleys per day and the average relative humidity from 1 p.m. to 3 p.m. at the 5-foot level were found to be related significantly at the 1 percent level to the evaporation. Average wind speed from 7 a.m. to 5 p.m. at the 7-foot level was related significantly at the 5 percent level to the evaporation. No measure of temperature including maximum, minimum, and afternoon average, and no value of air stability was found that gave a reliable estimate of evaporation during the 40-day period in 1960.

The following multiple regression equation relates certain weather measures to evaporation:

$$X_1 = 13.781 + 0.196X_2 - 0.232X_3 + 0.034X_4$$

where X_1 is total evaporation (cm.³) at 5 feet from 7 a.m. to 5 p.m.; X_2 is average wind speed (m.p.h.$\times$10) at 7 feet from 7 a.m. to 5 p.m.; X_3 is average relative humidity (percent, with decimal point ignored) at 5 feet from 1 p.m. to 3 p.m.; X_4 is sunshine intensity in total langleys per day.

The coefficient of multiple correlation for the above equation is 0.913, the standard error of estimate is 3.58. The standard error of estimate for each pair of variables is: wind and relative humidity, 4.04; wind and sunshine, 4.17; and relative humidity and sunshine, 4.71. The combination of wind and relative humidity gives the smallest error, while the combination wind and sunshine is only slightly higher. Sun and relative humidity give the largest error. The reason is the interrelation of the

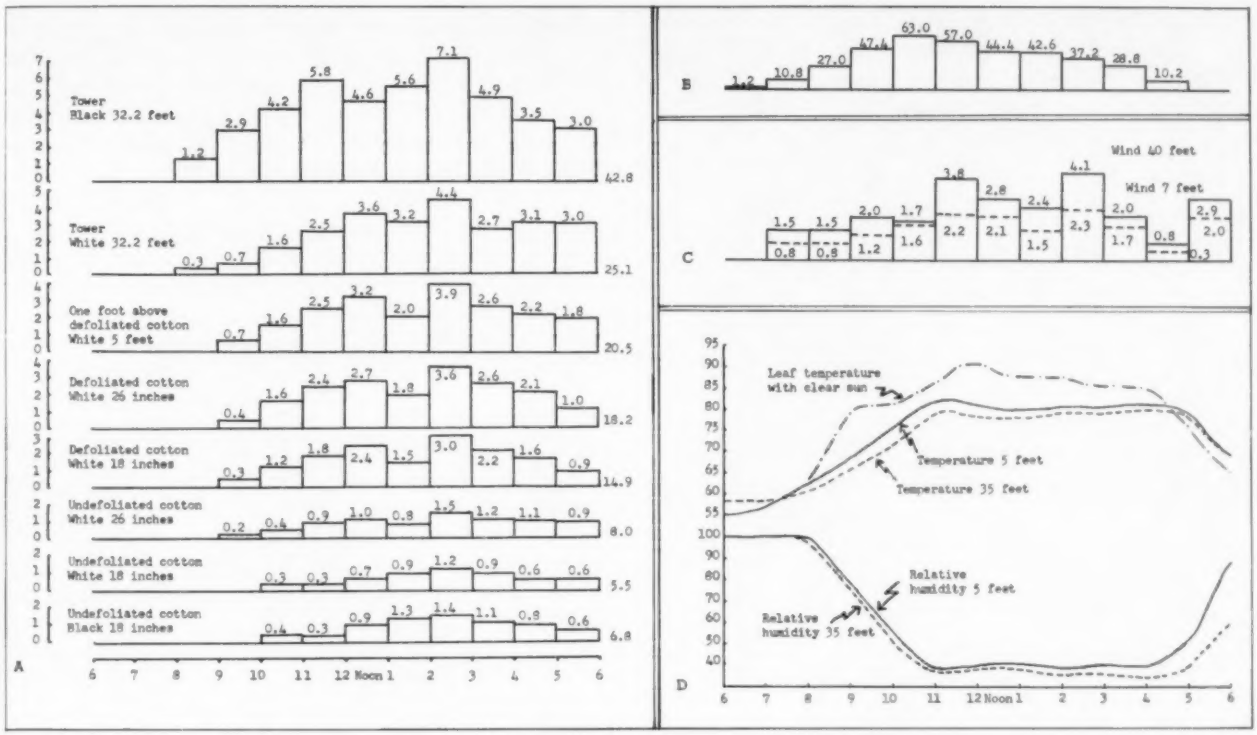
Tower Black 32.2 feet
Tower White 32.2 feet
One foot above defoliated cotton White 5 feet
Defoliated cotton White 26 inches
Defoliated cotton White 18 inches
Undefoliated cotton White 26 inches
Undefoliated cotton White 18 inches
Undefoliated cotton Black 18 inches
A
B
C
Wind 40 feet
Wind 7 feet
Leaf temperature with clear sun
Temperature 5 feet
Temperature 35 feet
Relative humidity 5 feet
Relative humidity 35 feet
D
6 7 8 9 10 11 12 Noon 1 2 3 4 5 6

FIGURE 6.—Hourly weather observations in or near cotton fields, Stoneville, Miss., October 12, 1960. (A) Total hourly evaporation in cm.^{3} (B) Total hourly solar radiation in langleys hr.$^{-1}$ (C) Average hourly wind speed in m.p.h. (D) Temperature in °F. and relative humidity in percent.

two variables; i.e., sunny days are generally dry (low relative humidity) and vice versa. The partial correlation coefficients are: wind, 0.65; relative humidity, 0.52; and sunshine, 0.46. Wind is shown to be the most important single factor in the multiple regression equation, despite the fact that it had a smaller simple correlation coefficient. The effect of holding the mutually related relative humidity and sunshine constant is to increase the importance of wind.

Figures 6 A–D show detailed measurements for one day during the experiment, October 12, 1960. High pressure with dry mild air centered over Tennessee extended into the Delta. A few tenths of altocumulus clouds around sunrise cleared by 8 a.m. Small, scattered, fair weather cumulus prevailed from 10 a.m. to 5 p.m. Dew was heavy at 7 a.m., disappearing from defoliated cotton about 9 a.m. and from undefoliated cotton about 10 a.m. Light dew formed again on exposed surfaces on both fields about 6:30 p.m. Such weather is typical of a fairly good cotton picking day in the Delta.

Figure 6A shows hourly evaporation totals at different heights and different exposures. As indicated earlier, evaporation increased with increasing exposure (lack of leaf and stalk obstruction) and with increasing height above the ground. Besides the variation in total amount, it is of interest to note the time lag of maximum evaporation that occurred within the cotton fields as compared with more exposed locations. The first measurable evaporation occurred on the tower during the hour 8–9 a.m. Measurable evaporation did not occur at the 18-inch level in the leafed field until 2 hours later, 10–11 a.m. Evaporation at the exposed locations showed an early peak during the hours of 11 a.m. to 1 p.m., with another peak from 2–3 p.m. The early peak, although greatly damped in amplitude, extended to the 26-inch level in the leafed field. At the 18-inch level in the leafed field, there was a single maximum at 2–3 p.m., but the black atmometer did show a rather sharp increase from 11 a.m. to 1 p.m.

Figure 6B shows the greatest hourly solar radiation, 63 langleys, occurred from 10 to 11 a.m. Scattered small cumulus clouds caused sunlight to fluctuate considerably after 11:20 a.m. The maximum hourly evaporation at all levels occurred from 2–3 p.m., which was several hours after the time of maximum solar radiation.

Figure 6C shows an early maximum of wind from 11–12 a.m. The greatest wind was measured from 2–3 p.m., which was also the period of greatest evaporation at all levels.

Figure 6D shows the temperature and relative humidity variation throughout the day. Temperature reached a maximum and relative humidity a minimum about 11

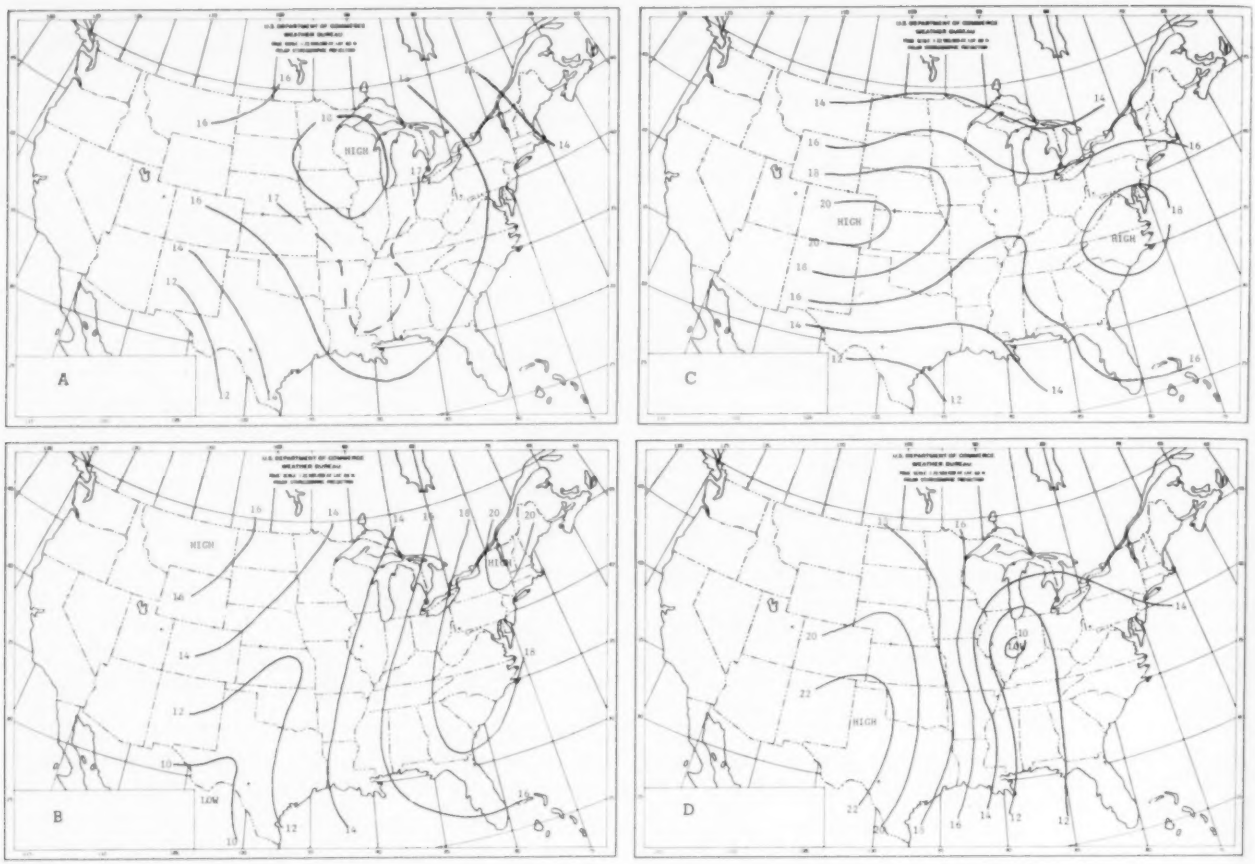

FIGURE 7.—Average sea level pressure in millibars at 12 a.m. (A) Heavy dew. (B) No dew with southerly winds. (C) No dew because of rain. (D) No dew with northerly winds. Stoneville, Miss., September 30–November 8, 1960.

a.m. and only minor changes occurred until after 4 p.m.

Leaf temperature readings as shown in figure 6D, were made when the sun was not obscured by clouds. Small electrically recording temperature probes, normally used to measure temperature inside fruit, were taped onto the bottom portion of leaves. Leaves that were measured were alive and green but rather dry and apparently transpiring very little. The maximum difference between the leaf temperature and the air temperature at 5 feet occurred shortly after noon, during a period of maximum sunlight. At that time, the leaf temperature was 11° higher than the surrounding air temperature. Differences between leaf and air temperature on this day were typical of readings made on several other fairly clear days. The leaf temperature was a little below the air temperature early in the morning until the dew was nearly all evaporated (usually between 8 and 10 a.m.), then the leaf was warmer than the air until just before sunset. When the leaf no longer received direct solar radiation (usually 4–5 p.m.), it became colder than the air. During the period of dusk, with clear skies, the leaf was about 5° cooler than the air, which of course is a necessary condition for dew formation. On the day shown in figure 6D, dew had begun to form on well exposed leaf and stalk surfaces by 6:30 p.m.

6. RELATION OF DEW AND EVAPORATION TO PRESSURE PATTERNS

Dew intensity and sea level pressure patterns.—Figure 7 shows the average sea level pressure pattern for 13 cases of heavy dew. High pressure is the significant feature; however, there are two different locations of the high center that give dew in the Delta. The small knob of high pressure that appears over central Mississippi in figure 7A reflects four cases where a high pressure system just to the south of the Delta was associated with heavy dew. The larger and more pronounced high pressure system to the north represents the average center on the nine other nights of heavy dew.

Figure 7B shows the average sea level pressure pattern for four nights of no dew. Figure 7C shows the pattern of five nights on which rain fell and no dew formed and figure 7D shows the average pattern for the two remaining nights of no dew.

The nights comprising figure 7B were grouped together because the wind was from the south in the Delta. The wind at 40 feet averaged 4.3 m.p.h. and the cloud cover averaged 73 percent. North wind prevailed during the nights grouped in figure 7D; here the wind was much stronger, 11.8 m.p.h., and the cloud cover was about the same, 72 percent.

It is interesting to note that the three maps of no dew seem to form a series showing a trough of low pressure, or a front, moving from northwest through the Delta. With an approaching front, increasing cloudiness prevents dew. When the front is overhead, rain combined with cloud cover prevails, and immediately after the front has passed, gusty winds prevent dew.

Strong frontal passages as far south as the Delta are rare in September and the first half of October; during that period cloudiness and wind associated with weak fronts or instability lines are the usual conditions limiting dew formation. Later in the year, active fronts and more pronounced low pressure systems are the limiting factors. In most cases, cloudiness is the limiting factor in dew formation before the middle of October. It is very rare to have a night with no dew before mid-October. After the middle of October, wind is the main limiting factor and nights with no dew become somewhat more frequent.

Evaporation and sea level pressure patterns.—Figure 8A shows the average sea level pressure pattern at 12 a.m. on the days when evaporation totaled 30 cm.[3] or greater. Figure 8B shows the same data for six days when the evaporation totaled less than 10 cm.[3] The first map, showing strong drying conditions, features a low pressure trough from the Texas Panhandle through southwestern Nebraska to Lake Superior, a high pressure center just south of the Delta, and relatively strong pressure gradient just north of the Delta that would bring dry air and rather gusty winds from the west. Figure 8B, showing poor drying weather, features a weak trough from southern Texas through western Arkansas to Lake Michigan, high pressure over Colorado and the Virginias, and a weak pressure gradient over the Delta that would bring light, moist south to southeast winds over the Delta.

The charts indicate that the strength of the westerly wind over the area just west of the Delta is the most important synoptic feature. Strong westerly winds give good drying conditions, while southeasterly winds give poor drying conditions. As a measure of the strength of the westerly winds, the 12 a.m. sea level pressure at Galveston (p_{GLS}) was subtracted from the pressure at Sioux City (p_{SUX}) and the following regression equation developed:

$$\text{Evaporation (at 5 feet)} = 19.49 - 0.07\ (p_{SUX} - p_{GLS})$$

The correlation coefficient relating the sea level pressure difference between the two stations to the evaporation has been about the same magnitude as the correlation coefficient relating the local wind speed at 7 feet to the evaporation reading.

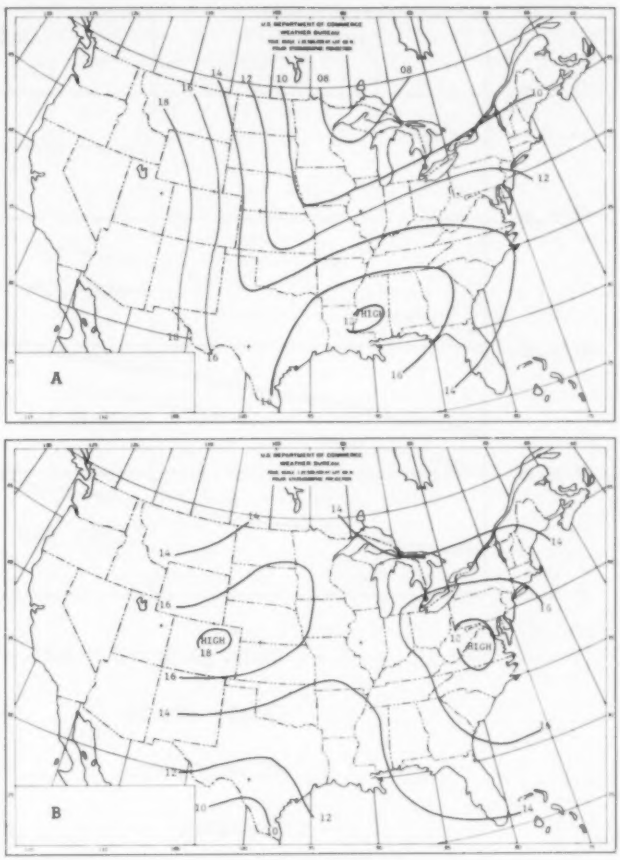

FIGURE 8.—Average sea level pressure in millibars at 12 a.m. (A) Six days with evaporation from Livingston atmometers at 5 feet above the ground (one foot above defoliated cotton) of 30 cm.[3] or more. (B) Six days when evaporation was less than 10 cm.[3] Stoneville, Miss. September 30–November 8, 1960.

7. ESTIMATING PICKING TIME

Figure 9 shows a cotton picking guide designed jointly with the Cotton Harvesting Section of the U.S. Department of Agriculture. The graph is based on average conditions measured during the falls of 1958 and 1959. The three major variables are: time of year, leaf cover, and dew intensity. Minor modifications are made by considering cloudiness and wind. By using the guide, an individual farmer in the Mississippi Delta can make an early morning estimate of when his cotton will be dry enough to harvest.

8. CONCLUSION

Observations taken within cotton fields during the harvest season indicated that relative humidity variation was strongly influenced by the amount of leaf cover. Daytime humidities were higher deep within a leafed plant zone than near the top. Relative humidity at midday averaged 9 percent lower in defoliated fields

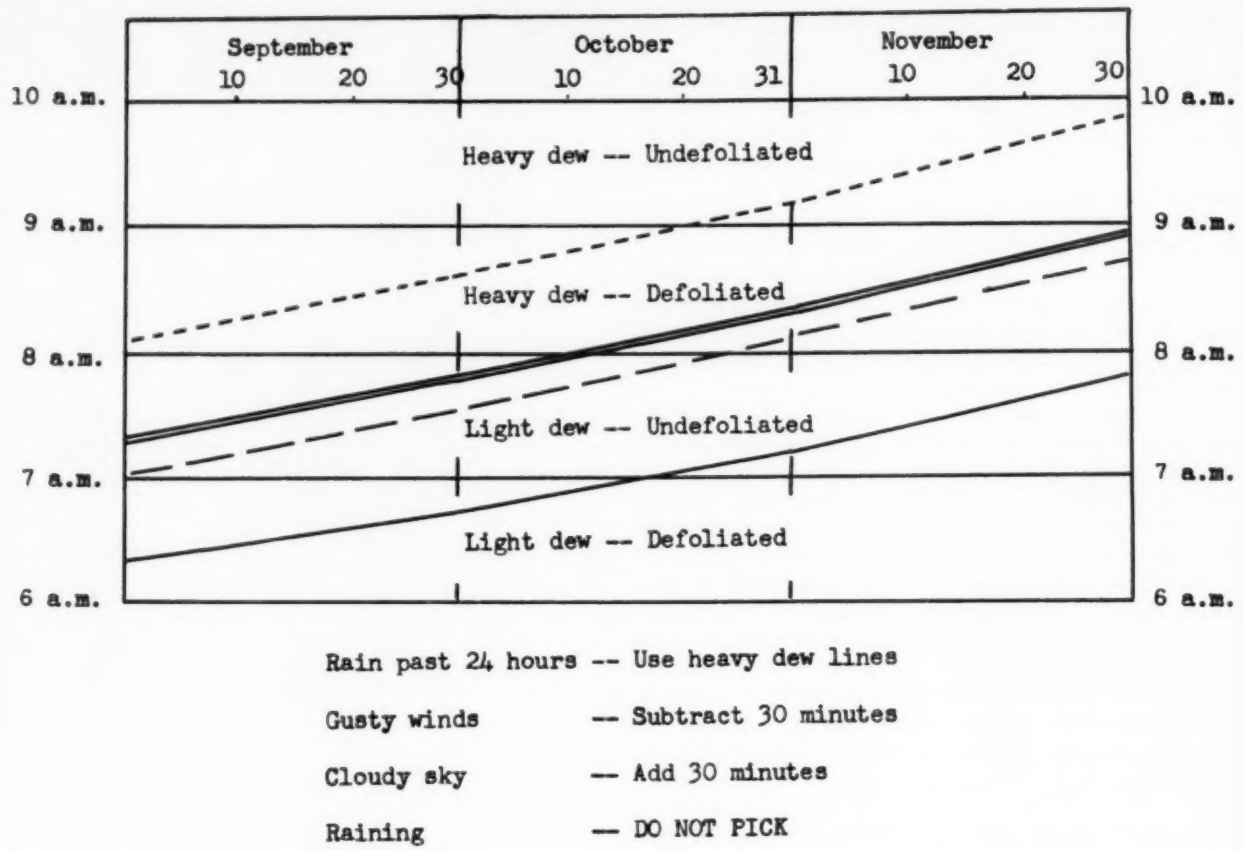

FIGURE 9.—Daily guide for beginning mechanical cotton picking, Mississippi Delta Area, designed jointly by the Cotton Harvesting Section, ARS, and the Weather Bureau.

than in leafed fields. It normally stayed below 50 percent, an estimate of "safe" picking conditions, for an additional hour in defoliated fields.

Wind and sunlight within a cotton field were found to be inversely proportional to the amount of leaf cover. The decrease of wind and sunlight within the cotton field was related to the variation of relative humidity at the same level. Sunlight was much reduced within a leafed cotton field. Less than a third of the sunlight measured at the top of 4-foot-high cotton penetrated to within 1½ feet of the ground. Wind increased with increasing height above the ground and decreasing amounts of obstruction. At 2 feet above the ground in the cotton fields, daytime winds in a leafed field averaged only 6 percent of the wind at 7 feet above the ground and in a defoliated field they averaged 25 percent of the wind at 7 feet above the ground.

Dew is the most frequent wetting factor in cotton fields at harvest time. Heavy dew occurred with clear skies, light winds, stable air, and high nighttime humidities in cotton fields. In the cases studies here, a large high pressure system at sea level over, or north of, the Delta was associated with heavy dew; low pressure, especially in the form of a northeast-southwest trough in the area, was associated with no dew.

High values of evaporation were favored by strong sunlight, low humidities, and strong winds. Evaporation was twice as great in a defoliated field as in a leafed field. In addition to the difference in total evaporation, there was a time lag in evaporation in the leafed field. A strong westerly flow of air, as indicated on the sea level map, was the best synoptic predictor of high rates of evaporation in the Delta.

The cotton picking guide designed jointly with the Cotton Harvesting Section of the U.S. Department of Agriculture gives the farmer an early morning estimate of when his cotton will be dry enough to harvest. Further studies relating weather variations to seed cotton moisture variation and objective techniques for forecasting dew and evaporation are expected to refine the guide with an end in mind of giving the farmer a technique for planning his picking activities at least 12 hours in advance.

ACKNOWLEDGMENTS

The studies reported in this paper are part of a joint project with the Cotton Harvesting Section of the U.S. Department of Agriculture and the Delta Branch of the Mississippi Agricultural Experiment Station. Grateful acknowledgment is expressed to Engineers E. B. Williamson and O. B. Wooten for design and implementation of the project. Valuable suggestions were made by Dr. Wm. L. Giles, Station Superintendent (now Vice President for Agriculture of Mississippi State University), and by the Cotton Quality Improvement Committee of the Delta Council. Timely insecticide applications by the Entomology Section saved the experimental site from possible damage on several occasions during the 3-year project and valuable assistance was received from the Cotton Physiology Section. Mr. L. L. Means, Chief, Public and Agricultural Forecasts Section, Weather Bureau, provided encouragement and numerous helpful suggestions throughout the project.

REFERENCES

1. O. B. Wooten, and R. A. Montgomery, "The Effects of Relative Humidity and Spindle Moisture on Machine-Picked Cotton," *Cir. 204*, Mississippi State University, April 1956.
2. O. B. Wooten, R. A. Montgomery, and J. A. Riley, "Relationship of Moisture to Machine Picking of Cotton," Paper presented at Southeast Sectional Meeting, American Society of Agricultural Engineers, Feb. 1959.
3. J. A. Riley and E. B. Williamson, "Relative Humidity in Cotton Fields at Harvest Time," *Bul. 581*, Mississippi State University, July 1959.
4. E. B. Williamson and J. A. Riley, "The Interrelated Effects of Defoliation, Weather, and Mechanical Picking on Cotton Quality," Paper presented at Winter Meeting, American Society of Agricultural Engineers, Dec. 1960.
5. G. B. Crowe and H. R. Carns, "Economics of Cotton Defoliation," *Bul. 552*, Mississippi State University, June 1955.
6. J. A. Riley and E. B. Williamson, "Defoliation—a Modification of Cotton Harvesting Conditions Through a Modified Microclimate," *Proceedings*, Cotton Defoliation and Physiology Conferrence, Greenville, S. C., Jan. 1961.
7. R. Geiger, *The Climate Near the Ground*, Translation by M. N. Stewart and others of the 2d German edition of *Das Klima der Bodennahen Luftschicht* issued Aug. 1956, The Harvard University Press, 494 pp., 1957.
8. B. E. Livingston, "Atmometers of Porous Porcelain and Paper, Their Use in Physiological Ecology," *Ecology*, vol. XVI, No. 3, July 1935.
9. R. E. Huschke (Editor), *Glossary of Meteorology*, American Meteorological Society, Boston, Mass., 1959, 638 pp. (p. 163).

Weather Note

THE "DOUBLE EYE" OF HURRICANE DONNA

C. L. JORDAN

Department of Meteorology, Florida State University, Tallahassee, Fla.
and

LT. FRANK J. SCHATZLE, USN

Airborne Early Warning Squadron Four, Roosevelt Road, Puerto Rico
[Manuscript received June 13, 1961]

On the afternoon of September 6, 1960, hurricane Donna presented a striking picture on the radarscope of a U.S. Navy hurricane reconnaissance aircraft [1] as illustrated by figure 1. The structure of the inner portion of the storm as indicated by the radar was very unusual in that not only was the exact center of the storm clear of precipitation echoes but there was also a relatively wide ring in the storm interior with little or no radar return. Descriptions of the core of this storm given to the press following the flight led to newspaper stories of a "double eye," and at least one newspaper headline referred to "two-eyed" Donna. These accounts were misleading since they failed to mention that the "eyes" were concentric. In the transmitted weather reports, the storm core was described in terms of two concentric wall clouds and the inner diameter of each of the radar rings was given. As will be discussed below, this "double eye" structure persisted for at least several hours and connections between the inner and outer rings, if present, were very weak. At the time of the photographs presented in this note, hurricane Donna was located at approximately 21.5° N., 69.5° W., and was moving toward the west-northwest at a speed of about 8 kt.

A low-level penetration of the storm core was attempted from the south-southwest shortly after the time of the photograph presented in figure 1. The aircraft [2] was at an altitude near 1,000 feet and penetrated to a point about 32 miles from the center of the inner ring or just outside the edge of the outer ring. At this point the penetration attempt was abandoned because of excessive engine cooling due to the heavy rain. Surface wind speed estimates based on the state of the sea reached 100 kt. at 45 miles from the storm center and the maximum value was entered as "120+". The central sea level pressure of the storm at this time was near 940 mb.

A photograph of the scope of the vertically scanning radar taken during the attempted low-level penetration

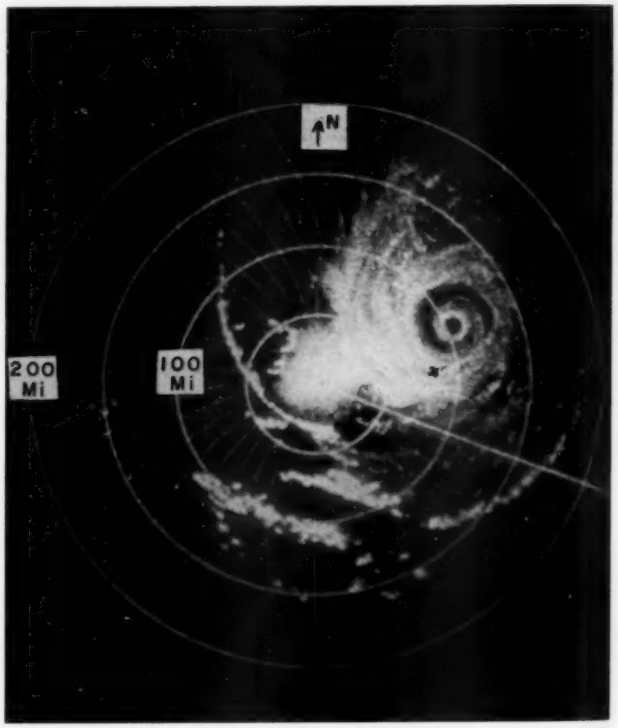

FIGURE 1.—A photograph of the scope of an APS–20E radar in a U.S. Navy hurricane reconnaissance aircraft taken at approximately 2100 GMT, September 6, 1960. The aircraft position (at the center of the photograph) was about 10 miles south of Grand Turk Island and about 105 miles west-southwest of the center of hurricane Donna. The aircraft was at an altitude of about 1500 ft. and on a heading of 110°. Some of the echoes to the south and southwest of the aircraft at a range of 75–150 miles were from the mountains of Hispaniola. The APS–20E is an S band (10.4 cm.) radar with a peak power of 2.0 megawatts. The beam width, as defined by the half-power points, is approximately 1.5° in the horizontal and 6.0° in the vertical. The symmetrical spiralling pattern of light lines was due to interference from other electronic equipment.

[1] Of the Airborne Early Warning Squadron Four then located at the Naval Air Station, Jacksonville, Fla.

[2] The aircraft was of the Super Constellation type, U.S. Navy designation WV-3.

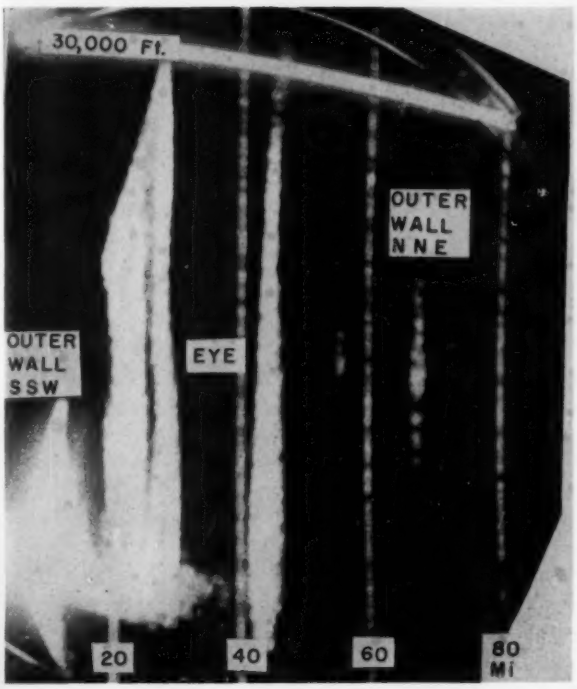

FIGURE 2.—A photograph of the range-height scope of the APS–45 radar in a U.S. Navy hurricane reconnaissance aircraft taken about 30 minutes after figure 1. Height is shown on the vertical scale and slant range from the aircraft on the horizontal scale. The aircraft was at a relative position given approximately by "x" on figure 1 and was at an altitude of about 1,000 ft. The view is directly across the storm center toward the north-northeast. The APS–45 is an X band radar (3.2 cm.) with a peak power of 450 kilowatts. The beam width, as defined by the half-power points, is approximately 3.0° in the horizontal and 1.0° in the vertical.

FIGURE 3.—A photograph of the plan-position scope of the APS–45 radar taken at approximately 2215 GMT, September 6, 1960. The aircraft was at the position indicated by the "+" and at an altitude of about 8,300 ft. The 20-mile and 40-mile range circles to the southeast of the center and the 60-mile circle in the north-northeast sector can be seen faintly.

(fig. 2) gives additional information on the structure of the storm core. This range-height view, taken from a relative position indicated by the "x" in figure 1, was directed across the eye from south-southwest toward north-northeast. The cross-section of the inner ring is clearly shown but, because of attenuation, the outer ring on the opposite side is barely discernible. This radar, the APS–45, is subject to much greater attenuation than the APS–20E, from which figure 1 was obtained, because of the shorter wavelength which is used. The inner wall cloud is shown on the range-height scope as nearly vertical and the echoes extend above 30,000 ft. The diameter of this inner "eye" varied from about 10 miles at the lower level to about 13 miles at the high levels.

The "clear" zone between the inner and outer rings on figure 2 is confused to some extent on the side nearest the aircraft by return from the sea which shows up in the form of a horizontal fanshaped pattern. The small faint echo in the "clear" space on the far side of the inner ring should perhaps be associated with the small echo in the same region on figure 1. The time difference of the two photographs is only about 30 minutes.

The radar appearance of the inner ring was more characteristic of convective type echoes than the outer one and it extended to somewhat greater heights. The maximum height of the inner ring during the several hours that it could be seen on this flight was about 45,000 ft., while the clouds forming the outer ring appeared to be more stratiform in character and gradually died out on the range-height scope above 30,000 ft. In view of the greater strength and height of the inner echo, it could be argued that, at this time, the inner radar ring should be considered as the true wall cloud of the eye.

Following the low-level penetration attempt, a climb to the 700-mb. level was made and the storm core was penetrated from the northeast with relatively little difficulty. The space between the radar rings was free of clouds in a layer which was estimated to extend from about 3,000 ft. to about 25,000 ft. However, only a limited area was visible during the penetration and, un-

fortunately, the exit was made after dark. The stratocumulus between the two radar rings consisted of well-formed concentric horizontal rolls and appeared to be unusually low. The ocean surface was not visible through the stratocumulus so that we have absolutely no information on the distribution of wind between the inner and outer rings. Unfortunately, the research aircraft of the National Hurricane Research Project did not enter Donna on this day.

There was a thick layer of cirrus or high altostratus extending out from the inner core and covering the area between the two rings. The inner core of the storm was described by one of the pilots as resembling a giant "tastee freeze". Inside the inner ring, the stratocumulus was nearly overcast but the sea surface could be seen in spots. Cirrus was absent over most of the inner "eye" and there were no clouds above the stratocumulus which, in this area, extended to about 6,000 ft.

A photograph of the APS–45 scope taken during the penetration of the inner radar ring (while the radar was on horizontal scan) is shown in figure 3. The "clear" ring shows up nicely but it is shown as being somewhat narrower than indicated in figure 1. This difference is not surprising in view of the shorter wavelength of this radar and the fact that the aircraft was much closer to the cloud systems. The narrowest portion of the "clear" ring and the greatest suggestion of a connection is shown on the north side of the center. This is almost directly opposite to what was shown in figure 1 but there is a time difference of a little more than 2 hours between these two photographs.

The "double eye" structure was observed throughout a period of about 5 hours when the afternoon flight of September 6 had the hurricane on its radar. The inner ring appeared to be weakening as the aircraft moved away from the storm but it was noted on the subsequent flight a few hours later. Limited information is available from this later flight because the radar was not functioning properly. The eye reorganized during the night and on the following day an orthodox eye was found with a diameter of about 25 miles. About 12 hours prior to the time of figures 1 and 2, there was no evidence of a "double eye" and the eye diameter was reported as 20 miles.

A rather poorly documented case of a "double eye" was reported in a hurricane of 1947 [3] and the same type of structure has been reported in several typhoons in recent years. Fortner [1] described typhoon Sarah of 1956 at the time when it had "an eye within an eye". In some of the spectacular typhoon cases, the inner convective system appears as a giant cumulonimbus centered in a large "eye". The "inner eye" within the cumulonimbus vortex has been observed to be as small as 2 miles. In these cases, winds well in excess of typhoon force were observed in the relatively clear space separating the inner and outer wall clouds. In other cases in recent years [2], the radar has indicated a very narrow ring of relatively weak return just outside a ring-shaped wall cloud but these weak areas were not apparent from visual observations made from the reconnaissance aircraft.

To our knowledge, all cases of "double eyes" in intense tropical cyclones have been of the concentric type. There are often radar features, the so-called "false eyes", outside the storm core which could be misinterpreted as the eye of the storm by inexperienced observers. These, however, do not have closed circulations about them and are hardly detectable, if at all, in the wind and pressure fields.

REFERENCES

1. L. E. Fortner, Jr., "Typhoon Sarah, 1956," *Bulletin of the American Meteorological Society*, vol. 39, No. 12, Dec. 1958, pp. 633–639.
2. C. L. Jordan, D. A. Hurt, Jr., and C. A. Lowrey, "On the Structure of Hurricane Daisy on 27 August 1958," *Journal of Meteorology*, vol. 17, No. 3, June 1960, pp. 337–348.
3. U.S. Navy, "A Note on the Double Eye Phenomena as Observed During Hurricane 11–20 Sept. 1947," *NAVAER* 50–IR–207, Chief of Naval Operations, Washington, D.C., 11 pp.

DISTRIBUTIONS OF WEEKLY AVERAGES OF DIURNAL TEMPERATURE MEANS AND RANGES ABOUT HARMONIC CURVES[1]

CHRISTOPHER BINGHAM

The Connecticut Agricultural Experiment Station, New Haven, Conn.
[Manuscript received April 11, 1961]

ABSTRACT

The distributions of weekly averages of diurnal temperature maxima, minima, means, and ranges are found to be non-normal, although the errors in using the normal distribution do not impair the usefulness of derived estimates of probability. The central tendency and the variance are estimated by harmonic regression. This enables the estimation of probabilities for any week from as few as five parameters. A three-term harmonic curve fitted to individual years is adequate to describe the course of temperature.

1. INTRODUCTION

Useful probability statements about the occurrence of diurnal temperature means or ranges cannot be made without knowledge of the form of the distribution of the values and a practicable means of estimating the parameters which specify the distribution. The present paper explores the distributions of the weekly average of the daily mean temperature ($=\frac{1}{2}$ (max+min)) and the weekly average diurnal range, as well as the related distributions of the weekly average diurnal maxima and minima.

2. HARMONIC REGRESSION

The fundamental tool which will be used in this development is harmonic regression. It is well known that any set of data, $x_1, x_2, \ldots, x_{2n}$ at equally spaced times $t_1, t_2, \ldots t_{2n}$ may be exactly fitted by a series of the form

$$y=a_0+\sum_{p=1}^{n} A_p \cos(pt-\phi_p), \quad t \text{ measured in degrees.} \quad (1)$$

This is the sum of cosine curves, each with semi-amplitude A_p and time of maximum $t=\phi_p/p$. Equation (1) can also be written in the form used herein,

$$y=a_0+\sum_{p=1}^{n} (a_p \cos pt+b_p \sin pt) \quad (2)$$

where

$$a_p=A_p \cos \phi_p;\ b_p=A_p \sin \phi_p; \text{ and } a_p^2+b_p^2=A_p^2,\ p=1, \ldots, n. \quad (3)$$

Such a sum will be called an n-termed Fourier series, and $(a_p \cos pt+b_p \sin pt)$ will be called the pth term. In many applications it is found that very few terms are needed to give an excellent fit to the data, so that the residuals from the curve are of the same magnitude as the basic errors of observations. For instance, Craddock [6] observed that over much of the Northern Hemisphere, a two-term series provided an adequate fit to the mean monthly temperature. He did not, however, examine any variability between years of the coefficients of the two-term curve which best fit each year. Without this knowledge, a proper error term for significance tests for the reality of given terms is not available. Bliss [4] remedied this deficiency, describing a technique paralleling the standard analysis of variance for the fitting of orthogonal polynomials.

The mathematical model underlying Bliss's analysis is the following. Each observation for the jth unit of time in the ith year, y_{ij}, is considered as a sum

$$y_{ij}=(a_0+\alpha_{i0})+(a_1+\alpha_{i1}) \cos t_j+(b_1+\beta_{i1}) \sin t_j + (a_2+\alpha_{i2}) \cos 2t_j+(b_2+\beta_{i2}) \sin 2t_j + \ldots +(a_r+\alpha_{ir}) \cos rt_j+(b_r+\beta_{ir}) \sin rt_j+\epsilon_{ij} \quad (4)$$

where $t_j=j/k\ 360°$, $j=0, 1, 2, \ldots, k-1$ (if the units are weeks, $k=52$). The ϵ_{ij} are independently distributed normal deviates with zero means and common variance σ^2. The vectors $(\alpha_{i0}, \alpha_{i1}, \ldots, \alpha_{ir}, \beta_{i1}, \beta_{i2}, \ldots, \beta_{ir})$ are independent observations from a $2r+1$ variate multivariate distribution with zero mean vector. This model covers both the case of a single curve applicable to every year (when the variances $V(\alpha_{i0})=V(\alpha_{i1})= \ldots = V(\beta_{ir})=0$), and the case of random variation of the curve from year to year. In the latter case the variance components of the coefficients enter into the variance of y_{ij}. For details on the analysis of variance see Bliss's [4] bulletin. His analysis is designed to test several hypotheses. The

[1] This work was supported in part by funds of a regional project in agricultural climatology, NE-35.

simplest such hypothesis is that $a_j^2+b_j^2=0$, for particular values of j. One can also test the adequacy of r terms to fit the data, and the reality of the between years variance components associated with the coefficients. Significance tests are made using the F-test for variance ratios.

It should be pointed out that a certain arbitrariness must occur in the above model. This is the choice of a zero point from which we measure the time t. To illustrate this, let us suppose that

$$y_{tj}=(a_0+\alpha_{t0})+(a_1+\alpha_{t1})\cos t_j+(b_1+\beta_{t1})\sin t_j +(a_2+\alpha_{t2})\cos 2t_j+(b_2+\beta_{t2})\sin 2t_j.$$

Then if $0\leq\Theta<360°$, y can equally well be expressed by

$$y_{tj}=(a_0+\alpha_{t0})+(a_1'+\alpha_{t1}')\cos t_j'+(b_1'+\beta_{t1}')\sin t_j' +(a_2'+\alpha_{t2}')\cos 2t_j'+(b_2'+\beta_{t2}')\sin 2t_j', \quad (5)$$

where $t_j'=t_j+\Theta$ and $a_1'=a_1\cos\Theta-b_1\sin\Theta$

$$b_1'=a_1\sin\Theta+b_1\cos\Theta$$

$$a_2'=a_2\cos 2\Theta-b_2\sin 2\Theta$$

$$b_2'=a_2\sin 2\Theta+b_2\cos 2\Theta,$$

with a similar relationship holding for the α's and the β's. If one fits a curve of the form (5) to data, exactly the same curve is obtained as when the more conventional form is fitted. It is easily seen that the variance component contributed by α_t will, in general, be different from that contributed by α_1'. However, the sum of the components for a given term will be unchanged. That is, $V(\alpha_t)+V(\beta_t)=V(\alpha_t')+V(\beta_t')$. Further,the semi-amplitudes A_t will be unchanged by the change of origin. Since the analysis of variance does not separate the two components of each term, this is sufficient to ensure that the analysis is invariant under any choice of origin.

Estimates, a_{t0}^*, a_{t1}^*, . . . , b_{tr}^*, of the coefficients, $(a_0+\alpha_{t0})$, $(a_1+\alpha_{t1})$, . . . , $(b_r+\beta_{tr})$, for the tth year are easily made as follows.

$$a_{t0}^*=\frac{1}{k}\sum_{j=0}^{k-1}y_{tj}$$

$$a_{tm}^*=\frac{2}{k}\sum_{j=0}^{k-1}y_{tj}\cos mt_j \quad (6)$$

$$b_{tm}^*=\frac{2}{k}\sum_{j=0}^{k-1}y_{tj}\sin mt_j, \quad m=1,2,\ldots,r; \quad t_j=\frac{j}{k}360°.$$

Estimates for the mean coefficients a_0, a_t, . . . , b_r are obtained by averaging the above a_{tm}*'s and b_{tm}*'s over years. These are least squares estimates, and hence if the assumptions stated are fulfilled, they are the best unbiased estimates; further, if the error component is normally distributed they are also maximum likelihood estimates. The estimates remain unbiased even when the restriction of independence of residuals is removed.

Using the estimates a_{t0}^*, . . . , a_{tr}^*, b_{t1}^*, . . . , b_{tr}^* one can compute an "expected" value, $\hat{y}_{tj}$, for the jth week of the tth year by

$$\hat{y}_{tj}=a_{t0}^*+a_{t1}^*\cos t_j+b_{t1}^*\sin t_j+\ldots +a_{tr}^*\cos rt_j+b_{tr}^*\sin rt_j. \quad (7)$$

Adequacy of the model is seen in the deviations

$$d_{tj}=y_{tj}-\hat{y}_{tj} \quad (8)$$

of observed values from their "expected" values. These deviations will occasionally be referred to simply as d, without subscripts. Thus the use of this model produces two additional arrays, d_{tj} and $\hat{y}_{tj}$, similar in form to the original data. Any operations or computations that may be performed on the original data, y_{tj}, may be performed on the d_{tj} and on the $\hat{y}_{tj}$. For example, to the sample variance for the jth week,

$$s_j^2(y)=\frac{1}{f-1}\left[\sum_{t=1}^{f}y_{tj}^2-\frac{1}{f}\left(\sum_{t=1}^{f}y_{tj}\right)^2\right] \quad (9)$$

where f is the number of years in the sample, corresponds the variance of the deviations d_{tj} for the jth week.

$$s_j^2(d)=\frac{1}{f-1}\left[\sum_{t=1}^{f}d_{tj}^2-\frac{1}{f}\left(\sum_{t=1}^{f}d_{tj}\right)^2\right]. \quad (10)$$

Bliss applied this technique to a 14-year record of monthly mean temperatures at New Haven, Conn. His findings confirmed those of Craddock: A two-term series accounted for more than 97 percent of the observed sum of squares. It is well known that the variance of the temperature is higher in winter than in summer. Bliss found that a simple sine curve fitted to the log-variance of monthly mean temperatures adequately described the yearly trend of this variance. Concurrently I applied the technique to the monthly averages of the diurnal temperature range for the same period at New Haven [3]. Both the first and second terms of the regression curve were significant. The trend of the range was quite unexpected with maxima in May and October and absolute and relative minima in January and July, respectively. The distributions of both the mean and the range were normal for all practical purposes, although there were very slight indications of systematic skewness.

3. METHOD AND DATA

To carry out the laborious calculations for the application of the technique to weekly averages of temperature maxima, minima, means, and ranges, electronic data processing equipment was necessary. A program was written for the IBM 650 with the following functions. From cards containing weekly sums or averages of the maximum and minimum temperatures, coefficients a_{tp}* and b_{tp}*, $p=1, 2, 3$, of the three-term Fourier curve which

best fitted the data (maximum, minimum, mean, or range, depending on a coded instruction card) of each individual year were computed. Simultaneously sums of powers needed for moments up to the fourth were accumulated. From these "annual" coefficients the expected values $\hat{y}_{ij}$ for each week were computed. In addition, the raw moments of the deviations, $d_{ij}=y_{ij}-\hat{y}_{ij}$, were accumulated, y_{ij} being the observed and $\hat{y}_{ij}$ the expected values for a given week and year (equation (7), (8)). Finally the machine calculated an analysis of variance. Later it was found useful to write a program to convert raw moments to moments about the mean and compute

$$g_1=k_3/k_2^{3/2} \text{ and } g_2=k_4/k_2^2 \tag{11}$$

where k_i, $i=2$, 3, 4, are Fisher's k-statistics [8]. I also found it advantageous to write a program to carry out a harmonic analysis of unreplicated data and to synthesize curves from the estimated coefficients.

The complete set of programs was carried out on the data from only two stations, Storrs, Conn., and Keedysville, Md. both for the years 1926–56. In addition the mean and the range were studied for Uniontown, Pa., Eau Claire, Wis. both for 1926–56, and for Easton, Md. for two independent periods, 1896–1926, and 1926–56. These last will be referred to as Easton I and Easton II, respectively. The climatological year starting March 1 and omitting February 28 and 29 was used throughout.

4. CENTRAL TENDENCY

The mean squares from the analysis of variance for the harmonic regression fitted to the maximum, the minimum, the range, and the mean at Storrs are given in table 1. The sums of squares may be easily calculated using the degrees of freedom. The correct F-tests were applied according to Bliss [4]. The 30-year averages of the mean and the range for Easton II together with the average harmonic curve are shown in figures 1 and 2 respectively.

Maximum, Minimum and Mean.—As was expected, the first (sine curve) term of the Fourier series accounted for approximately 90 percent of the total sums of squares for the maximum, the minimum, and the mean. The fit appeared excellent. In a few cases the second or third terms were significant (i.e., larger than one could expect from chance variation under the null hypothesis) but in terms of the percentage of sum of squares accounted for ($<<1$ percent) they were trivial. However, the interactions of terms by years all were significant and for the second and third terms were more important than the average effect of these terms. This indicates that the shape of individual years cannot in general be adequately described by a simple sine curve, despite the good fit to the averages.

An interesting feature was the consistency over a wide area of the departures of the average values for the period

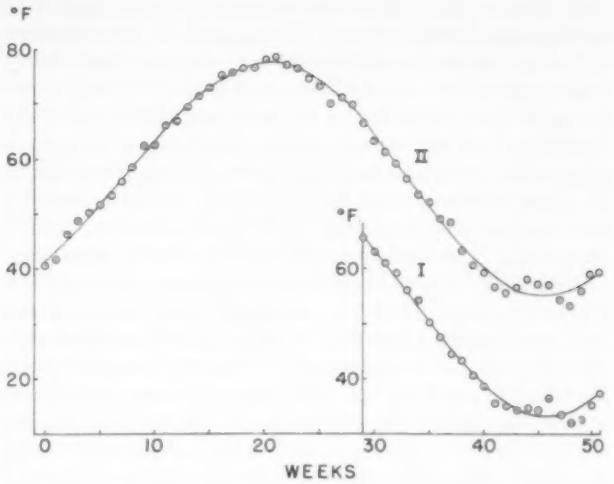

FIGURE 1.—30-year average of mean weekly temperature and the fitted harmonic curve, Easton, Md., 1896–1926 (designated I), and Easton, Md., 1926–1956 (designated II). Week 0 begins March 1.

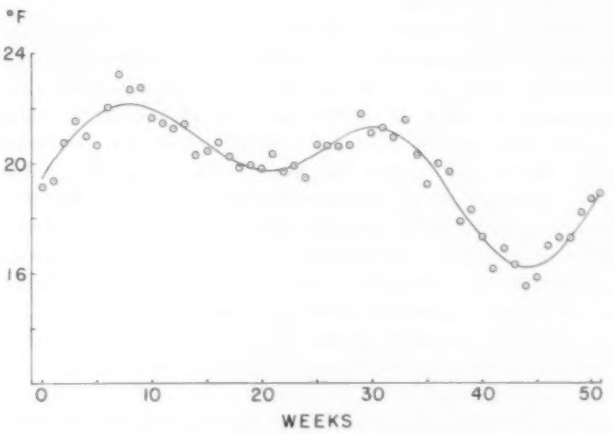

FIGURE 2.—30-year average of weekly average diurnal temperature range and the fitted harmonic curve, Easton II, 1926–1956.

TABLE 1.—*Mean squares from analysis of variance of harmonic regression, applied to weekly averages of diurnal temperature maxima, minima, ranges, and means, Storrs, Conn., 1926–1956*

Row	Source of variation	D.F.	Mean squares			
			Maximum	Minimum	Range	Mean
1	Between years	29	*113.649	*73.631	‡65.891	‡80.546
2	1st term	2	‡216080.805	‡173223.360	‡2631.135	‡193884.295
3	2d term	2	‡494.045	12.245	‡578.350	96.540
4	3d term	2	14.715	*227.890	‡295.545	47.425
5	Scatter about curve	45	*33.370	†49.283	*15.696	‡32.424
6	1st term x year	58	‡72.379	‡51.113	‡22.515	‡66.064
7	2d term x year	58	†43.060	‡32.114	‡23.743	‡32.081
8	3d term x year	58	*36.092	*29.750	*14.552	‡29.283
9	Residual	1305	25.868	23.206	11.424	21.105

*P<.05.
†P<.01.
‡P<.001.

1926–1956 of the maximum, minimum, and mean from the average Fourier curve. The magnitude and direction of the deviations for all four eastern stations were almost indistinguishable. In addition, at Keedysville and Storrs, the pattern of deviations of the mean was almost perfectly reproduced by the corresponding deviations of the maximum and the minimum. The time of year when the fit was least good and when the bulk of the sum of squares for scatter arose was the period from mid-December to mid-February. The last two weeks of December were considerably below the fitted curve, January above it, and February again below it. Although differing in detail the same general pattern of winter temperatures was observed in both independent 30-year samples from Easton, Md. (see fig. 1). The warm January is reminiscent of the fabled "January thaw." However, the date of the "thaw" is reportedly well defined at January 20–23 [11] [14]. This does show up clearly in the Easton I record but is not visible in the Easton II record or at other stations analyzed for the later period. This casts doubt on the reality of this "singularity," especially in view of the occurrence of maximum variability in January. No other such similarities in deviations are apparent in both records from Easton.

Range.—As shown in figure 2, the range followed the pattern uncovered in the preliminary analysis of the monthly data at New Haven [3]. We observed pronounced maxima in early- to mid-May and in mid-September with a summer relative minimum considerably above the winter minimum. The summer dip was least pronounced at Keedysville and Eau Claire but was clearly present in all records, including both independent Easton records. There were few, if any, recognizable similarities in deviations from the fitted curve between the stations. However, at all stations, the first two terms of the Fourier series were highly significant, with the third of lesser importance although still significant. The interaction of terms by years was quite uniformly significant. This, of course, indicates that there is considerable variation between years in the shape of the yearly course of diurnal range. Of considerable interest is close agreement of the phase of the first term (fundamental sine curve) with that of the sun. This apparently reflects the close relationship between the diurnal range and the energy input. That this relationship is not overpowering is, however, clearly shown by the spring and fall maxima. Despite first guesses that these maxima were corollaries of clearer skies in both spring and fall, sunshine and cloudiness records showed that in fact the spring period tended to be cloudier than the summer, although the high daytime gains and nighttime losses of radiation due to clear skies in the fall remain an acceptable explanation for the autumnal maximum. An examination of the daily temperature record for Mt. Carmel, Conn. suggested a possible explanation. It was observed that there was a considerable number of days when the daytime temperature went very far above the nighttime minimum but returned to previous levels after sundown. In the late spring, the annual course of insolation is considerably ahead of the course of soil temperature, and hence, in general, ahead of the course of nighttime air temperatures. This makes it possible when conditions are right, for the temperature to rise sharply in the daytime and yet return at night, as we observed, to about the same level as the previous night. This behavior is corroborated by a comparison of the variances (between year and within year) of the maximum and the minimum temperatures. During these spring months the variance of the maximum is definitely greater than that of the minimum.

5. DISTRIBUTIONS

The analysis as discussed to this point has provided an efficient method for estimating a central tendency or location statistic for the distributions of temperatures and temperature ranges. Instead of 52 individual means, we have as few as three coefficients (for a sine curve) which give the location of the distribution for every week. However, for statements of probability, knowledge of the shape of the distributions is required. If it can be shown that the distributions are normal, or Gaussian, then the mean and the variance completely specify the distribution. On the other hand, if the distributions are non-normal, higher moments are necessary to specify or to approximate them. In addition, for the analysis of variance to be fully applicable, several assumptions should be met: The deviations of each observation from the theoretical regression curve for the year should be (i) normally distributed, (ii) homoscedastic (i.e., of equal variance), and (iii) independent. To examine the distributions of the observations and to test the first and second of these assumptions, moments were computed and the following procedure carried out. The sample variance for each week, $s_j^2(y)$, $j=0, \ldots 51$, (equation (9)) was computed from the observed values under consideration, to be referred to as y, the maximum, minimum, range, or mean. I also computed $g_1(y)$ and $g_2(y)$ (equation (11)) as measures of skewness and kurtosis. In addition, I calculated the same statistics $s_j^2(d)$, $g_1(d)$, $g_2(d)$ for the distributions of the deviations, d, of the observed values from the best fitting annual curves (see equation (10) for example). This process gave 52 values, one for each week, of the sample statistics just mentioned, for each of the two related distributions.

Variance.—The observed variance of the maximum and the minimum for Storrs and Keedysville changed smoothly over the year, as did the variance of the mean for all stations. Corroborating the previously mentioned tendency, the variance of these variates was considerably higher during the winter months than during the summer, with a reasonably smooth transition between the extremes (see figs. 3, 4, 5). Unfortunately for strict fulfillment of the conditions of the analysis of variance, the variance of the deviations, d, about the individual curves showed the same pattern, although to a reduced degree. In the case

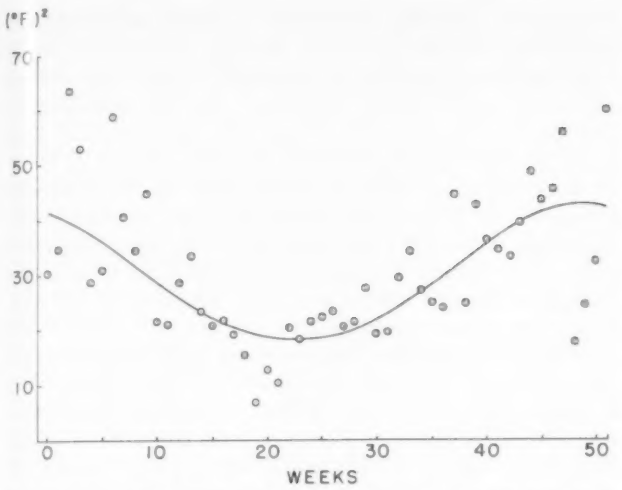

FIGURE 3.—Sample variance of weekly average diurnal maximum temperature and transform of the sine curve fitted to the log variance, Storrs, Conn. 1926–1956.

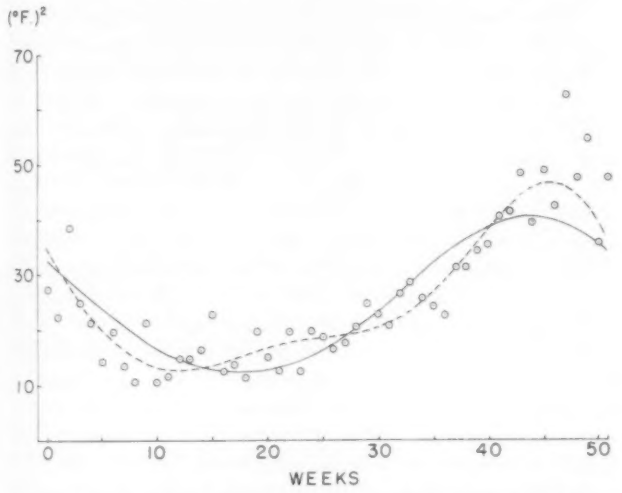

FIGURE 4.—Sample variance of weekly average diurnal minimum temperature and transforms of the sine curve (solid line) and the two-term Fourier curve (dashed line) fitted to the log variance, Storrs, Conn., 1926–1956.

of the range there were indications that the variance followed a double maximum pattern. Hardly visible at Storrs, it was more apparent at Keedysville, and still more so at Uniontown. Furthermore, it could be discerned in both independent Easton records. (The observed variance of the range at Uniontown is shown in figure 6.)

Since the trends in the variance were pronounced, we summarized the pattern by applying to the variance the same techniques of harmonic regression previously used on the temperature variates themselves. In order to minimize the non-normality of the distribution of the variance, it was transformed to its logarithm before the analysis was carried out [2]. As Bliss indicated, the annual course of the log variance of the mean could be approximated by a simple sine curve. The same was true for the log variance of the maximum temperature. In both cases neither the second nor the third term was significantly different from zero. However, the analysis of variance indicated that, for the minimum, the higher terms were significant. The second term component was quite pronounced at Storrs while the third term was important at Keedysville, although at both stations the sine curve was clearly the dominating feature. The range exhibited a markedly different character. The log variance showed a significant second term trend, but little evidence of any single wave. For all four variates, when the deviations, d, about the annual curves were considered, the analysis showed that the F values for all terms decreased although the same relative importance of terms seemed to be the rule.

Correlations Between the Variates.—Of related interest to the course of the variance of the individual variates is

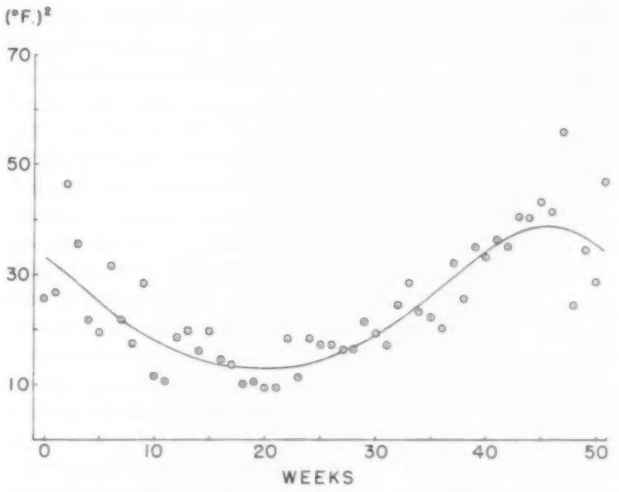

FIGURE 5.—Sample variance of weekly average diurnal mean temperature and transform of the sine curve fitted to the log variance, Storrs, Conn., 1926–1956.

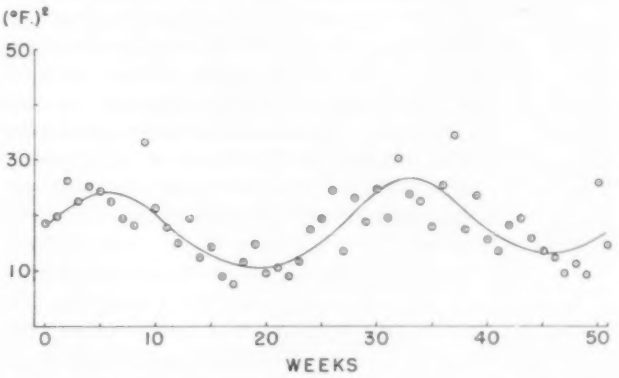

FIGURE 6.—Sample variance of weekly average of diurnal temperature range and transform of the two-term Fourier curve fitted to the log variance, Uniontown, Pa., 1926–1956.

the course of the correlation between them. Because the maximum-minimum and the mean-range coordinate systems are orthogonal, the correlation between the average maximum and the average minimum temperatures contains all the available information on the various correlations. Although not computed directly in our original program, this correlation is easily calculated from the variances of the maximum, minimum, and range as

$$r\,(\max, \min)=\frac{s^2_{\max}+s^2_{\min}-s^2_{\text{range}}}{2s_{\max}\times s_{\min}}. \tag{12}$$

This calculation was carried out for the two stations, Keedysville and Storrs, for which all these variances were available. At both stations, the correlation r was always positive, reaching a maximum in winter and a minimum in summer. Like the variance of the mean, it followed a fairly smooth trend between these extremes. To obtain a quantitative description of its seasonal course we transformed r to $z=\tanh^{-1}r$, in order to stabilize its variance and minimize the non-normality of its distribution [9] and carried out a harmonic regression on each station.

The variance about a regression curve fitted to z derived from samples of 30 is theoretically $1/27=0.037037$. We can insert this as an added line in the analysis of variance with infinite degrees of freedom. This can be used in place of the ordinary error row in an analysis of variance of replicated data to test the adequacy of the fit and the reality of the regression. For both Storrs and Keedysville the scatter of z about a sine curve, when tested in this manner, was not significantly different from the theoretical variance ($P\geq 0.2$, $F<1.2$), indicating there was no removable systematic variation in the residuals about the curve. The sine curve was highly significant ($P\leq 0.01$). Thus we may conclude that the transform, z, of the correlation between the weekly averages of maximum and minimum temperatures follows a sine curve. The only apparent regular departure from the sine curve is in April and early May when, at Keedysville, there were eight successive weeks when the observed correlation was less than the "expected" correlation, calculated from the sine curve. At Storrs a similar feature was observed for the same eight weeks, with the exception of one week in which the observed correlation slightly exceeded the "expected." In addition to this, there were other similarities between the two stations in the observed correlations. This is a further reflection of the previously noted similarities in the temperature records at quite widely separated stations (340 miles).

One might hope that, by using the "expected" values of $r(\max, \min)$, $s^2_{\max}$, and $s^2_{\min}$, computed from the sine curves fitted to their transforms, one could recover the curve describing the course of the variance of the range by the formula,

$$s^2_{\text{range}}=s^2_{\max}+s^2_{\min}-2rs_{\max}\times s_{\min}. \tag{13}$$

I hoped in this way to obtain a purely mathematical explanation for the behavior of s^2_{range} based on simple assumptions concerning the behavior of the other second moments. The results, however, are not convincing. For Storrs, the curve of s^2_{range} computed in this way is far too flat, although its only notable feature, a peak at week 10, does reflect a similar peak in the observed variance. At Keedysville, where the observed variance of the range displayed a pronounced double maximum pattern, I found only a single peak at the time of one observed maximum, with a point of inflection at the less important of the two minima.

Homoscedasticity and Independence of Residuals.—The above analysis has made one thing clear: Our assumption of hooscemdasticity is not fulfilled. Although the mathematical model postulated implies some sort of a periodic form for the variance of the actual values, y, the variance of the deviations, d, from the annual curves should be constant. In the case of the average diurnal range this is nearly true. However, the other three variables are far from homoscedastic. In any case, the estimates of the regression coefficients are still unbiased estimates of the population values. It is difficult to assess the effect of this upon the tests in the analysis of variance. According to Cochran [5], the F-test for non-regressive designs is sufficiently robust as to be not misleading, although the more general case is not covered. Since, for the mean and the two extremes, the sine curve predominates, we can clearly accept the adequacy of the overall fit, although the tests cannot be considered exact. Since the variability of the variance of the range is far less prominent and regular, the tests should be less affected by heteroscedasticity.

Of equal or greater importance, perhaps, although more difficult to assess, is the possibility of dependent residuals. Direct tests for this are available [1] but laborious to apply and, as they stand, are not readily applicable to our computing scheme. Bliss [4] states that the technique of fitting separate curves to each year will have the effect of removing serial correlation between weeks, and leaving substantially independent residuals. From inspection of individual years, the observed residuals appear to be random. On the assumption of independent residuals, it follows that the moments for each week, as computed from the residuals, are independent and thus also g_1 and g_2 computed from these moments are independent. Serial correlation in these should tend to inflate the significance of trends in these statistics. Thus we would expect that if the residuals are independent, the F values in tests for the reality of regression curves fitted to the annual course of g_1 and g_2 should be lower for the distribution of the residuals than for the distribution of the raw observations. This, as we shall see, was observed and can be considered evidence of independence. However, no conclusive test has been found to clarify this point.

Tests for Normality.—We now examine the assumption of normal distributions for our variates. Being able to work with normal distributions is desirable for three

reasons. Firstly, such normality is assumed in our use of variance ratio tests in the analysis of variance, although it has been shown [5] that departures from normality, if not extreme, have little effect on the F test. Secondly, the normal distribution is known and easy to apply. Thirdly, if a distribution is normal all information about the values of the parameters defining it is subsumed in the sample mean and variance [7]. Furthermore, the powerful central limit theorem, applicable because we are considering averages of several observations in our distributions, tells us that the distributions approach normality.

A further consideration is also important: the use to which the probability statements derived from the distribution will be put. If extreme accuracy at all levels of probability is required, for instance, we must be extremely stringent regarding our tests of the distribution. On the other hand, in practical climatological applications we are not interested in, for example, the difference between a once-in-20 and a once-in-25 event. Even if tests show that almost certainly there is some departure from the normal curve, we may accept a normal approximation if the errors in probability estimated from our approximation do not impair the usefulness of the estimates.

As measures of departures from normality I chose, as previously mentioned, $g_1=k_3/k_2^{3/2}$ and $g_2=k_4/k_2^2$ where k_i are Fisher's k statistics. Departure of these from zero is indicative of non-normality. Both statistics are asymptotically normally distributed with mean zero and variance depending, in the null case, only on the sample size. Skewness or assymmetry is measured by g_1 while g_2 measures kurtosis. For ease in machine computation, g_2 was chosen in preference to

$$a=\frac{\sum|x_i-\bar{x}|}{s}$$

recommended by Geary and Pearson [10]. The g_1's and g_2's can be tested in two ways. First, compare the observed distributions of the g's with those expected for samples drawn from independent normal populations. The ordinary significance test using a standard error is of this type. Second, examine the yearly course of g_1 or g_2 for meaningful patterns. An improbably regular pattern is as clear evidence of the presence of non-zero skewness or kurtosis as are high values of g_1 and g_2.

The chief obstacle to the first type of test is our ignorance of the exact distributions of g_1 and g_2 under the null hypothesis. It is known that for samples as small as 30, such as concern us here, the distribution of g_1 is not far from normal while that of g_2 is strongly positively skewed. When the cumulative sample frequencies for the g's at Keedysville were plotted on probit paper, the curves reflected this expectation. The distributions of the g_1's were quite linear indicating approximate normality while the g_2's exhibited a concave upward curve characteristic of positively skewed distributions.

TABLE 2.—*Number of exceedences of the 1st, 5th, 95th, and 99th percentiles in 52 values of* $g_1(y)$ *and* $g_1(d)$ *calculated from weekly averages of diurnal temperature maxima, minima, ranges, and means, Keedysville, Md., 1926–1956*

	$g_1(y)$			$g_1(d)$		
	>upper 5 percent	<lower 5 percent	Total	>upper 5 percent	<lower 5 percent	Total
Maximum	4	1	5	1	1	2
Minimum	2	3	5	2	2	4
Range	3	1	4	2	3	5
Mean	5	1	6	1	0	1
	>upper 1 percent	<lower 1 percent	Total	>upper 1 percent	<lower 1 percent	Total
Maximum	1	0	1	0	0	0
Minimum	2	2	4	0	0	0
Range	0	0	0	0	0	0
Mean	1	0	1	0	0	0

Although the exact distribution of g_1 is unknown, Geary and Pearson [10] have given approximate extreme percentage points. A comparison of the observed frequencies of g_1 beyond these points seemed the optimal procedure. Since these percentage points are not available for g_2 for sample size less than 100, this comparison was not possible for g_2. In table 2 are given the number of times the upper and lower 5 percent and 1 percent levels for g_1 are exceeded for the 52 weekly distributions of the observations, y, and the residuals, d. We see that the agreement is as good as could be expected for the distribution of the deviations, d, about the annual curves although there are improbably few (i.e., no) values beyond the 1 percent point. However, in the distribution of the observations, y, themselves, the most striking feature is the appearance of four $g_1(y)$'s beyond the 1 percent point among the 52 g_1's derived from the minimum temperature. Further, the upper 5 percent point of $g_1(y)$ for the maximum and the mean is exceeded too often. Thus a certain degree of non-normality is indicated in all the original variates except the range. There is, however, no indication that this is true for the deviation from the annual curves, d. This last result is important since it is assumed in our mathematical model.

Clearly, the above tests lose much of their validity if there is appreciable serial correlation between weekly values since this makes the g_1's serially correlated. This affects the shape of the observed distribution of the 52 values of $g_1(y)$ for each variate. Thus the second type of test referred to above may be more applicable. This can best be done by fitting a regression curve on time to the computed statistics to uncover any significant pattern over the year. If the regression accounts for a significant part of the variation, it indicates a real departure from the expected values of zero. Because of the general robustness of the F-test, the departure of the distributions of the g_1's and g_2's from normality should not invalidate tests of significance of a regression curve. Accordingly, as previously mentioned, a three term harmonic curve was fitted to each of all available sets of g_1's and g_2's, with

somewhat mixed results. For the distribution of d there are no more F values significant at the 5 percent level than one would expect, with the exception of g_1 for the maximum temperature. For this, the second term for Storrs is significant and at Keedysville both the second and third terms are significant, although in both cases they are quite small. One may conclude, however, that there was no appreciable systematic skewness or kurtosis in the residual variation, whether one considers the mean, range, maximum, or minimum.

When we examine the observations y, there is a consistent pattern among the $g_1(y)$'s. For four out of the six records analyzed, including Easton II, the second term of the curve fitted to the course of $g_1(y)$ for the mean temperature was significantly different from zero. In the fifth record, Easton I, the amplitude of the second term was more than twice as large as any other, although not quite significant. Eau Claire, on the other hand, demonstrated a strong first term and small second and third terms. This discrepancy may possibly be traced to climatic differences between the Atlantic coastal and the Lake States. The same double maximum pattern was even more apparent in $g_1(y)$ for the minimum temperatures. At both stations analyzed, Storrs and Keedysville, the second term was highly significant, an almost identical pattern emerging. There appeared to be a tendency toward positive skewness in the fall and especially in the spring and negative skewness in the summer and especially in the winter.

We conclude that the distributions of the deviations d from annual curves are Gaussian for all four variates, while the observations y of the minimum and the mean have a skewness that changes seasonally. Since this pattern of skewness is most pronounced in the minimum and since the mean, as defined herein, is in part derived from the minimum, the primary pattern of non-normality is likely to be in the distribution of the minimum temperatures.

Although the tests discussed so far have not indicated any real departures from normality in the distributions of the range and the maximum, one further test placed in doubt the normality of the distributions of these variates, too. By the central limit theorem, the distribution of averages of independent g_1's or g_2's should be approximately normally distributed with zero expectation and variance $1/n$ times the variance of a single value. Thus if we consider the mean $\overline{g}_i$ of the 52 values of g_i, $i=1, 2$, we can treat it as a normal deviate with variance $1/52\ \mathrm{V}(g_i)$. These then can be compared with the percentage points of the normal distribution. Any means outside, say, the 5 percent level would indicate a significant average departure from normality. Since we have no a priori knowledge of the direction in which deviations from the null hypothesis should occur, the proper test to use is the two-tailed comparison. When this test was carried out, no average departures from zero were found for either the $g_1(d)$'s or the $g_2(d)$'s of the distributions of the deviations, d, for any of the four variates studied. Neither were there significant nonzero average departures in the $g_2(y)$'s. However, both the maximum and the range displayed definite signs of positive average skewness among the y's. At both Keedysville and Storrs $\overline{g}_1(y)$ surpassed the upper 5 percent level and, in the case of Storrs, the upper 1 percent level. For the range, all except one station, Storrs, with $\overline{g}_1(y)=-0.0041$, showed some positive skewness, with two records, Easton I and Uniontown, surpassing the 1 percent and 5 percent levels respectively.

Conclusions Regarding Distributions.—First, the variation of all four variates about the annual harmonic curves is Gaussian. This is important from a theoretical point of view, since it increases our faith in the underyling model. However, because we cannot predict the shape of the yearly course of the variate, this knowledge is of little use from a practical point of view. Second, we have quite clear indications of skewness but not kurtosis in the distributions of all four variates. In the case of the range and the maximum temperature, the average skewness is consistently and, in some cases, significantly positive. On the other hand, although they display no average skewness, the distributions of the mean and the minimum have skewness that varies systematically over the year. Thus, for completely exact climatological statements of probability, normal assumptions will not be sufficient.

In theory one should try to find the exact nature of the distribution for each of the four variates. In the present instance, this could be more misleading than any assumptions of normality. First, there are insufficient data to establish any distribution as being correct without doubt. Second, the variation in skewness, at least for the mean and minimum temperatures, suggests that the "correct" distribution may vary seasonally. This would greatly increase the difficulty of applying any distribution. An alternative which is more approachable is the use of the third and fourth moments in fitting ad hoc distributions to the variates using either one or several of the Pearson curves or the Edgeworth approximation. Since we have no evidence of the departure of the fourth moment from the value expected for the normal distribution, the third moment, as reflected in $g_1(y)$, should be sufficient. Further, due to the large sampling variation in $g_1(y)$ resulting from our use of small samples, our best estimate of the population skewnesses should be the values calculated from the fitted periodic regression curve, or in the case of the maximum or the range, from the yearly average. Even if such an approximation does not provide an exact fit, the degree of change from the normal approximation should indicate the magnitude of error.

Tables of the cumulative distribution functions of the first Edgeworth approximation for different values of γ_1, the population measure of skewness, are available [13]. Referring to these I found that for small departures from

symmetry ($|g_1| \leq 0.2$) use of this approximation does not markedly affect probability points given by the normal distribution. Assuming a standard deviation, σ, of 7° F. (near the maximum for any variate) at $g_1 = \pm 0.2$ the upper and lower 1 percent points are displaced approximately 1° F. with lesser changes nearer the median. Thus it seems safe to say that use of the normal distribution for the maximum and the range does not introduce any serious errors since the greatest average $g_1(y)$ (Storrs maximum) is 0.1643. For the minimum temperature at Keedysville which displayed the strongest systematic departures from zero of $g_1(y)$, the "expected" value of $g_1(y)$ ranged from about -0.48 to $+0.52$. It is true that the 1 percent level is quite distorted by this amount of asymmetry. However, the 5 percent level is only about a degree off (again letting $\sigma = 7°$ F.). Conversely, a deviation which by the normal distribution would be surpassed 5 times in 100 years would, under these circumstances, occur about 6.5 times in 100 years. Similarly the estimated 10 percent point would be exceeded about 11 times every 100 years. The Edgeworth approximation should be fairly accurate when the shape of a distribution is not far removed from the normal form. Since, as mentioned earlier, the central limit theorem assures that the distributions approach normality, the use of this approximation in the present case should be appropriate. Hence, these figures show that the use of the normal curve will be satisfactory on all levels of probability except beyond the 5 and 95 percentiles where one should probably apply some extreme value distributions.

6. PROBABILITY ESTIMATION

The above considerations on the distribution of temperature variates lead to a satisfactory method of estimating probabilities. Since we may assume for our purposes that the variates are normally distributed, specification of the means and variances completely determines the distribution. Our harmonic curves fitted to the variates provide the first of these parameters, while the curves fitted to the log variance provide the second. In the case of the maximum and mean temperatures both curves are essentially sine curves, with higher terms, even when satistically significant, changing the estimates little. The course of the minimum temperature is adequately described by a sine curve. The higher terms of the curve fitted to the variance do not seem to make an appreciable difference. For example, for Storrs the 5 percentile and the 1 percentile are changed a maximum of 0.8° and 1.2° F. by adding a second term. Similarly, the probability assigned to a given departure from the mean seems to be changed by at most 0.02 to 0.03. Since this is less than the level of accuracy ordinarily desired, the sine curve alone can be used. Hence for the maximum, the minimum, and the mean, the estimation of probabilities for any week of the year reduces to the fitting of six constants. I should point out that although a sine curve is adequate to describe the courses of these temperatures at the stations studied, the possibility is not excluded that at some locations higher terms may be necessary. Each term can, however, be specified by only two additional constants.

For the range, at least two terms, i.e., five parameters, should be used for estimating the central tendency. Since at some stations the second term in the curve describing the course of $\log s^2_{\text{range}}$ is of prime importance, five constants seem to be necessary to estimate the variance. However, in cases where there is no discernible pattern in the variance, it is probably best to use a single average variance derived from the row for scatter about the average curve. Thus for Storrs one would use 15.7 (° F.)^2 as the variance of the range (table 1, row 5).

Although the above discussion puts forward a relatively simple technique for estimating the mean and variance of temperatures from a small number of constants, there is a further simplification that may produce equivalent results, at least for the mean temperature. I noticed that not only does the log variance of the mean temperature follow a simple sine curve but also the time of the maximum variance is about 180°, or 6 months, out of phase with the temperature. For example, the yearly maximum of the mean temperature at Keedysville, computed from the best fitting simple sine curve, falls 137°27′ or 139.4 days after March 4 (the midpoint of week zero) while the maximum of $\log s_{\text{mean}}$ is at 313°48′ or 318.2 days after March 4 and 176°21′ or 178.8 days after the maximum temperature. This suggests that the log variance and the mean may be linearly related with a negative slope. When $\bar{y}$ was plotted against $\log s$, this was seen to be substantially the case. In fact, the logarithm so little changes the relationships among the standard deviations that an almost equally good fit to a linear relationship is obtained if one plots $\bar{y}$ against s. If one assumes that the phase difference between the log variance and the mean temperature is exactly 180°, which is very close to the observed difference, then one can rather easily compute the slope of the regression of $\log s$ on $\bar{y}$ from a knowledge of the amplitudes of the respective sine curves.

If

$$\begin{aligned}\bar{y} &= a_0 + a_1 \sin t + b_1 \cos t \\ &= a_0 + A_1 \cos (t - \phi_1)\end{aligned} \tag{14}$$

where A_1 is the semi-amplitude and ϕ_1 is the time in degrees of the maximum of the mean as measured from the start of the climatological year, and if

$$\begin{aligned}\widehat{\log s} &= a_0' + a_1' \sin t + b_1' \cos t \\ &= a_0' + B_1 \cos (t - \phi_1 - 180°),\end{aligned} \tag{15}$$

then

$$\frac{\bar{y} - a_0}{A_1} = \cos (t - \phi_1) = -\cos (t - \phi_1 - 180°) = -\frac{\widehat{\log s} - a_0'}{B_1}.$$

Thus

$$\widehat{\log s} = -\frac{B_1}{A_1}\bar{y} + \frac{B_1}{A_1}a_0 + a_0'. \tag{16}$$

Hence we can give the "regression" of $\log s$ on $\bar{y}$ from a knowledge of the sine curves fitted. To test the accuracy of this method, both the ordinary least squares line and the line computed from equation (16) were calculated for the mean temperatures at Storrs and at Easton I and Easton II and are given in table 3 together with the regression line calculated from equation (16) for the other stations studied. We note a remarkable homogeneity among the slopes of the regression lines for the three records which cover two Maryland stations, with the slope at Storrs quite close. However, when one crosses the Alleghenies to Uniontown, the relation changes radically, and is even more changed at Eau Claire. Even if the observed interstation homogeneity in the three easternmost stations is fortuitous, the stability of the regression lines between two independent records at Easton shows that it may be possible to estimate temperature probabilities for any week of the year from only five parameters, the overall mean, the phase angle, and the amplitude of the temperature curve, and the amplitude and mean of the log variance. This relationship does, however, need further study, especially with respect to the geographical stability of the "regression" of $\log s$ (or s) on $\bar{y}$.

One point in the above discussion may need some explanation. It is a well-known fact that in drawing samples from a single normal population, s^2, the estimate of the population variance, and $\bar{y}$, the estimate of its mean, are independently distributed. How then do we have such a marked correlation between the means and the log variances, when we have seen that the distributions are not far from normal? The question is, however, meaningless since, although we have drawn 52 samples from normal or near normal populations, these populations have not been the same. There is neither a priori nor a posteriori evidence that the population of mean temperatures for week one is the same (i.e., has identical characteristics) as the population for any other week. In fact, our investigation has demonstrated that these distributions are definitely different. Thus one should not expect the independence between s^2 and $\bar{y}$ which would result if the populations were the same. A relationship between the true values (not merely the estimates) of the averages and variances of the mean temperatures, say, is clearly indicated by the data at hand. Its reality can be indicated statistically but its cause must be physical. In a similar vein the standard tests for equality of variance, say, between two different weeks are quite useless. In advance of such a test, we have a well established result that the variances are, in general, unequal.

TABLE 3.—*Regression equations of log s on $\bar{y}$ computed by least squares and by equation (6)*

Station	Least squares line	Equation (6)
Easton I	$\log s = 1.020113 - 0.006454\bar{y}$	$\log s = 1.02479 - 0.006543\bar{y}$
Easton II	$\log s = 1.018815 - 0.006057\bar{y}$	$\log s = 1.02260 - 0.006128\bar{y}$
Storrs	$\log s = 0.926768 - 0.005239\bar{y}$	$\log s = 0.92902 - 0.005277\bar{y}$
Keedysville	[1]	$\log s = 1.02814 - 0.006067\bar{y}$
Uniontown	[1]	$\log s = 1.18340 - 0.008311\bar{y}$
Eau Claire	[1]	$\log s = 0.89526 - 0.002067\bar{y}$

[1] Not computed.

7. PROBLEMS IN FURTHER APPLICATIONS

To this point we have spoken only about the probabilities of average temperatures or average diurnal ranges for a given week, without reference to the probabilities for derived quantities, or averages over longer periods such as months or seasons. If the mathematical model were completely correct, one could, theoretically, compute quite complicated probabilities concerning degree days, frost dates, etc., from a knowledge of the joint distribution of the coefficients of the curves which describe each year. This knowledge is also needed for efficient use of the parameters in relating them, as being in some sense a description of a yearly temperature regime, with other elements, climatological, agricultural, or physical. Before proceeding further, we should inquire to what degree the estimated coefficients for a given year do contain the salient features of that year. To this end, I tabulated the published departures of the monthly mean temperatures from the long-term normal for the regions or States in which our stations are located. Years were then picked by eye which had various characteristics, e.g., warmer than normal spring combined with colder than normal winter, etc. Then, using the best fitting harmonic curves for these years for the stations involved, the "expected" temperature, $\hat{y}$, for each week was computed and compared against the 30-year average curve. In every case the unusual pattern for which that year had been chosen was observed in the fitted harmonic curve. Although they lack fine detail, the curves for each year definitely reflect the course of the temperature for that year.

Determination of the distribution of the true coefficients is far more difficult since they cannot be observed directly. We can examine only estimated coefficients. A further complication is the previously discussed dependence of the coefficients upon our arbitrary choice of origin. Thus a full discussion of this problem would involve determining all relationships among the coefficients which are not changed by any choice of origin. However, despite the above objections, I considered it valuable to examine more carefully the estimates of the coefficients for the particular choice of origin we used. To provide a minimal test of normality in the marginal distributions of the separate coefficients, the ranked estimated coefficients for the curves fitted to the mean temperature were plotted against rankits (expected order statistics for the normal distribution [9]) for each of the two Easton samples. Departure from normality of the estimates should be reflected in non-linearity in the plotted points. In every case where any noticeable non-linearity occurred in one

record, it was not visible in the other. Thus I concluded that there was no evidence for rejecting the hypothesis of normality among the estimates of the coefficients. To the degree that non-normality in the distribution of the actual coefficients would be reflected in non-normality of the estimates, this indicates normality in the marginal distributions of the actual coefficients. Hence, they are probably distributed in a multivariate normal distribution. Further, we computed covariance and correlation matrices for the seven estimated coefficients for each of the two Easton samples, and then combined them to get an estimated covariance matrix based on a 60-year sample. It can easily be shown that for our choice of origin, the winter maximum of the variance of the mean temperature implies that there should be positive correlation between a_0 and a_1 and negative correlation between a_0 and b_1. Hence any test for the significance of these observed correlations should be single-tailed, and we should also compute the partial correlation $r(a_1, b_1|a_0)$. We found that there were several correlations of statistical significance, i.e., larger than one could expect to occur by chance alone. However, their practical significance is negligible since they are all less than 0.5 in absolute value. The physical or climatological meaning of such correlations is not clear, especially in view of the fact that any one may be reduced to zero by some choice of an origin in fitting the polynomials.

There is one further problem which would limit the application of this method, even were the above problems solved. There appears to be considerable difficulty in making a meaningful correspondence between the parameter space and the space of "year types." In other words, there is no clear way to pick out all those sets of coefficients $a_0, a_1 \ldots, a_3, b_1, \ldots, b_3$, which, when used in a harmonic curve, would produce a "warm spring." Unless one can accomplish this, knowledge of the distribution of the coefficients cannot be fully applied.

There are many applications, however, of the average curve computed for a location, in which the form of the distribution of the yearly coefficients is of minor importance. Prescott [12] used maps of the phase and amplitude of sine curves fitted to monthly temperatures for stations in Australia to locate suitable homoclimes for new crops. Except for the difficulties attached to solving polynomial equations involving trigonometric terms, expression of the yearly course of temperature by a periodic curve provides a means of locating the time when the average temperature is at a maximum or a minimum. If

$$y=a_0+a_1 \cos t+b_1 \sin t+a_2 \cos 2t+b_2 \sin 2t+ \ldots,$$

the relative maxima and minima occur at those values for t for which

$$-a_1 \sin t+b_1 \cos t-2a_2 \sin 2t+2b_2 \cos 2t- \ldots=0.$$

Similarly, the day on which the average maximum, minimum, or mean temperature passes some critical value can be computed from the coefficients of the average curve. In the case of the mean temperature, of course, this type of problem is generally simple since the temperature can be considered to follow a sine curve. However, for more complex curves, a process of successive approximation seems to be necessary.

REFERENCES

1. R. L. Anderson and T. W. Anderson, "Distribution of the Circular Serial Correlation Coefficient for Residuals from a Fitted Fourier Series," *Annals of Mathematical Statistics*, vol. 21, 1958, pp. 59–81.
2. M. S. Bartlett, "The Use of Transformations," *Biometrics*, vol. 3, No. 3, Mar. 1947, pp. 39–52.
3. C. Bingham, "Analysis by Harmonic Regression of Diurnal Temperature Range" (abstract), *Bulletin of the American Meteorological Society*, vol. 39, No. 8, Aug. 1958, pp. 441–442.
4. C. I. Bliss, "Periodic Regression in Biology and Climatology," *Bulletin* 615, The Connecticut Agricultural Experiment Station, New Haven, Conn., 1958, 55 pp.
5. W. G. Cochran, "Some Consequences When the Assumptions for the Analysis of Variance Are Not Satisfied," *Biometrics*, vol. 3, No. 3, Mar. 1947, pp. 22–38.
6. J. M. Craddock, "The Variation of the Normal Air Temperature Over the Northern Hemisphere During the Year," a paper of the Meteorological Research Committee (London), M.R.P. No. 917. (A copy is available in the Library of the Meteorological Office.)
7. H. Cramér, *Mathematical Methods of Statistics*, Princeton University Press, 1946, 575 pp. (pp. 494–495).
8. R. A. Fisher, *Statistical Methods for Research Workers*, 6th edition, Oliver and Boyd, Edinburgh, 1936, 339 pp. (p. 75).
9. R. A. Fisher and F. Yates, *Statistical Tables for Biological, Agricultural and Medical Research*, 3d edition, Oliver and Boyd, London and Edinburgh, 1948, 112 pp.
10. R. C. Geary and E. S. Pearson, *Tests of Normality*, London, 1938, 15 pp.
11. H. Landsberg, *Physical Climatology*, 2d edition, Gray Printing Co., Inc., Dubois, Pa., 1958, 446 pp. (p. 152).
12. J. A. Prescott, "The Value of Harmonic Analysis in Climatic Studies," *The Australian Journal of Science*, vol. 5, 1943, pp. 117–119.
13. H. R. Tolley, "Frequency Curves of Climatic Phenomena," *Monthly Weather Review*, vol. 44, No. 11, Nov. 1916, pp. 634–642 (see table, pp. 640–641).
14. E. W. Wahl, "The January Thaw in New England (An Example of a Weather Singularity)," *Bulletin of the American Meteorological Society*, vol. 33, No. 9, Nov. 1952, pp. 380–386.

THE WEATHER AND CIRCULATION OF JUNE 1961

A Hot, Dry Month in the West

L. P. STARK

Extended Forecast Branch, U.S. Weather Bureau, Washington, D.C.

1. RECENT MONTHLY TRENDS

From March 1961 thru June 1961 there was a noticeable trend in the monthly weather anomalies and circulation over the United States. Temperatures in the eastern half of the United States tended to become progressively cooler than normal while temperatures in the western half of the country continued a warming trend. At the same time, there was a gradual shift in the area of heavier than normal precipitation from northern and eastern portions to the Southern States and a noticeable tendency toward drought conditions in parts of the West.

A corresponding trend was apparent in the circulation in the mid-troposphere. Comparison of successive monthly mean 700-mb. charts for March through June shows the gradual displacement westward of a long-wave trough from the western Atlantic at the beginning of the period to the Ohio Valley by June. There were other areas in which apparent retrograde motion of major systems occurred, but in none was it so pronounced or so important to the weather in the United States.

2. MONTHLY MEAN CIRCULATION

The planetary wave pattern at 700 mb. in June 1961 (fig. 1) consisted of well-defined trough and ridge systems from the western Pacific eastward to Eurasia. While this is shown by the height contours alone, it is better indicated by the height departures from normal (dotted lines in fig. 1).

In the Atlantic the circulation was characterized by westerlies that averaged considerably faster than normal in a jet maximum that extended from Newfoundland to the United Kingdom. The strong westerlies resulted from the moderately deep Icelandic Low in phase with a strong ridge in the Atlantic. The primary Icelandic Low was 310 feet deeper than normal and was displaced considerably eastward to the Norwegian Sea from its normal position near Baffin Island [1].

The Aleutian Low was similarly displaced. Its normal position in June [1] is in the Bering Sea, and it is usually accompanied by a broad cyclonic flow in the central Pacific north of 30° N. The observed flow (fig. 1) shows that the deepening trough in eastern Asia and amplification in mid-Pacific contributed to the anomalous position of the Aleutian Low in the Gulf of Alaska. Deepening of the trough in the Gulf of Alaska was probably assisted by local baroclinic processes, suggested by the distribution of monthly mean 1000–700-mb. thickness (fig. 2), as well as by barotropic transport of vorticity from upstream.

Growth of the ridge in the central Pacific was a great change from May (see fig. 1 of [2]) when a trough was located in this area. Heights at 700 mb. increased as much as 400 ft. from May to June in the western Aleutians as the trough was replaced by a strong ridge in June.

Over North America the Canadian portion of the ridge in the West was somewhat farther east and generally 100 feet or more stronger than normal. Its companion trough downstream was west of its normal position and a little deeper than normal. This shortening of the half wavelength between the ridge and the trough resulted in a vigorous northerly component of the height anomaly field from northeastern Canada to Mexico.

There were pronounced changes in the circulation at 700 mb. from the first half of June (fig. 3A) to the last half of the month (fig. 3B). Elements of the circulation over and near North America for June 1–15 included a continental ridge and two major troughs, one in the Gulf of Alaska and the other in eastern Canada, oriented in a modified omega pattern. Flow over the United States was quite weak except along the northern border. These features are shown clearly by the contours of height and height anomaly in figure 3A.

From the first half to the last half of the month the circulation was characterized by retrogression and general flattening of the pattern at higher latitudes over North America (fig. 3). This was associated with weakening of the Low in the Gulf of Alaska. At the same time heights increased in western United States as much as 200 ft. over the Great Basin. Meanwhile, the trough in eastern North America retrograded to the Ohio Valley and joined with the trough that moved eastward from Baja California.

In summary, June was a month of relatively low index circulation over the United States. This was associated not with blocking as was May, but with a strong meridional flow that was responsible for unseasonable extremes of temperature in many parts of the country.

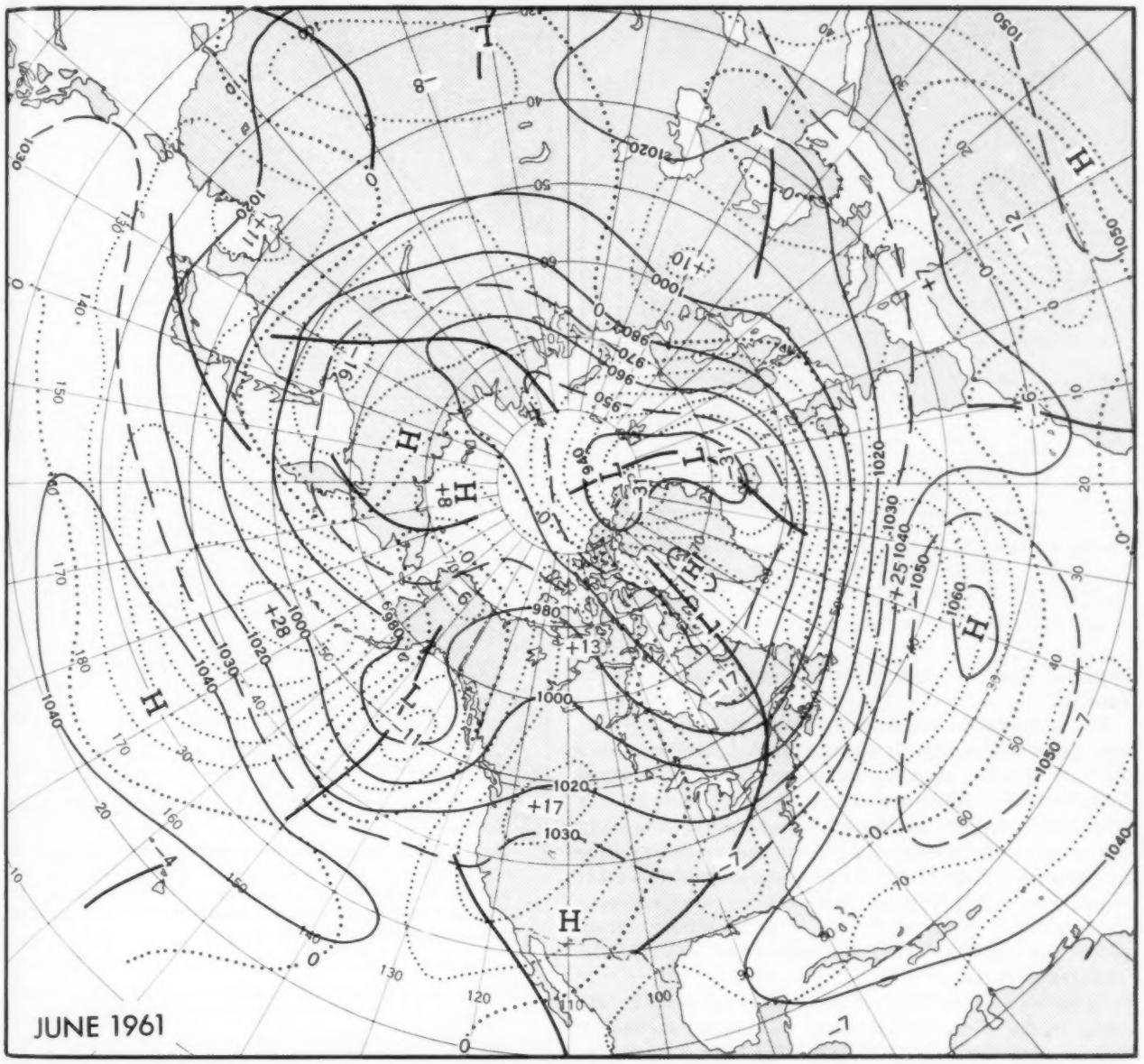

FIGURE 1.—Mean 700-mb. contours (solid) in tens of feet, and departures from normal (dotted) in 50-ft. intervals, for June 1961. The meridional nature of the height anomaly field was indicative of the low index condition over North America and the Pacific.

3. WEATHER RELATED TO THE CIRCULATION

TEMPERATURE

Hot, dry weather in the West was associated with many new temperature records principally in Montana, California, and Oregon, while unusually cool conditions prevailed over much of the East.

Temperatures in June (fig. 4) averaged about 2° to 4° F. cooler than normal from the Southern Plains to the Mid-Atlantic States and from the Lower Great Lakes to the Gulf of Mexico. This area was dominated by below normal heights and cyclonically curved contours on the monthly mean 700-mb. chart (fig. 1). The strong ridge in western North America steered numerous anticyclones southward from northern Canada (Chart IX of [3]) to the Northern Plains then southeastward across the Middle Atlantic States in a slightly confluent zone. A secondary track of Highs extended from western Hudson Bay to southern Quebec. In both instances daily anticyclones

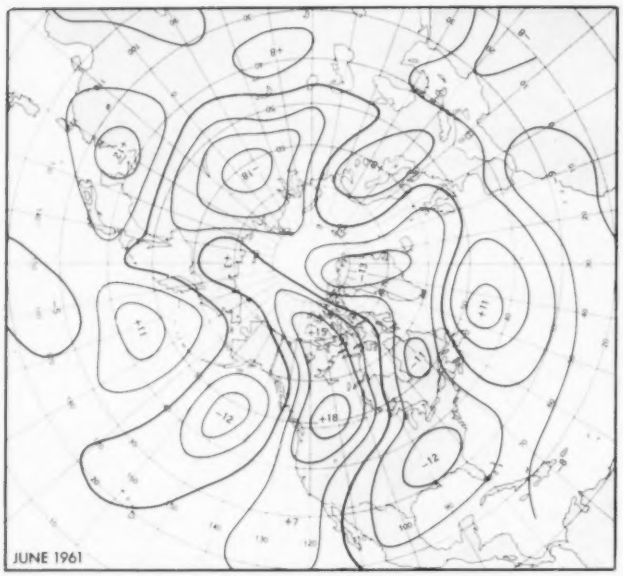

FIGURE 2.—Mean thickness (1000–700 mb.) departure from normal (isopleth interval 50 ft.) for June 1961. Cool air masses dominated the East and subsiding air warmed the West.

bypassed the Great Lakes, a very atypical occurrence in June [4].

The average thickness from 700 to 1000 mb. (fig. 2) was below normal along an axis from Labrador to the Gulf of Mexico, generally coincident with the area of below normal surface temperatures (fig. 4). Few records were established in the East beyond several new daily minimum temperatures. At Norfolk, Va., a new all-time minimum for June of 48° F. was recorded on the 17th; record low monthly mean temperatures were reported at Louisville, Ky. (68.9° F.) and Vicksburg, Miss. (75.1° F.), and the coldest June since 1903 was reported at Shreveport, La.

In contrast to the East, temperatures were exceptionally warm in the West. A large area was 6°–10° F. warmer than normal (fig. 4). This region was located under the upper level ridge where subsidence was widespread and where heights exceeded normal by as much as 170 ft. (fig. 1). Many areas in the West reported heat waves of varying duration, but one of the most intense was at

TABLE 1.—*New monthly maximum temperature records in June 1961.*

Location	Maximum temperature (°F.)
San Francisco, Calif.	106
Bakersfield, Calif.	113
Medford, Oreg.	109
Pendleton, Oreg.	108
Winslow, Ariz.	105
Salt Lake City, Utah	104
Yakima, Wash.	103
Rapid City, S. Dak.	106

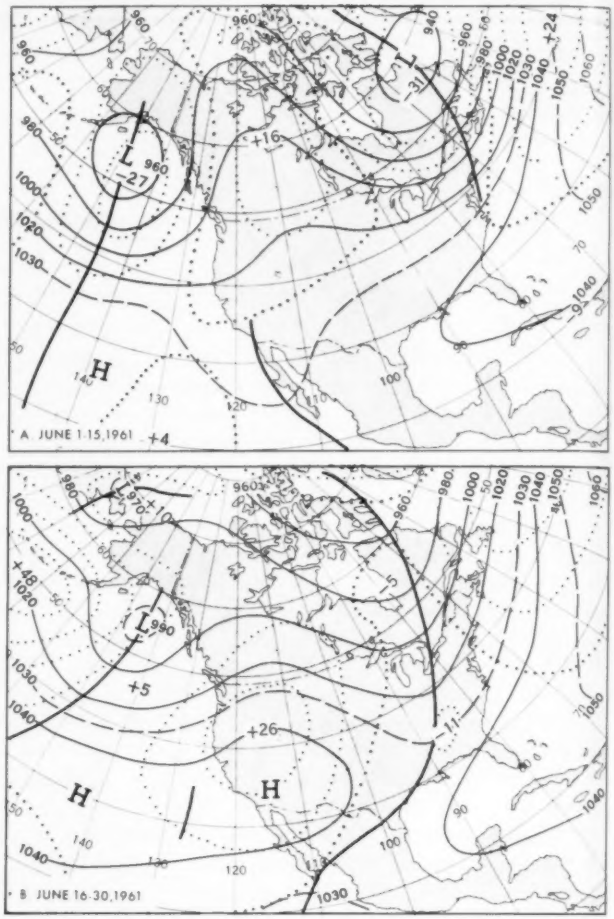

FIGURE 3.—Mean 700-mb. contours (solid) and departures from normal (dotted), both in tens of feet for (A) June 1–15, 1961, and (B) June 16–30, 1961. Retrogression of the trough in the East and intensification of the ridge in the West were important factors during June.

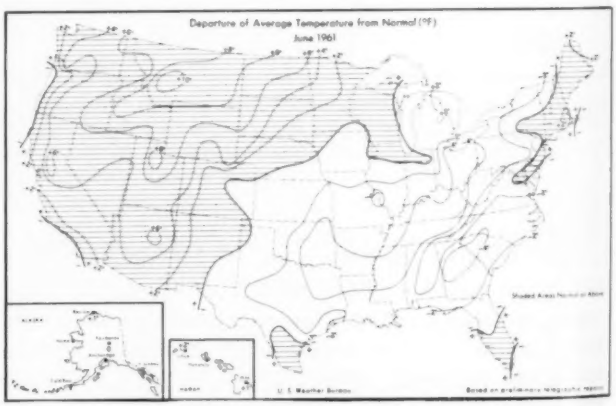

FIGURE 4.—Departure of average temperature from normal (°F.) for June 1961. Many new temperature records were established, especially in the West. (From [5].)

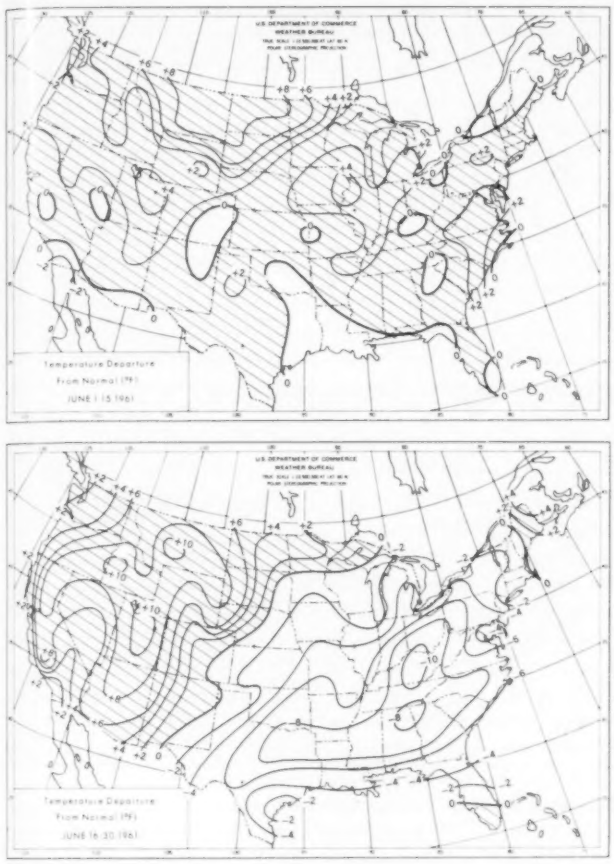

FIGURE 5.—Departure of average temperature from normal (°F.) for (A) June 1–15, 1961, and (B) June 16–30, 1961. Note that (B) most closely resembles figure 4.

Las Vegas, Nev., where the daily maximum temperature ranged from 110° to 113° F. from June 17 to 26. Most cities in Montana had the warmest June of record. Other spectacular records include new maximum temperatures for June as shown in table 1.

Above normal temperatures were not confined to the United States. The core of warm thickness and above normal heights extended northward to the Beaufort Sea. Reports from the Canadian Meteorological Branch, Department of Transport, indicate that temperatures exceeded normal by 6° to 8° F. from southern Alberta to Great Slave Lake and by more than 4° F. from there to 70° N.

Temperature anomalies discussed above can be examined less grossly by considering the 15-day averages (fig. 5). The large changes in the circulation (fig. 3) from the first half of June to the last half are clearly reflected in these temperature changes. Temperatures for June 1–15 (fig. 5A) were above normal over much of the United States. Maximum departures exceeded 8° F. in Montana and

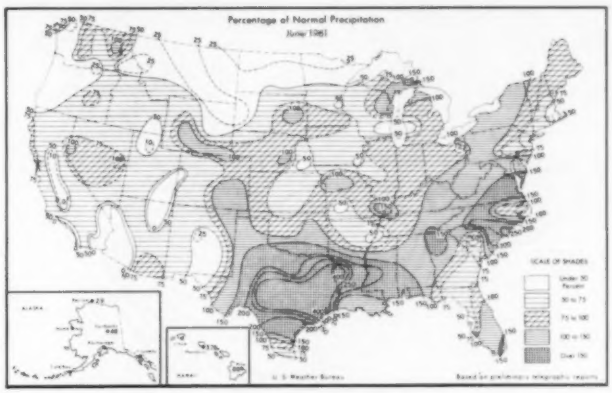

FIGURE 6.—Percentage of normal precipitation for June 1961. Only the South and parts of the East received more than normal rainfall. (From [5].)

North Dakota, the region in which positive height departures were largest (fig. 3A).

During the last half of June (fig. 5B) large-scale cooling in the East caused temperatures to decrease 6° to 10° F. from Texas to the Atlantic coast. In the West, influenced by the anticyclogenesis aloft (fig. 3B), the area of warmth expanded to the southern border and intensified by about 5° F. in most States.

Widespread warmth over western North America occurred when deepening in the Gulf of Alaska reinforced the ridge that normally lies along the Canadian Rockies. Consequently, there was little penetration of western North America by Pacific air masses as the average jet axis swept northward off the west coast instead of eastward along its usual path in middle latitudes. All aspects of the mean circulation that supported the heat in the West also favored a relatively dry month in this area.

PRECIPITATION

Quite dry conditions prevailed over most of the western half of the country (fig. 6), while precipitation was generally heavy in most of the South and in portions of the East.

Rainfall in the West was effectively inhibited by the 700-mb. flow (fig. 1). The anticyclone in the West and its associated ridge were sufficiently strong to present a barrier to the transport of moisture from the Pacific. In addition, the desiccating nature of anticyclonic conditions and the predominantly downslope direction of the anomalous flow contributed to the dry weather. There were few monthly records established in the West, but rainfall was appreciably below normal and contributed to prolonging a period of light precipitation in that region.

The average 700-mb. flow (fig. 1) was conducive to heavier than normal rainfall along and eastward from the trough in the central States. Features of the 700-mb. chart favoring heavy precipitation in Texas included the trailing trough, below normal heights, and easterly

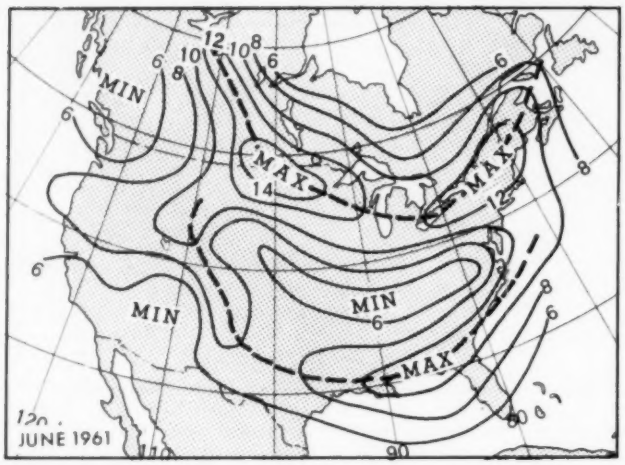

FIGURE 7.—Number of days with fronts in equal area (66,000 n. mi.²) quadrilaterals for June 1961. Heavy precipitation occurred along the axis of maximum frontal frequency in the South; in the North fronts were "drier" due to virtual exclusion of moisture from Gulf of Mexico by strong northerly flow.

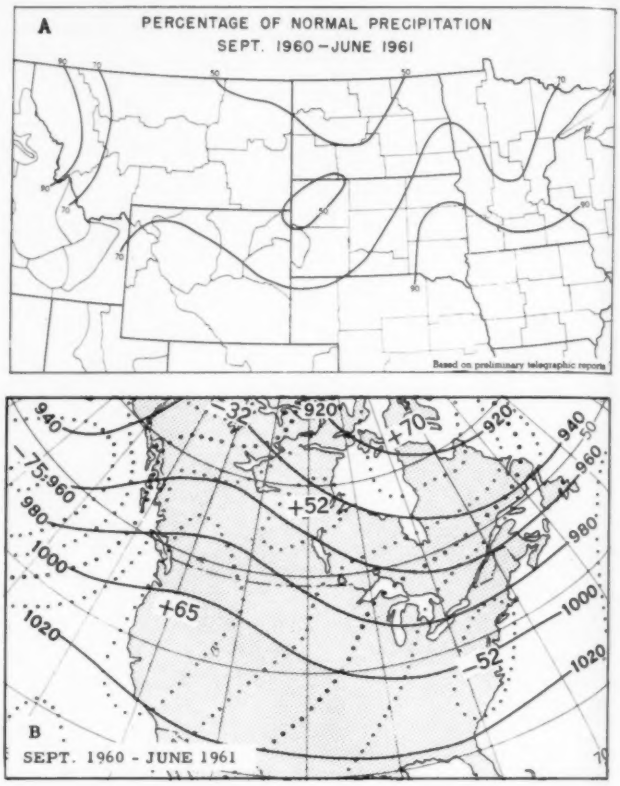

FIGURE 8.—(A) Percentage of normal precipitation (from [5]), and (B) mean 700-mb. contours (solid) in tens of feet and departures from normal (dotted) in 25-ft. intervals, with centers labeled in feet. Both for September 1960–June 1961.

anomalous wind components. In addition, temperatures were fairly cool (figs. 2 and 4) from the surface to 700 mb. and the influx of moisture at the surface (Chart XI of [3] was moderately strong from the Gulf of Mexico to Oklahoma. Thus, conditions were optimum for overrunning and heavy precipitation in this area. Record amounts for June were observed at Waco and Abilene, Tex., and Shreveport, La.

The distribution of precipitation can also be considered as a function of frontal activity. Figure 7 shows an axis of maximum frontal frequency from Texas to southern Alabama to North Carolina. The location of this average frontal zone corresponds well to the area of heavy precipitation, as would be expected. However, the area of ma xi mum frontal occurrence from North Dakota to the Lower Great Lakes shows a higher frequency than that in the South, yet the precipitation "fit" was relatively poor, except in New York and Pennsylvania. The flow at all levels west of the trough at 700 mb. contained a northerly component, carrying dry air into the country. Therefore, fronts in the West were ineffective in producing rain of any consequence, a major factor in the perpetuation of drought in this area.

DROUGHT

A significant shortage of precipitation in the last ten months has produced a drought of particular severity in portions of the States shown in figure 8A (from [5]). The 700-mb. mean circulation for most of the United States and Canada for the period September 1960 to June 1961 (fig. 8B) was prepared in order to detect any correspondence between the flow and the drought. Anomalous precipitation is not uniquely defined by mean 700-mb. contours, but there are components of this circulation that seem to augment or inhibit the production of precipitation. In this instance the flow itself implies little and, in fact, resembles grossly the normal circulation that consists of a ridge over the western mountains and a trough over eastern North America. However, the dotted isopleths in figure 8B representing the anomalous components of the 700-mb. heights clarify the situation. Note, first, that heights were all above normal in the drought area, and, second, that the direction of anomalous flow was northerly. Although both conditions favor dry weather, the latter is most frequently associated with a deficiency of precipitation on mean circulations.

It would be an over-simplification to attempt to explain the drought solely in terms of the anomalous 700-mb. flow, but there was a significant contribution. Statistical evidence [6] indicates that winter precipitation in North Dakota is negatively correlated with 700-mb. heights in southern Idaho and positively correlated with heights in the Middle Atlantic States (both correlation coefficients exceed 0.5). It follows that anomalous northerly flow components of the type portrayed in figure 8B should be associated with a dry regime in the Dakotas.

REFERENCES

1. U.S. Weather Bureau, "Normal Weather Charts for the Northern Hemisphere," *Technical Paper No. 21*, Washington, D.C., 1952, 74 pp.
2. R. H. Gelhard, "The Weather and Circulation of May 1961—Persistent Cool Weather in the United States," *Monthly Weather Review*, vol. 89, No. 8, Aug. 1961, pp. 299–305.
3. U.S. Weather Bureau, *Climatological Data—National Summary*, vol. 12, No. 6, June 1961, Charts IX and X.
4. W. H. Klein, "Principal Tracks and Mean Frequencies of Cyclones and Anticyclones in the Northern Hemisphere," U.S. Weather Bureau, *Research Paper No. 40*, Washington, D.C., 1957, 60 pp.
5. U.S. Weather Bureau, *Weekly Weather and Crop Bulletin, National Summary*, vol. XLVIII, Nos. 27 and 28, July 3 and 10, 1961.
6. C. K. Stidd, "The Use of Correlation Fields in Relating Precipitation to Circulation," *Journal of Meteorology*, vol. 11, No. 3, June 1954, pp. 203–213.

Weather Bureau Technical News

ISOTOPE-POWERED AUTOMATIC WEATHER STATION

The latest development in the automatic observation of weather is the incorporation of a radio-isotope power plant into the apparatus of automatic stations. This allows unattended operation of the station up to the limit of instrument life and eliminates the difficulties met with in other automatic stations from lack of a continuous power source. The first such station was set up in August on or near Graham Island in the Canadian Arctic about halfway between the Joint Canadian-United States Arctic Weather Stations at Eureka and Resolute. Power is generated by the heat spontaneously produced by radio active decay of pellets of strontium-90, in the form of strontium titanate, enclosed in a small (5-inch) shielded cylindrical capsule. The heat is transformed directly into a continuous flow of electricity by 60 pairs of thermocouples arranged like spokes around the cylindrical heat source. The whole generator is shielded in 4.4 inches of lead and covered by an outer skin of stainless steel. The overall dimensions are 20 inches long by 18 inches in diameter.

The generator cylinder is the bottom element in a larger cylindrical container 8 feet long. The top compartments of this house the electrical apparatus, recording equipment, radio transmitters, and the barometer. Excess heat from the generator serves to maintain an interior operating temperature of 70° F. The anemometer and thermometer are exposed on a mast beside the cylinder, the lower 5 feet of which is buried in the ground.

Observations of wind direction (to nearest 10° heading), wind speed (0 to 150 kt. ±1 kt., 1 and 8 minute average), pressure (28.00 to 32.00 in., ± 0.02 in.), and temperature (−75° to +120° F., ±1° F.) is transmitted by radio in 8 bit binary digital form once every 3 hours simultaneously on two frequencies, 3.36 and 4.97 megacycles. The transmitter output is 250 watts on each frequency with range up to 1500 miles depending on the frequency. The transmission consists of call letters and data measurements plus one repeat. Provision has been made in the package for measuring other elements such as precipitation, humidity, sky cover, etc., whenever suitable sensors become available.

The measuring and transmitting equipment are designed and fabricated to provide reliability consistent with the long life of the isotope, to use a minimum of electricity, and to produce accurate weather data in usable form. Since the generator sustains no wear from moving parts, long-term maintenance-free operation is possible. The generator could power the station for more than ten years.

Although these stations will always be located in remote or completely uninhabited areas such as the present site, great care was taken in the development of a safe fuel form and adequate, reliable shielding. Strontium becomes a biological problem only if it is absorbed by some living organism. This danger can be eliminated by using an insoluble compound. To provide at the same time a fuel material dense enough to conserve space and relatively easy to produce, strontium titanate was selected. This compound remains stable even beyond its melting point of 3000° F., and its rate of solubility in fresh water is so low it has not been measured. In salt water its solubility is measured in parts per billion. The shielding within the generator consists of several layers of an alloy called Hastelloy-C. It would take centuries to corrode, even if immersed in sea water. The outside shielding of the generator cylinder is ¾ ton of lead with a final covering of stainless steel. The whole generator is designed so sturdily that it could survive a plane crash or an explosion without releasing its fuel.

The station was designed and built by the nuclear division of the Martin Company, Baltimore, Md., under a contract with the U.S. Atomic Energy Commission, Office of Isotopes Development in cooperation with the U.S. Weather Bureau. The site was suggested by the Department of Transport of Canada and the station was installed by a joint Canadian and United States work party.

Publications By Weather Bureau Authors

D. I. Blumenstock, "A Report on Typhoon Effects Upon Jaluit Atoll," *Atoll Research Bulletin*, No. 75, April 15, 1961, issued by Pacific Sciences Board, National Academy of Sciences, National Research Council, Washington, D.C.

P. F. Clapp, "The Long View of the Weather," *Harvard Alumni Bulletin*, vol. 63, No. 9, Feb. 18, 1961, pp. 393–400.

S. Fritz, "Meteorological Observations from Satellites," *The New Scientist*, vol. 10, 1961, pp. 504–507.

C. S. Gilman and V. A. Myers, "Hurricane Winds for Design Along the New England Coast," *Journal of Waterways and Harbors Division*, Proceedings of the American Society of Civil Engineers, vol. 87, No. WW2, May 1961, Part 1, pp. 45–65.

C. D. Hopkins, Jr., "Water Supply Forecasts in Northern New England," pp. 105–117, *Proceedings of the 1959 and 1960 Annual Meetings*, Eastern Snow Conference (no date).

D. S. Johnson, "Image Sensing as Applied to Meteorological Satellites," *Journal of the Society of Motion Picture and Television Engineers*, vol. 69, No. 1, Jan. 1960.

H. E. Landsberg, "Solar Radiation at the Earth's Surface," *Solar Energy*, vol. V, No. 3, July–Sept. 1961, pp. 95–98.

J. Namias, "Factors Leading to Variations in Monthly and Seasonal Snowfalls over Eastern United States," pp. 167–184, *Proceedings of the 1959 and 1960 Annual Meetings*, Eastern Snow Conference (no date).

B. Ratner, "Do High-Speed Winds Aloft Influence the Occurrence of Hail?" *Bulletin of the American Meteorological Society*, vol. 42, No. 7, July 1961, pp. 443–446.

J. A. Riley, "Climate of the Delta Area of Mississippi," *Bulletin 605*, Mississippi State University, Agricultural Experiment Station, Sept. 1960.

J. A. Riley (with W. W. Watson), "Plastic Greenhouse Studies in Mississippi Delta," *Bulletin 607*, Mississippi State University, Agricultural Experiment Station, Dec. 1960, 6 pp.

S. Twomey, "On the Deduction of the Vertical Distribution of Ozone by Ultraviolet Spectral Measurements from a Satellite," *Journal of Geophysical Research*, vol. 66, No. 7, July 1961, pp. 2153–2162.

H. Wexler and D. S. Johnson, "Meteorological Satellites," *Bulletin of the Atomic Scientists*, vol. XVII, Nos. 5–6, May–June 1961, pp. 185–190.

U.S. GOVERNMENT PRINTING OFFICE: 1961